Wave Dissipation in Mangroves

Parameterization of the drag coefficient based on field data.

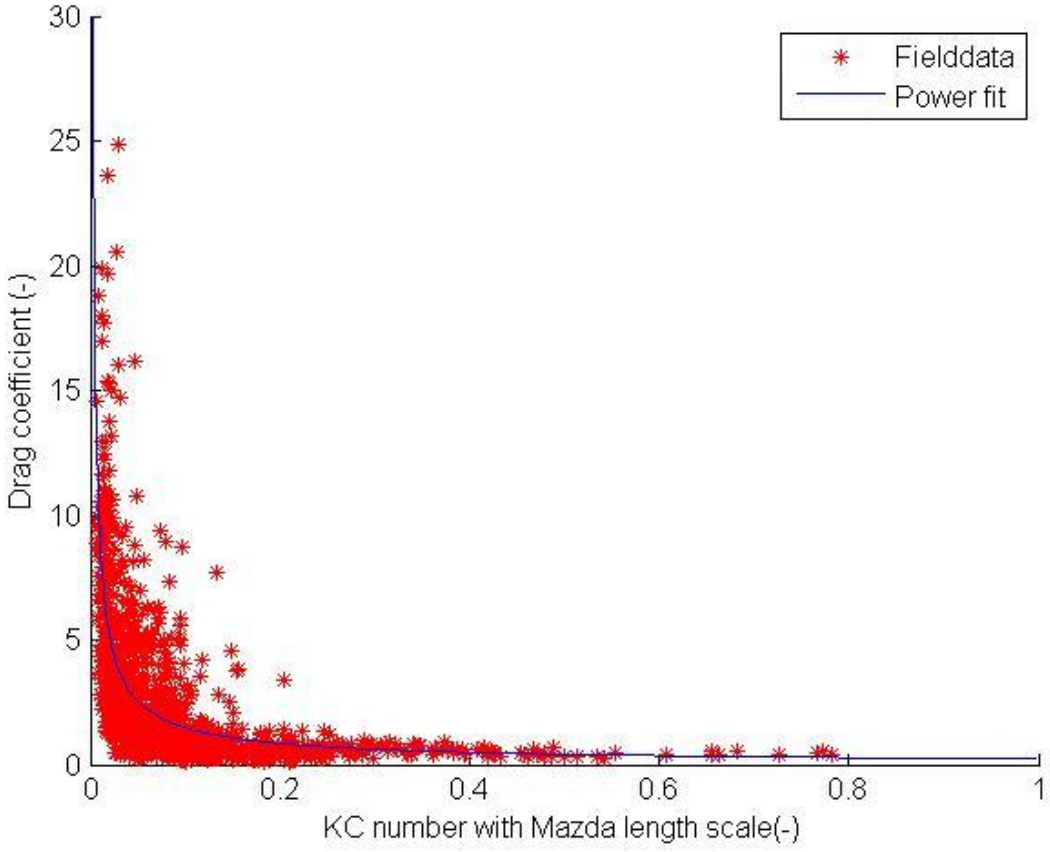

M.Sc Thesis
J.M. Hendriks
February 2014
University of Twente
Deltares

Graduation Committee:
dr. ir. C.M. Dohmen-Janssen
ir. E.M. Horstman
dr. D.S. van Maren
dr. ir. T. Suzuki

UNIVERSITY OF TWENTE.

Deltares
Enabling Delta Life

ACKNOWLEDGEMENTS

This report is the result of my M.Sc. thesis performed at Twente University and Deltares, as the final part of the master, Water Engineering and Management at Twente University.

The data used in this thesis have been collected and provided by Erik Horstman, who also closely collaborated in this thesis. I would like to thank him for his contribution and all the time he has put into providing me with feedback.

Large part of the execution of this M.Sc. thesis has been performed at Deltares research institute in Delft. They kindly provided me with the workspace and knowledge needed in order to bring this thesis to a good result. I would like to thank everyone at Deltares who helped me with parts of this thesis, but especially Claire Jeuken for making all necessary arrangements, and Bas van Maren for providing valuable contacts and feedback when needed.

Next, I would like to thank Tomohiro Suzuki, for the insight he provided in the SWAN vegetation module he created, the suggestions he made for interesting relations to investigate, and the time and effort he has put into the meetings and feedback.

In general I would like to thank for the time and effort they have put into helping me to come to this final result, all the members of my graduation committee:

dr. ir. C.M. Dohmen-Janssen
ir. E.M. Horstman
dr. D.S. van Maren
dr. ir. T. Suzuki

Last but not least I would like to thank my friends and family for supporting me throughout my study, and providing me with feedback when needed.

Jurjen Hendriks

Enschede, February 2014

SUMMARY

Mangrove forests cover large parts of sheltered coastlines in the tropical and subtropical parts of the world. Over the past decades, mangrove forests have gained more interest because of their unique ecosystems, and the coastal defence function they provide, due to their attenuating effects on waves. Even though several theoretical and field studies have been performed, and a numerical model exists to simulate wave attenuation in mangroves, available models still require calibration of a certain coefficient. This coefficient cannot simply be calculated from observed vegetation and/or wave characteristics.

The most extensive model available has been first developed by Dalrymple et al. (1984), and models the mangroves as a field of vertical cylinders. This field of cylinders affects the waves propagating through it. This formulation has been implemented in SWAN (a numerical wave model), by Suzuki et al. (2011b). Even though this model is a representation of reality based on the physical processes, there is no explicit formulation available for calculating the drag coefficient which is required in this model. Instead, the drag coefficient for a certain transect has to be resolved by a calibration procedure, resulting in a constant parameter value.

Over the years, many studies have been performed looking into drag coefficients in general, and in more recent years, vegetation drag coefficients in mangroves gained interest (e.g. Mazda et al., 2006). In these studies, the effects of several parameters on the drag coefficient (such as the Reynolds number and the KC number) have been shown. Even though for some parameters the impact on wave attenuation has already been shown in studies, there is no explicit parameterization for the drag coefficient which takes into account all these effects and has been tested on field data as well.

In this report, the data of a field campaign by Horstman et al. (2012) is used to further investigate the different variables determining the drag coefficient in mangrove vegetation. The aim was to develop a generic expression, describing this drag coefficient as a function of vegetation and wave characteristics within the mangroves.

In order to do this, the field data has been used to calculate the drag coefficients required to obtain the observed effects, for numerous short datasets (bursts) of observed wave propagation through mangroves. The resulting large set of values for the drag coefficient C_D, was analysed in relation to a number of variables, representing both the vegetation and the wave characteristics. From these variables the most significant relation was found with the KC-number with the Mazda length scale implemented instead of vegetation diameter.

$$KC_M = \frac{uTA}{(V - V_M)}$$

In which u is the maximum orbital flow velocity (m/s), T is the peak period (s), V is the control volume of water (m^3), A is the projected surface of the vegetation within this control volume (m^2), and V_M is the volume of the mangroves within the control volume (m^3).

A multi variable analysis has been performed to analyse the combined impact of several parameters and to derive a definition for the drag coefficient. Due to the variation in the data, several formulations did show up with comparable results. However, based on literature and physical meaning, a basic parameterization only using the KC-number with Mazda length scale has been selected as the best representation of the data:

$$C_D = 0.24 * {KC_M}^{-0.78}$$

In which C_D is the drag coefficient (-), and KC_M is the KC number with Mazda length scale (-) as defined before.

When implementing this equation in the SWAN model, small improvements were obtained compared to the old situation with a single constant drag coefficient for each transect. This new equation slightly increased the R-squared and correlation values of predicted vs. observed energy dissipation rates. However, the greatest improvement lies in the fact that both transects available in the data are represented by the same equation, rather than both having a different value in the old situation. This is a first step towards more generic modelling of vegetation-induced wave dissipation.

Even though the first results show some clear relations, due to much noise in the data, not all effects could be studied in detail. Improvements of the parameterization are likely to be possible. In order to do so, more field data and controlled laboratory tests are advised.

TABLE OF CONTENTS

1. INTRODUCTION

Currently, a large part of the world's population is living in coastal areas. Even though the sea brings great benefits to the people living in these areas, it poses danger as well. Natural hazards such as storms and tsunamis are witnessed all around the world, sometimes resulting in large natural disasters. Due to the ongoing population increase in combination with the effects of climate change, such as sea level rise and increasing storm surges, the risks of coastal disasters are likely to increase in the coming decennia.

Even though engineering technologies enable us to defend the coastal areas to a certain level, these engineering solutions are often quite expensive. Moreover, they are often harmful to ecosystems and are not a sustainable solution. Due to for example land subsidence, coastal defence structures need to be reinforced after a while. This has increased awareness of the potential downsides of the established engineering solutions to coastal protection issues and increased attention for the role of ecosystems in coastal defence. One of the ecosystems that has gained attention for their natural coastal defence services are mangrove forests.

Although research has been done into the effects that mangroves have on waves, and thus to what extent they provide coastal protection, it is still very hard to actually predict these effects. Without being able to do so, it is difficult to use mangroves as an integral part of a coastal defence system. Furthermore, it is hard to convey the actual importance of mangroves to the local population without knowing the exact effects. This thesis will aim to improve this understanding and the ability to model wave attenuation in mangroves.

In this introduction, first the general context will be introduced with a short summary of the research done so far into this topic. Next, the research objectives of this thesis will be presented. Last, the research approach and report structure will be clarified.

1.1 GENERAL CONTEXT

This general context will start with a short introduction on mangroves, after which their interaction with waves and the physical processes involved will be discussed. After this previous field studies will be presented, followed by the available models and the gaps herein.

1.1.1 MANGROVES

Mangrove forests are situated at sheltered intertidal areas, found around tropical and subtropical coastlines (Giri et al., 2011). Mangroves cover approximately 137.760 km^2 worldwide (Giri et al., 2011). A distribution of the mangroves worldwide can be found in figure 1.

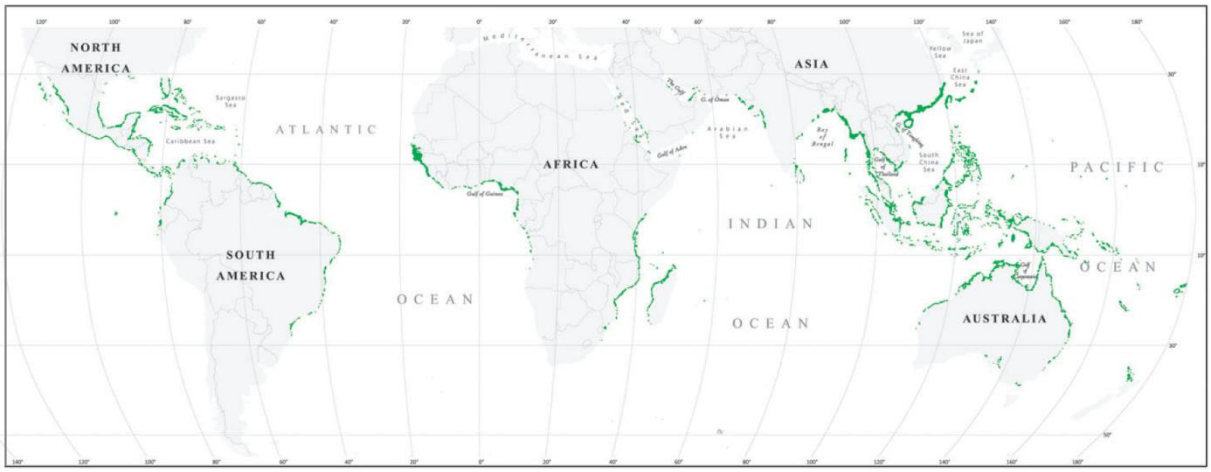

FIGURE 1 DISTRIBUTION OF MANGROVES WORLDWIDE (ADAPTED FROM GIRI ET AL. 2011)

Mangrove vegetation consists of trees and shrubs that are able to survive in saline environments. A great distinction between mangroves and normal trees comes from the aerial roots found at mangroves (Tomlinson 1986). Since mangroves are situated at intertidal flats which are submerged periodically, the mangroves need these aerial roots for oxygen uptake. The most common root types found in mangroves are pneumatophores, knee roots and stilt roots (figure 2). The aerial roots of mangroves will be submerged by the sea at least part of the tidal cycle .

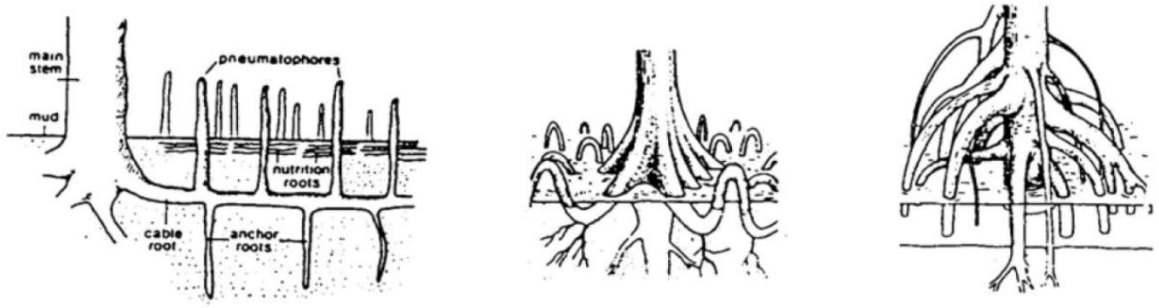

FIGURE 2 MANGROVE ROOT SYSTEMS (FROM LEFT TO RIGHT): PNEUMATOPHORES, KNEE ROOTS AND STILT ROOTS (DE VOS 2004)

1.1.2 MANGROVE WAVE INTERACTION

Waves propagating through vegetation fields lose part of their energy due to the interaction with the vegetation (Mendez and Losada, 2004). As waves propagate through mangroves, they will experience resistance from the trunks, aerial roots and in some cases the canopy as well. Due to the often extensive root systems of mangroves, this drag can become quite significant and wave attenuation in mangroves has been found to contribute to the protection of the shore (Danielson et al., 2005). Burger (2005) investigated this interaction, and the most important variables playing a role in this attenuation process. He concluded that the actual wave dissipation depends on both vegetation characteristics and hydraulic conditions.

For mangrove-wave interactions, this study focusses on wind and swell waves. Wind and swell waves are occurring almost continuously and, as can be seen in Figure 3, these waves are associated with the highest relative energy. Wind and swell waves have typical periods of about 2-20 seconds.

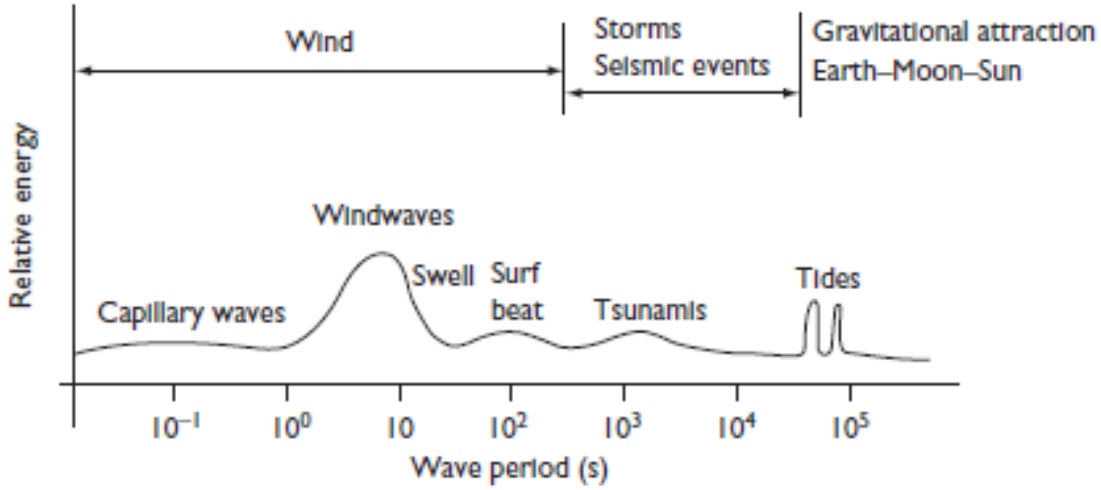

FIGURE 3 WAVE ENERGY SPECTRUM, SHOWING THE RELATIVE ENERGY OF DIFFERENT WAVE TYPES COMPARED TO EACH OTHER (REEVE ET AL., 2004)

1.1.3 PHYSICAL PROCESSES

The most important physical cause for the energy loss in vegetation is the friction being caused by the vegetation. This friction consists of both drag friction and skin friction. Skin friction is generated by the water flowing around the vegetation, creating a small boundary layer depending on the smoothness of the vegetation. Drag friction is caused by the form of the vegetation creating turbulence in its wake. The balance between the two types of friction depends on the flow regime. The flow regimes range from creeping flow, where no separation takes place and skin friction is the dominant friction factor, to flows with a completely turbulent boundary layer, where drag friction is the dominant friction force. A good overview of the regimes has been made by Sumer and Fredsoe (2006), which can be found in figure 4.

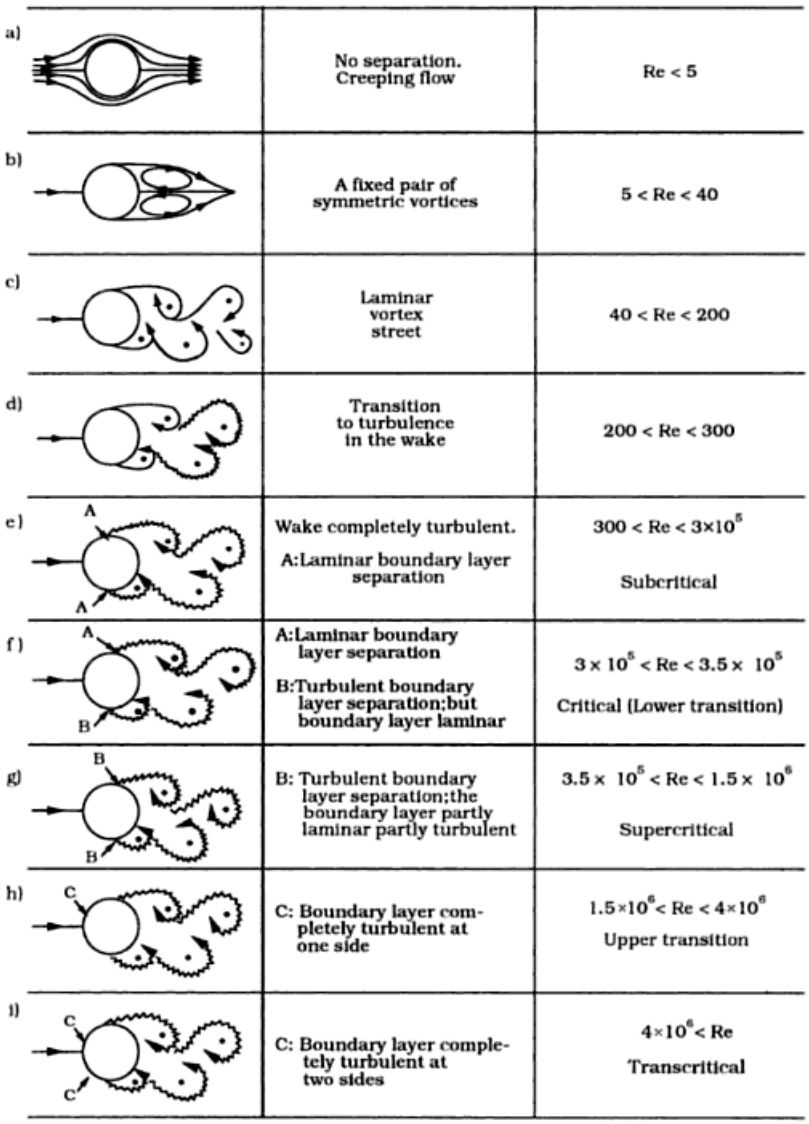

FIGURE 4 FLOW AROUND A CYLINDER AT DIFFERENT FLOW REGIMES (SUMER AND FREDSOE, 2006)

Although the energy loss is temporally and spatially varying, in general a time averaged value is used in literature. Since the timescale in which the variations in flow speed (and thus energy loss) take place is small (cf. the wave period), for the total average energy loss over time this will have no effects.

1.1.4 FIELD STUDIES

Over the last decades, several field studies have been performed into the attenuation of waves in mangroves (e.g. Brinkman et al 1997, Mazda et al 1997a, Massel et al, 1999, Mazda et al 2006, Quartel et al 2007, Vo-Luong and Massel 2006,2008, and Bao 2011). Even though each of these field studies measured and represented wave attenuation in a different way, during all of these studies the wave attenuation effects of mangroves have been proven. The rates of wave attenuation differ a lot though, depending on the mangrove characteristics and wave conditions for the different locations. The dissipation in these field data goes as high as 50-70% energy loss

in the first 20 metre of mangroves. A short overview of the available field studies can be found in table 1. A complete overview of these field studies and their results can be found in appendix I.

TABLE 1: OVERVIEW OF PREVIOUS STUDIES INTO WAVE ATTENUATION IN MANGROVES. WAVE ATTENUATION IS QUANTIFIED BY THE RATIO OF THE WAVE HEIGHT REDUCTION (ΔH) AND THE INCIDENT WAVE HEIGHT (ΔH) PER UNIT DISTANCE (X): $R = \Delta H/(H{\cdot}\Delta X)$ (HORSTMAN ET AL., SUBM.).

Location	Vegetation	Incident wave height *H* & period *T*	Wave attenuation
Tong King Delta, Vietnam (Mazda et al., 1997a)	Sparse *Kandelia candel* seedlings (1/2 year-old), planted	*H* = - *T* = 5-8 s	*r* = 0.01-0.10 per 100 m
	Dense 2-3 year-old *Kandelia candel*, up to 0.5 m high, planted	*H* = - *T* = 5-8 s	*r* = 0.08-0.15 per 100 m
	Dense 5-6 year-old *Kandelia candel*, up to 1 m high, planted	*H* = - *T* = 5-8 s	*r* = 0.15-0.22 per 100 m
Vinh Quang, Vietnam (Mazda et al., 2006)	*Sonneratia* sp., 20 cm high pneumatophores, canopy starts 60 cm above bed, planted	*H* = 0.11-0.16 m *T* = 8-10 s	*r* = 0.002-0.006 m^{-1}
	No vegetation	*H* = 0.11-0.16 m *T* = 8-10 s	*r* = 0.001-0.002 m^{-1}
Can Gio, Vietnam (Vo-Luong and Massel, 2006)	Mixed *Avicennia* sp. and *Rhizophora* sp.	*H* = 0.35-0.4 m *T* = - s	energy reduction factor = 0.50-0.70 over 20 m (including a cliff)
Do Son, Vietnam (Quartel et al., 2007)	Mainly *Kandelia candel* bushes and small trees	*H* = 0.15-0.25 m *T* = 4-6 s	*r* = 0.004-0.012 m^{-1}
	Non-vegetated beach plain	*H* = 0.15-0.25 m *T* = 4-6 s	*r* = 0.0005-0.002 m^{-1}
Red River Delta, Vietnam (Bao, 2011)	Mixed vegetation	*H* = 0.15-0.27 m *T* = - s	*r* = 0.0055-0.01 m^{-1}
Can Gio, Vietnam (Bao, 2011)	Mixed vegetation	*H* ~ 0.55 m *T* = - s	*r* = 0.017 m^{-1}
Cocoa Creek, Australia (Brinkman, 2006; Brinkman et al., 1997)	Zonation: *Rhizophora* sp. (front), *Aegiceras* sp., *Ceriops* sp. (back)	*H* = 0.01-0.07 m *T* ~ 2 s	energy transmission factor = 0.45-0.80 over 160 m
Iriomote, Japan (Brinkman, 2006; Brinkman et al., 1997)	*Bruguiera* sp., 20-30 cm high knee roots	*H* = 0.08-0.15 m *T* ~ 2 s	energy transmission factor = 0.15-0.75 over 40 m
Oonoonba, Australia (Brinkman, 2006)	Zonation: *Sonneratia* sp. (front) and *Rhizophora* sp. (back)	*H* = 0.04-0.25 m *T* ~ 6 s	energy reduction factor = 0.9-1.0 over 40 m

1.1.5 MODELLING MANGROVE WAVE INTERACTION

Currently, there are two main approaces to simulate and/or predict the wave attenuation by mangroves. These are the bottom friction approach and the cylindrical structures approach (Suzuki, 2011a).

In the bottom friction approach, for example used by Quartel et al. (2007), the vegetation is represented by an increased bottom friction. The shear stress experienced by waves propagating through a mangrove stand is determined by the following equation (Quartel, 2007):

$$\tau_b = \frac{1}{4} * \rho f_w \, {u_b}^2 \qquad (1.1)$$

In which τ_b is the bed shear stress induced by waves, u_b (m/s) is the peak orbital velocity near bed, f_w is the bed friction factor (-), and ρ is the water density (kg/m^3).

This simple approach requires reliable data to calibrate and validate the bulk friction parameter that represents all friction and drag effects due to both the bottom and the vegetation. Once calibrated for a location, the approach is easy to use. There is however no validity of the friction parameter outside the calibrated area or for different conditions. Furthermore, this method is a simplification of reality and does not improve understanding of the processes taking place, but only allows to estimate the magnitude of the wave dissipation.

The second approach is the cylindrical structures approach. This approach represents the vegetation as cylindrical structures for which the drag forces and thus the energy losses can be resolved. This approach only deals with one average, representative cylindrical stem size. By integrating the forces over one wave period, the time averaged energy loss can be calculated. This has been shown by both Dalrymple et al. (1984) and Kobayashi et al. (1993) to be the following:

$$\varepsilon_v = \frac{2}{3\pi}\rho C_D b_v N \left(\frac{kg}{2\sigma}\right)^3 \frac{sinh^3 k\alpha h + 3\sinh k\alpha h}{3k\cosh^3 kh} H^3 \qquad (1.2)$$

In which ε_v is the time averaged rate of energy dissipation (N/ms), ρ is the water density (kg/m^3), C_D is the drag coefficient of the vegetation (-), b_v is the plant area per unit height of each vegetation stand (m), N is the number of vegetation stands per unit horizontal area (m^{-2}), k is the wave number (m^{-1}), h is the water depth (m), α is the relative vegetation height with respect to the water depth (-) and H is the wave height (m).

The energy loss is thus directly related to the frontal surface area of the vegetation, a certain drag coefficient and the wave properties. Although these vegetation characteristics and the wave properties are relatively easy to determine, a calibration procedure is required to obtain the drag coefficient (Mendez and Losada, 2004).

1.1.6 MODEL IMPLEMENTATION

The first implementation of the Dalrymple formulation into a numerical model has been performed by Burger (2005). He attempted to implement a vegetation module to the SWAN model. SWAN is an Eulerian model based on the action balance equation (TUDelft, 2013, Booij et al. 1999). The model gives a full spectrum representation of the action balance equation with all physical processes modelled explicitly, and therefore is considered a third-generation model (Booij et al. 1999). Time has been removed as a variable from the action balance equation in the SWAN model in order to improve computing time. This results in the model only being able to run for stationary conditions.

An official SWAN module for wave damping due to vegetation has been developed by Suzuki et al. (2011b), based on the Burger (2005) implementation. The main differences between the implementation of Suzuki et al. and Burger can be found in the implementation of vegetation density, and an adjustment in the implementation of the wave frequency and wave number. The SWAN vegetation module created by Suzuki et al. (2011b), allows for multiple layers of vegetation, each with their own specifications. In order to show the applicability of their model, Suzuki et al. (2011b) ran the SWAN vegetation model with field data of wave attenuation in mangroves obtained by Vo-Luong and Massel (2006). The results of this model run showed reasonable agreement with the observations (figure 5). Just as for the Dalrymple formulation though, this model still requires the calibration of the drag coefficient.

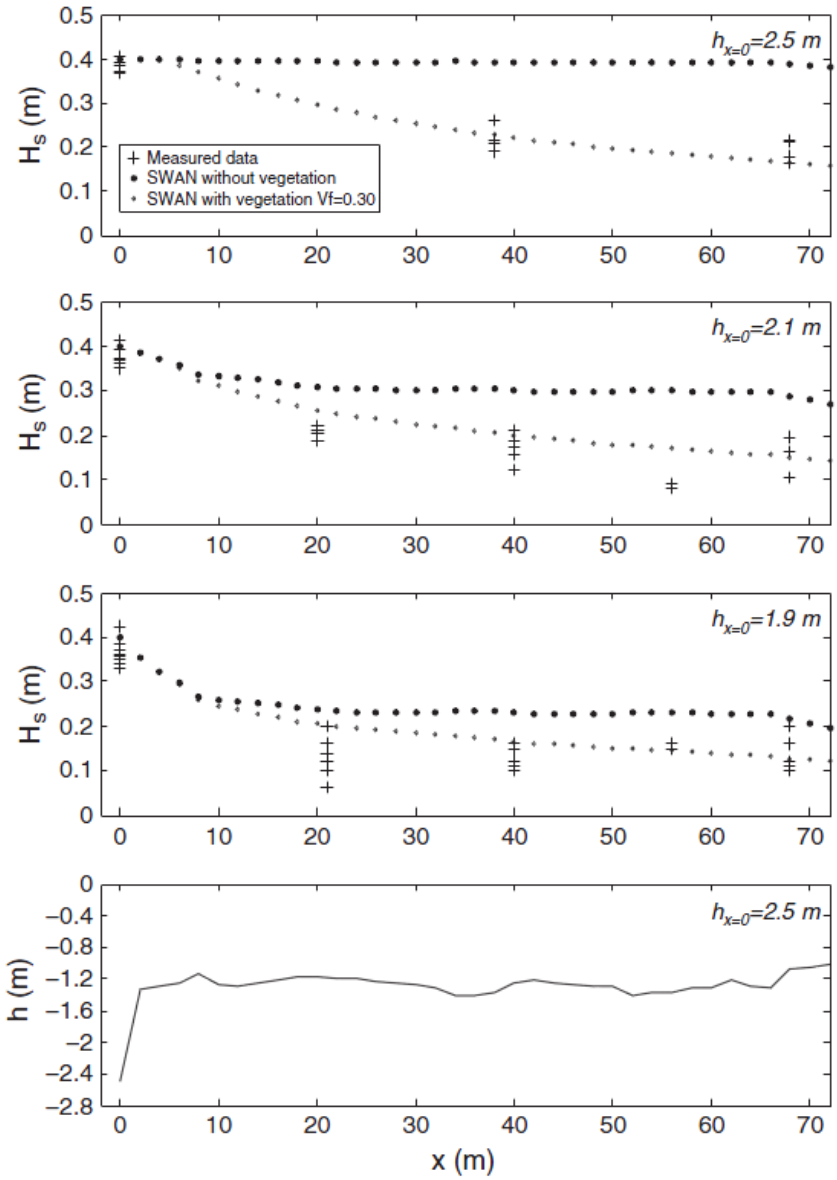

FIGURE 5 SWAN MODEL OVER VO-LUONG AND MASSEL (2006) DATA (SUZUKI ET AL, 2011B)

1.1.7 DRAG COEFFICIENT

The vegetation's drag coefficient is often used as a calibration parameter to obtain model results that compare favourably with field observations. However, research has shown that this drag coefficient is not constant, but can vary depending on different variables. From general flow theory around cylinders, the Reynolds number can be found to influence the drag coefficient (e.g. Dennis and Chang 1970, Son and Hanratty 1968). When looking more specifically at drag experienced by vegetation under wave conditions, an adaptation in the Reynolds number has been proposed by Mazda et al (1997b), including vegetation characteristics in the Reynolds number, which they showed to have more correlation with the drag coefficient. Another influencing variable was presented by Mendez and Losada (2004), showing the influence of the Keulegan-Carpenter number on the drag coefficient. Contrary to the standard Reynolds number, this Keulegan-Carpenter number includes the vegetation diameter. Other studies by for example Tanino and Nepf (2008), showed a relation between relative spacing of the vegetation elements

and the drag coefficient. This indicates that vegetation density might also influence the drag coefficient.

Considering these relations found in literature, many variables are shown to be influencing the drag coefficient. These include both wave characteristics and vegetation characteristics. Hence, the calibration of a fixed value for the drag coefficient based on set of field data, seems not very helpful for the prediction of wave attenuation in mangroves of a different constituency or under different conditions.

1.2 RESEARCH OBJECTIVES

Although some relations have been shown between the drag coefficient and both vegetation characteristics and wave characteristics, it remains unclear which and to what extent vegetation and wave parameters determine the drag coefficient. Currently, when trying to model the wave attenuation in mangroves for a certain location, field tests are needed to acquire data from which a drag coefficient can be derived. Acquiring this data is a time consuming and expensive process.

In order to assess the wave attenuation by different mangrove forests, a wave propagation model is required that predicts the vegetation effects for a certain area without doing extensive field studies. The missing link between the current models and applicability to a random mangrove forest is the drag coefficient. Providing a better parameterization of this drag coefficient, based on vegetation parameters and wave conditions, will improve the general applicability of the vegetation module of the SWAN model.

Considering the above, the following main research objective has been specified for this Master's thesis:

Derive and validate a predictive relationship for the drag coefficient based on vegetation and wave characteristics, by using field observations and a numerical wave model.

Based on this main research objective, several research questions have been defined that need to be answered in order to reach this goal.

1 How to interpret wave attenuation observed in mangroves and to obtain drag coefficients from these field data?

1.1 To what extent can bottom friction, explain the observed wave energy losses in the field data?

1.2 What vegetation drag coefficients are corresponding to the observed energy losses in the field data?

2 How can the drag coefficient be parameterized based on environmental parameters such as wave conditions and vegetation characteristics?

2.1 What parameters are influencing the drag coefficient?

2.2 What relations between the drag coefficient and environmental parameters can be extracted from the field data?

2.3 How can these environmental parameters be parameterized into a new formulation of the drag coefficient?

3 How does this new formulation for the drag coefficient perform in a numerical model?

3.1 How does the adapted model, with the implementation of the new parameterization, perform when simulating the observed field conditions, compared to the current SWAN model?

1.3 RESEARCH APPROACH

The research approach for this thesis is described for each sub question separately within this chapter.

Question 1.1: In order to determine to what extent bottom friction can describe the energy losses observed in the field data, a simple one-dimensional SWAN model will be used. For each transect, only average data will be used in this process in order to clearly show the contribution of known processes, and the remaining energy losses which thus are attributed to the vegetation.

Question 1.2: In order to derive the drag coefficients which are corresponding to the observed wave energy losses, a database with all available data will be created. A calibration process will be performed with this database, resolving the representative drag coefficients by repeatedly running the SWAN model. This calibration will be done for each data burst, for each pair of consecutive sensors with available data.

Question 2.1: A literature study will be undertaken to determine what parameters are possibly influencing the drag coefficient. An additional quick first exploration of the obtained drag coefficients in combination with the observed field data will be performed as well. The combination of these two results in a list of variables, and when known, the type of relation they have with the drag coefficient.

Question 2.2: For each of the variables determined at question 2.1, the relevant data will be extracted from the database, and will be correlated with the drag coefficient through a fitting procedure using Matlab. The type of relation the data will be fitted to, will be based on information from literature and on the observed trends in the data.

Question 2.3: To construct a proper parameterization of the drag coefficient, a multi variable analysis will be performed. The input variables and relations will be based on the results of question 2.1 and 2.2. Several approaches will be used, resulting in a range of possible parameterizations. These will then be analysed and assessed in order to select the best formulation for the drag coefficient.

Question 3.1: After implementing the new formulation of the drag coefficient and running the model for all field data, the performance of the new model will be analysed. Thereto, the observed and simulated energy dissipation over a transect, from the first to the last available sensor, will be compared. This will be compared as well to a baseline score determined by the performance of the original model with a constant drag coefficient for each transect. The dataset used here, will be the same dataset as used before. No separate data is available for validation.

1.4 REPORT STRUCTURE

The structure of this report mainly follows the specified research questions. A flow diagram showing the research questions and the corresponding chapters of this report is presented in figure 6.

Chapter two will present the data used in this study, including an analysis of the wave attenuation observed in this data. The chapter will start with a general introduction of the available data, with information about the data itself and the locations and manner in which the data was acquired. Next, general trends in the data will be investigated to see whether these are in line with the expectations. Also, subsets of the data will be analysed to check for consistency and possible unknown effects or errors in the data. Furthermore this chapter will answer question 1.1, by seeing to what extend bottom friction on itself can represent the energy losses witnessed.

After the exploration of the data, chapter three describes the process of determining the drag coefficients from this data. Furthermore, this chapter will provide an overview of the drag coefficients derived from the data.

In chapter four, literature will be used in order to construct a list of variables that might possibly influence the drag coefficient. This list is used in chapter five in order to find a parameterization for the drag coefficient. In chapter six, this parameterization will then be validated.

The report will end with a discussion, conclusions, and recommendations for further investigations into the subject.

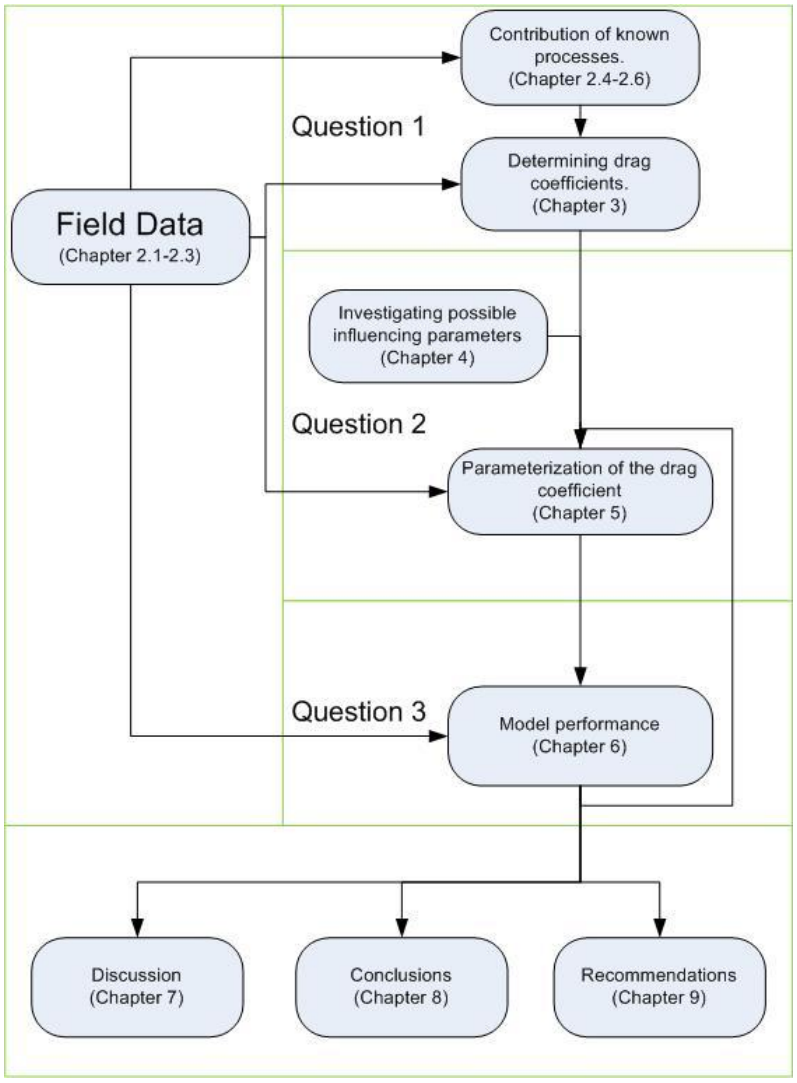

FIGURE 6 RESEARCH FLOWCHART

2 DATA EXPLORATION

To fulfil the aims of this thesis, field data is needed, including both vegetation characteristics and wave data. Field data acquired by Horstman et al. (2012) and pre-processed by Narra (2012), are used. This chapter will look both at the acquiring of this data as well as the quality of the data itself and the processes observed in the basic data.

First, this chapter summarizes how the data was collected. Secondly, the data itself will be introduced and visualized. Thirdly, the quality of the available data will be investigated. Next, an estimation will be made to see how much of the energy dissipation can be attributed to wave-mangrove interaction. Finally, spectral differences in wave attenuation will be discussed.

2.1 DATA DESCRIPTION

The data used for this thesis is a set of field data on wave attenuation in mangroves, which has been acquired by Horstman et al. (2012)/Horstman (2014) at two study sites, situated at the coast of Trang province in Thailand. These locations have been selected by Horstman (2014) because of the pristine condition of the mangroves in this region, a high vegetation diversity and a characteristic gradient in forest vegetation.

Two wave transects were selected, based on vegetation characteristics, positioning, and practical reasons. Both transects have multiple zones of vegetation, with either Avicennia or Rhizophora as the dominant species. Examples of these species can be found in figure 7. The locations and positioning of these transects are presented in figure 8. Although both transects show undisturbed mangroves, there are significant differences between the sites as well. The first transect, located in the Kantang district, is exposed to open sea, while the second transect, located in the Palian district, is situated at the side of a river estuary. Furthermore, there is a difference in the slopes between the two transects. And last, there is a difference in mangrove densities.

FIGURE 7 AVICENNIA AND RHIZOPHORA TREES (HORSTMAN ET AL., 2012)

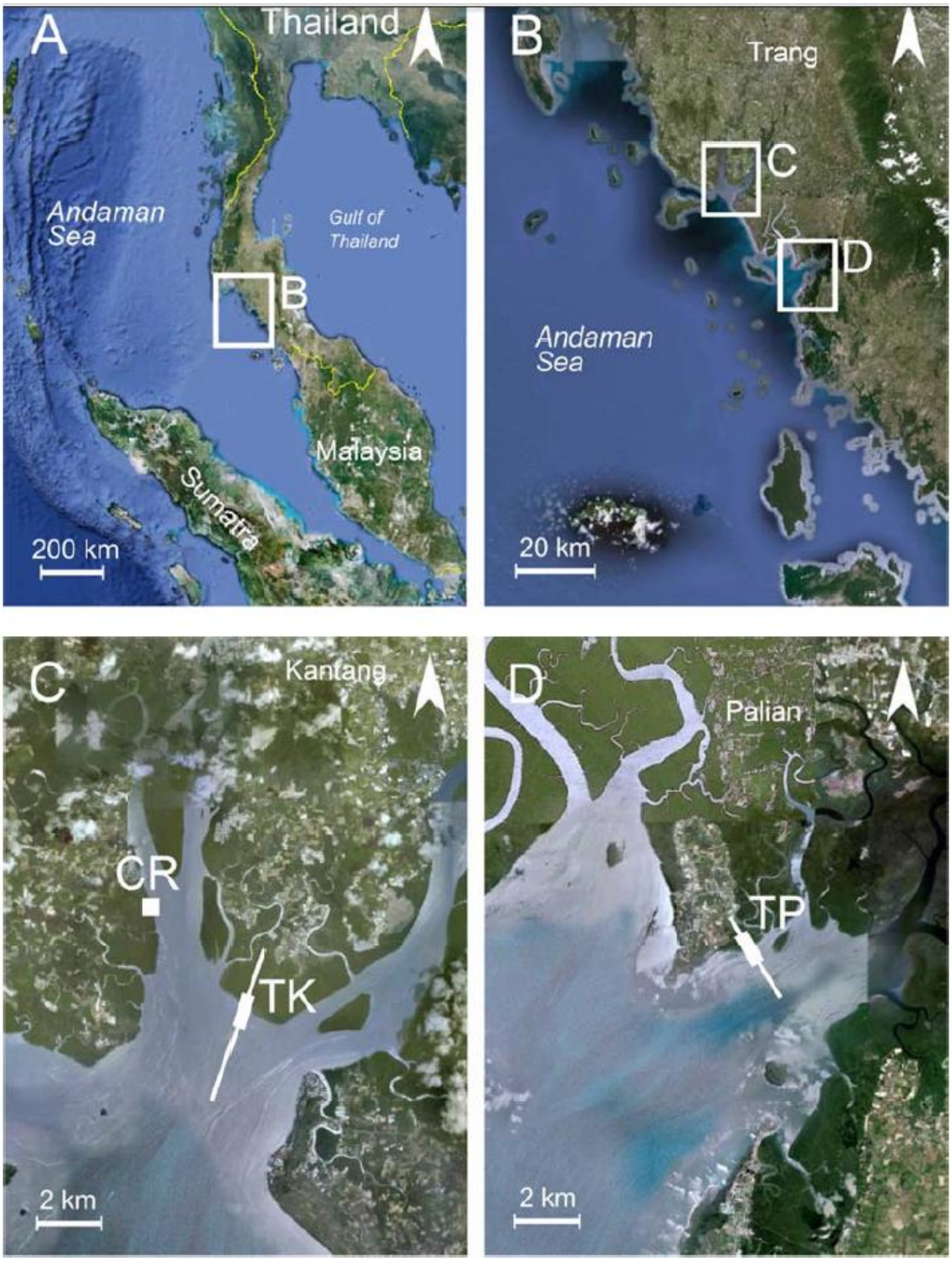

FIGURE 8 POSITIONING OF THE TWO WAVE TRANSECTS (HORSTMAN ET AL., 2012)

The Kantang transect, as measured by Horstman et al. (2012), has a total length of 532.3 metre in which a height difference of 1.7 metre is observed. The whole transect is submerged during spring high tides and is exposed during spring low tide.

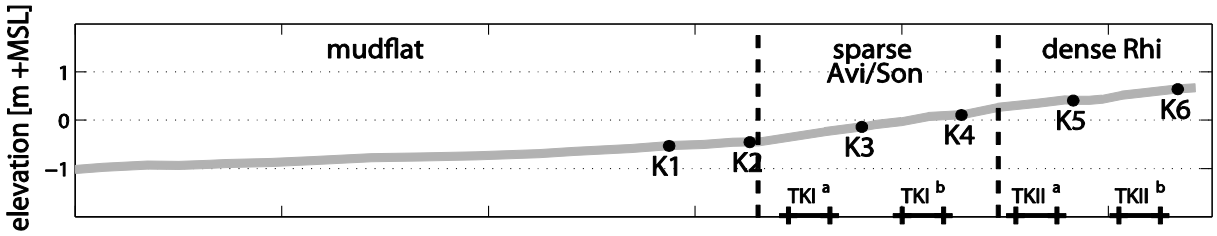

FIGURE 9 TOPOGRAPHY, VEGETATION ZONES AND SENSOR LOCATION ALONG THE KANTANG TRANSECT (HORSTMAN, 2014)

The transect can be divided in three zones (see figure 9): a mudflat, an Avicennia and Sonneratia zone with relatively sparse vegetation and a Rhizophora zone with dense vegetation. These zones with their characteristics can be found in table 2.

TABLE 2 ZONES OF THE KANTANG TRANSECT (ADAPTED FROM NARRA 2012)

Zone	Elevation change (m)	Length (m)	Slope (%)	Vegetation Density (‰)
Mudflat	0.58	327.44	0.18	0
Avicennia and Sonneratia	0.56	104.80	0.53	4.6-4.8
Rhizophora	0.56	100.03	0.56	6.0-10.4

The Palian transect is slightly shorter than the Kantang transect, measuring 493.7 metre. Even though it is shorter, the elevation difference, measuring 3 metre at this transect, is considerably larger. Again the whole transect is submerged at spring high tide and completely exposed at spring low tide.

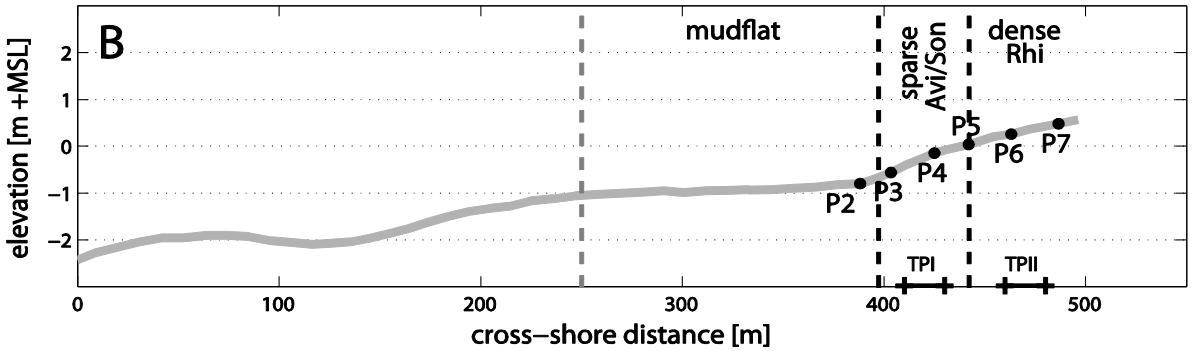

FIGURE 10 TOPOGRAPHY, VEGETATION ZONES AND SENSOR LOCATION ALONG THE PALIAN TRANSECT (HORSTMAN, 2014)

This transect shows the same zones as seen in the Kantang transect (figure 10). The zones with their characteristics for the Palian transect can be found in table 3.

TABLE 3 ZONES OF THE PALIAN TRANSECT (ADAPTED FROM NARRA 2012)

Zone	Elevation change (m)	Length (m)	Slope (%)	Vegetation Density (‰)
Mudflat	1.75	397.28	0.44	0
Avicennia and Sonneratia	0.71	43.82	1.62	4.5
Rhizophora	0.54	52.60	1.03	19.9

The vegetation characteristics vary over distance and height for each of these transects. The vegetation has been measured in 5 different layers by Horstman et al.(2012). For the Palian transect this has been measured in 2 zones (Avicennia and Rhizophora zones), while for the Kantang transect 4 zones have been defined (2 Avicennia and 2 Rhizophora zones), which roughly coincide with the partitioning by the sensors. This total vegetation data can be found in table 4 and 5.

TABLE 4 VEGETATION DATA FOR THE PALIAN TRANSECT

	Palian			
Zone	Avicennia		Rhizophora	
Sensor	2-4		4-6	
Height	Number ($400^{-1}m^{-2}$)	Diameter (m)	Number ($400^{-1}m^{-2}$)	Diameter (m)
0-5 cm	298884	0.005	21967	0.029
5-30 cm	4	0.66	21967	0.029
30-75 cm	4	0.57	6392	0.027
75-150 cm	3	0.66	2162	0.036
150-200 cm	3	0.61	1337	0.021

TABLE 5 VEGETATION DATA FOR THE KANTANG TRANSECT

	Kantang							
Zone	Avicennia				Rhizophora			
Sensor	2-3		3-4		4-5		5-6	
Height	Number ($400^{-1}m^{-2}$)	Diameter (m)	Number ($400^{-1}m^{-2}$)	Diameter (m)	Number ($400^{-1}m^{-2}$)	Diameter (m)	Number ($400^{-1}m^{-2}$)	Diameter (m)
0-5 cm	379070	0.005	180675	0.006	100921	0.006	28157	0.013
5-30 cm	190	0.043	195	0.048	6041	0.027	10237	0.024
30-75 cm	190	0.037	231	0.037	2661	0.023	3985	0.026
75-150 cm	190	0.031	171	0.040	1061	0.031	1777	0.027
150-200 cm	190	0.021	189	0.028	223	0.051	361	0.044

Wave conditions have been measured for each of the transects. The wave data were collected by six MacroWave (Coastal Leasing inc.) pressure sensors spaced along the transects. Pressure data were obtained at 10 Hz in bursts of 4096 samples (approximately 7 minutes) at an interval of 20 minutes. At each transect, the sensors have been deployed 3 times, at which the deployment periods vary from approximately one week to one month. The acquired data has been transformed into wave spectra by Narra (2012), which is the input for this thesis. More information about the collection of data is presented by Horstman et al. (2012) and Horstman (2014).

2.2 DATA INTRODUCTION

The field data acquired by Horstman et al.(2012) have been used by Narra (2012) to analyse the relations between mangrove density and wave dissipation. Narra found a positive correlation between vegetation density and energy dissipation over 100 metre distance. Furthermore, he found a negative correlation between water depth and energy dissipation. However, he also shows this relation differs per zone, and the variation in the data makes the uncertainty of the conclusions quite significant. All in all though, when comparing with previous studies, Narra concludes that the data shows similar trends.

Narra showed a clear decrease of energy for both transects when considering the average data (figure 11). However, one exception can be seen in sensor 4 for the Palian transect.

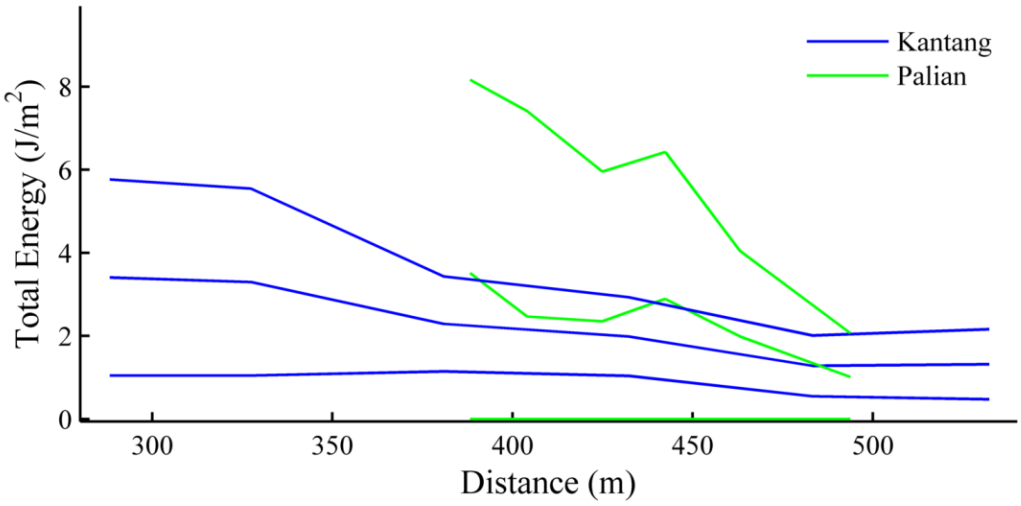

FIGURE 11 WAVE ENERGY OVER THE TRANSECTS (NARRA 2012) CENTRAL LINES SHOWING THE AVARAGE VALUES WHILE THE UPPER EN LOWER LINE REPRESENT THE STANDARD DEVIATION

From the raw data it is clear the measurements have been taken place in a wide range of conditions. For example the significant wave heights observed at the first sensor range from 1 to 43 centimetres for the Palian transect and 1 to 32 centimetres for the Kantang transect. The experienced peak periods seen for the transects do also vary. Peak periods range from 1.5 to around 18 seconds for both transects. An overview of the main statistics of the data as determined by Narra (2012) can be found in appendix II.

In the average wave energy spectra over a complete deployment of the sensors though, some differences can be observed between the transects (see figure 12 and 13).

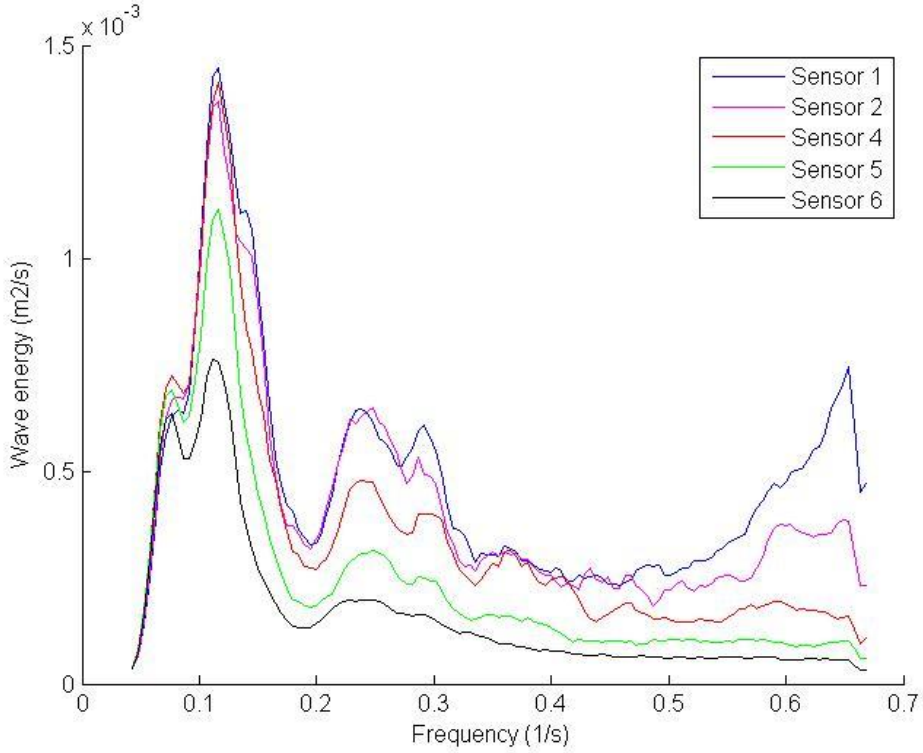

FIGURE 12 WAVE ENERGY SPECTRA AT THE PALIAN TRANSECT (MEASUREMENT 1)

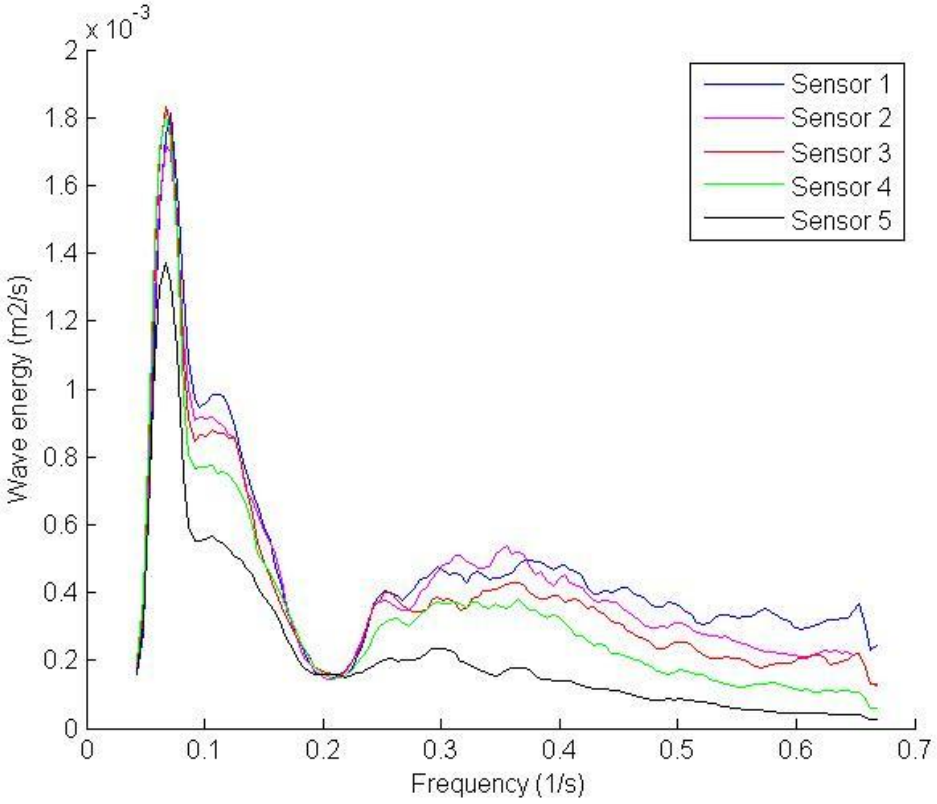

FIGURE 13 WAVE ENERGY SPECTRA AT THE KANTANG TRANSECT (MEASUREMENT 1)

The dominant waves at the Kantang transect are visible at a frequency of around 0.08 Hz. This is equivalent to a wave period of 12.5 seconds. For the Palian transect however the dominant

waves are visible at around 0.12 Hz, which is equivalent to a period of about 8.3 seconds. Furthermore, at the Palian transect an energy peak can be seen at very short waves (0.65 Hz). These differences in wave energy density spectra are most likely caused by the positioning of the transects.

2.3 DATA QUALITY

To get an initial idea of the quality of the data (and especially the variation within the data), bottom friction factors have been determined with Matlab, which represents the observed energy dissipation between two consecutive sensors. The determination of these friction factors is based on the bottom friction approach as introduced before, with an iterative process in which the friction factor is calibrated based on the energy calculated for the next sensor, compared to the measured energy at this sensor. An example of the results of such a run is plotted in figure 14.

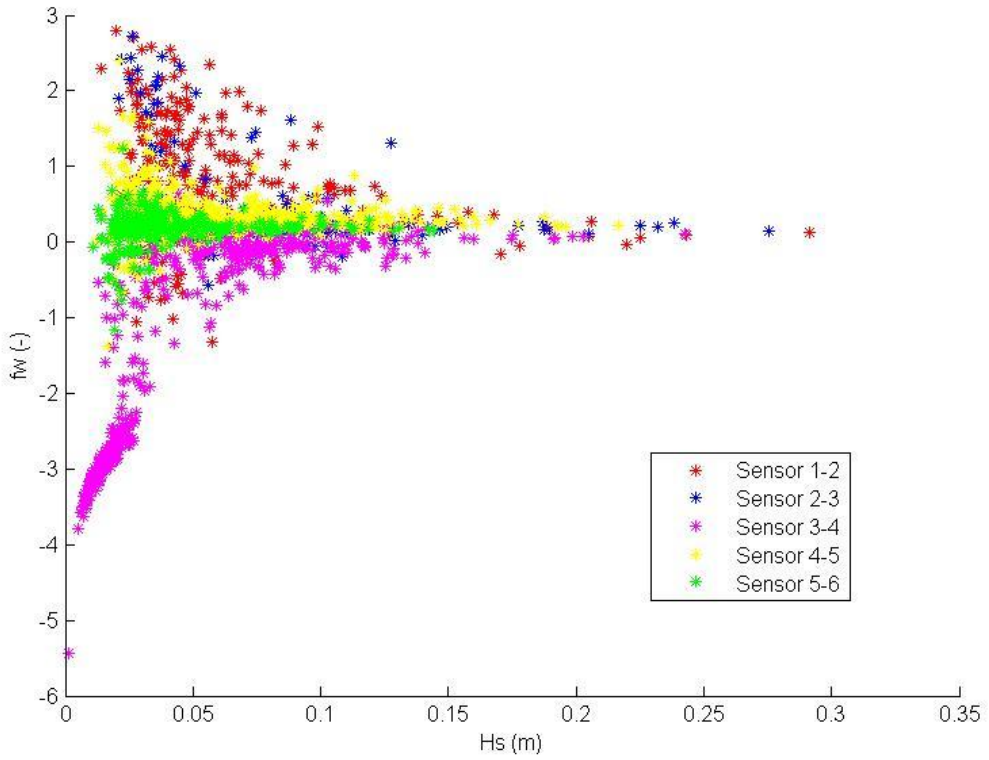

FIGURE 14 FRICTION FACTOR VS SIGNIFICANT WAVE HEIGHT FROM FIELD DATA

These plots show that the variation in friction factors is large and some sensors might be erroneous, resulting in negative friction factors. The variation can be explained easily by accuracy of the sensors used to measure the wave conditions. The accuracy of these sensors is only about 1 cm, thus at wave heights of 5 centimetres, there can be an error of 20% in the measured wave heights. For small energy losses between two sensors, these losses can easily turn into energy gains with this error. Even though lots of the scatter in this plot can be contributed to such sensor inaccuracy there are some data points which have been investigated further. This resulted in the identification of a faulty sensor in one of the measurements at the Palian transect (sensor 3 of measurement 2). This sensor (though working), is continuously outputting energy values which are too low, resulting in highly negative friction factors. This is especially visible at low wave heights.

Another striking sensor is sensor 3 at the last measurement of the Palian transect. This sensor as well seems to give low values compared to the surrounding sensors. However the differences are not significant enough to conclude this sensor is not trustworthy. The observed low energies might just as well be caused by some other effects such as wave reflection.

For the first case, in which the defect of the sensor is certain, the points have been removed from the dataset. For the second case however, where the certainty of the sensor defect cannot be proved, the data has been kept for now, and can be filtered out if necessary in further steps. More information about the faulty sensors and the most likely cause of the errors can be found in appendix III.

2.4 MANGROVE CONTRIBUTION

It is important to validate, whether mangroves have had influences in this dataset, since this influence is essential for the usability of this dataset. A first estimate of the contribution of mangroves to wave dissipation is obtained by running SWAN without vegetation and compare the computed wave heights with observations. The SWAN runs have been done both with and without bottom friction implemented.

In order to make the calculations, the topography of the transects has been inputted in SWAN. Since calculation times for these single runs will not be very important, no efforts have been made to optimize the model. Simply it is chosen to use a 10 centimetre grid size for the calculation, which should be more than sufficient for these runs. The output locations for data are the known locations of the sensors.

The average significant wave height has been determined from the datasets for each of the sensors. The average significant wave height of the first sensor of each transect serves as input for the SWAN model. Rather than determining the complete average wave spectrum, a JONSWAP (Hasselman et al., 1973) spectrum is assumed for the wave spectrum. The JONSWAP spectrum is chosen due to the relative resemblance with the data. Using this spectrum eliminates the need for defining a complete spectral input and simplifies the implementation in SWAN.

Bottom friction is implemented in SWAN according to the formulation of Madsen et al. (1988). Since no exact measurements have been done concerning the bottom patterns the equivalent roughness length (also known as Nikuradse height), had to be estimated. In literature, for bottom friction a Manning coefficient is often used. Typical values for this Manning coefficient in mangroves are 0.02-0.03 (e.g. Yanagisawa et al., 2009). When calculating this back to Nikuradse height, this is in the range of 2-20 cm. Since from the field observations the bottom has been observed to be relatively flat, and the sediment to be very fine, it is likely that the Nikuradse height is at the high low of this range. Furthermore, considering the low water depths and flow velocity, this 20 centimetre roughness height is unlikely. Because of these arguments, a Manning coefficient of 0.02 is implementation in this calculation.

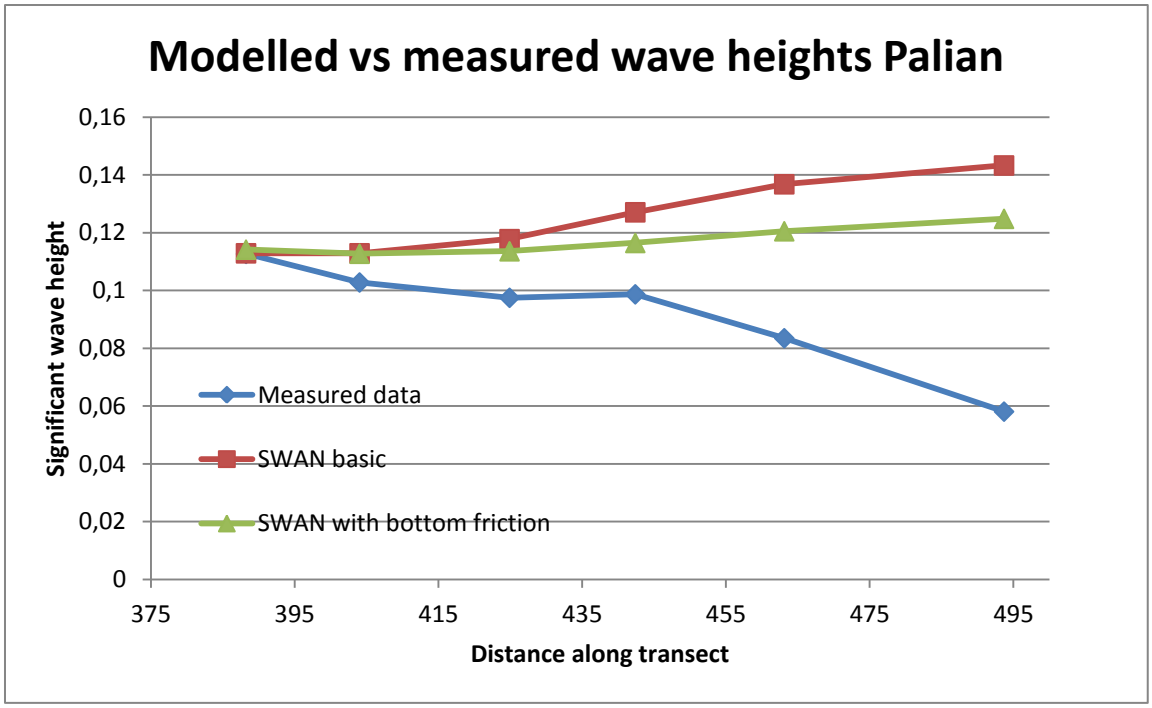

FIGURE 15 MODELLED VS. MEASURED WAVE HEIGHTS FOR THE PALIAN TRANSECT

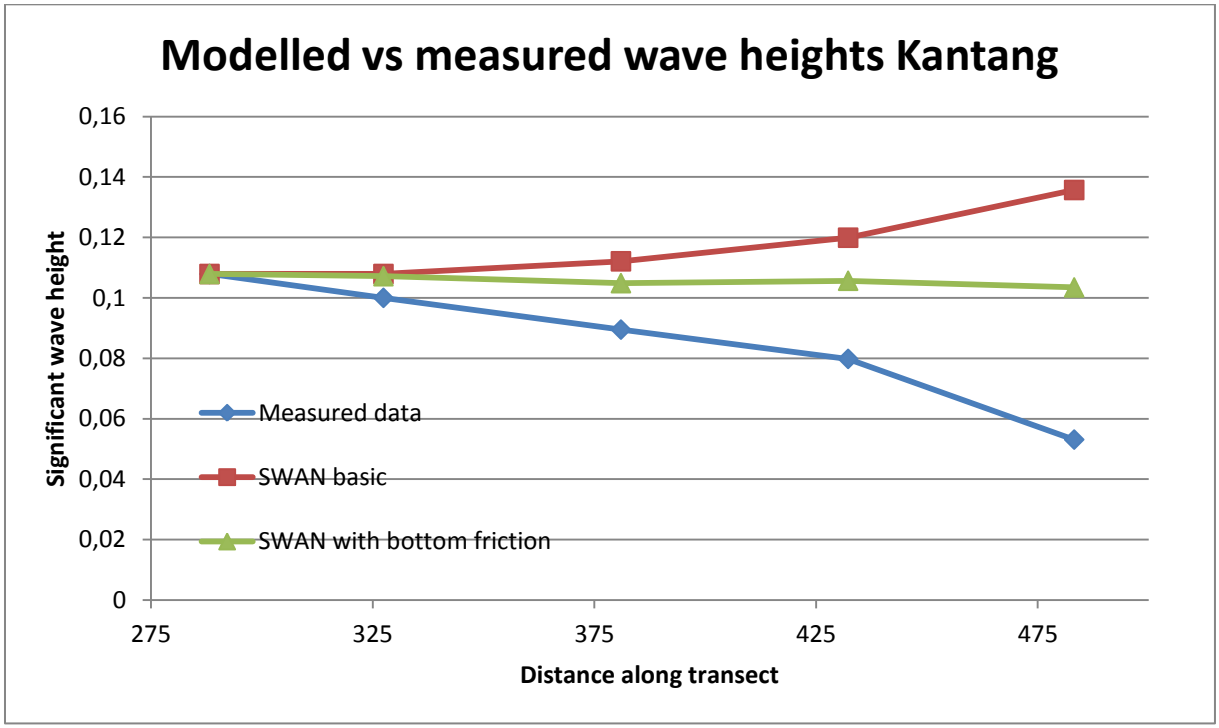

FIGURE 16 MODELLED VS. MEASURED WAVE HEIGHTS FOR THE KANTANG TRANSECT

For both cases, the observed wave attenuation was greater than the wave attenuation calculated with any of the model setups (Figure 15, Figure 16). This indicates that mangroves significantly add to wave attenuation in these data sets. Especially in the Palian transect, there are clear effects between sensor 4 to 6 (the last three sensors). This area (which has the highest mangrove densities found in these measurements), shows a sharp decrease in wave height from

the sensor data, while the modelled datasets cannot predict this. These effects must therefore be caused by the presence of the mangroves.

2.5 SPECTRAL DIFFERENCES IN WAVE ATTENUATION

In the previous analysis only the significant wave height and the corresponding frequency have been used. However, wave dissipation might vary over wave frequencies. To check whether this is the case, the percentage of energy loss between consecutive sensors has been calculated for each frequency band and plotted (see figure 21).

As expected, in general the energy losses between sensors 4-5 and 5-6 (high density mangroves) are higher than for the other two. Another clear trend which can be observed, is that more dissipation takes place at the higher frequencies (shorter waves). For these short waves, the influence of mangroves seems to become negligible, most of these waves are damped over the mudflat before even reaching the mangroves. The influence of the mangroves itself is most visible at the frequencies below 0.5 Hz. For the longest waves, dissipation seems to decrease rapidly, showing almost no energy losses in dense mangroves for waves at 0.05 Hz, and energy gains at this frequency for the mudflat and low density mangroves.

From this figure the preliminary conclusion would be that the influence of mangroves varies over the frequency bands. However, since only the total energy loss is considered, which also includes contributions of other processes (e.g. bottom friction), the spectral differences can in theory as well be caused by these other processes.

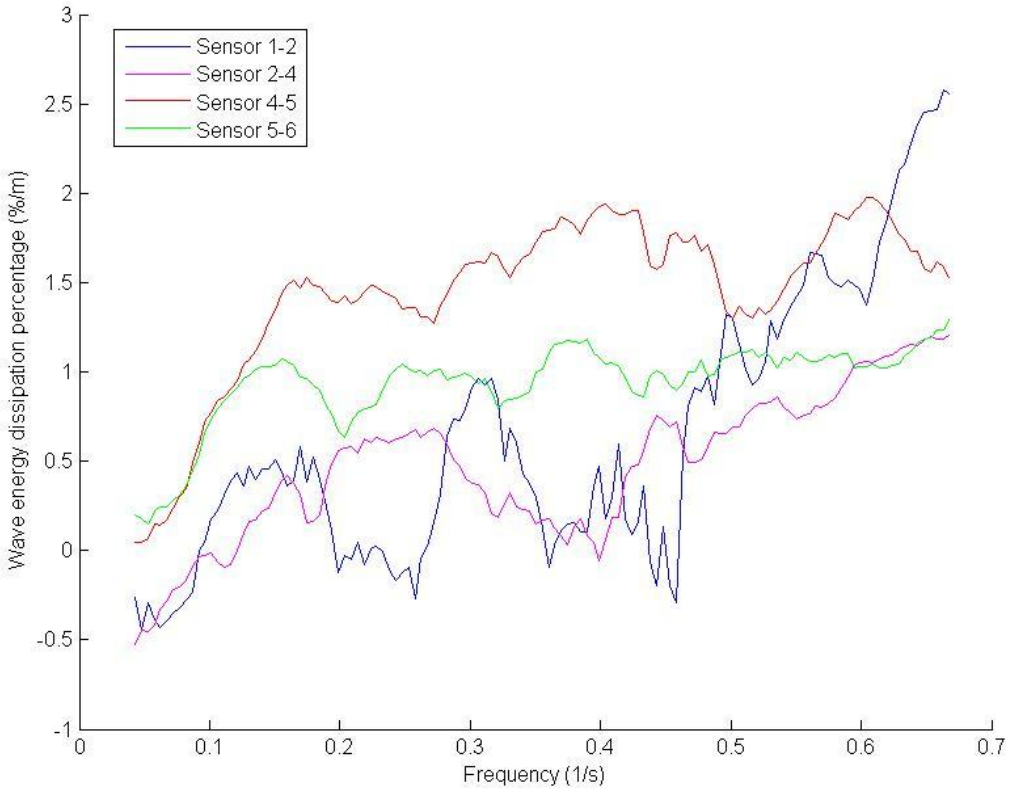

FIGURE 17 DISSIPATION PERCENTAGE SPECTRUM PALIAN TRANSECT

2.6 CONCLUSIONS

The available data, clearly reveal wave dissipation due to mangroves. The total wave attenuation cannot be modelled by the SWAN model without including wave-mangrove interaction. From the effects over the total wave spectrum, mangroves seem to have a different effect at different wave lengths. This however cannot be proven by this data only, so further investigations therein can be done when evaluating the actual drag coefficients.

3 DETERMINATION OF THE DRAG COEFFICIENTS

Based on the wave attenuation observed in the field, the SWAN software can be used to resolve the required drag coefficient to simulate the observed conditions. This chapter focuses on the process of this determination and describes the difficulties, and simplifications in the process. In order to determine the drag coefficients, both transects have been implemented in SWAN. This chapter starts with the description of this implementation. Next, the criteria for calibration of the drag coefficient are discussed. Last, the resulting drag coefficients will be presented.

3.1 IMPLEMENTATION IN SWAN

For the implementation of the transects in SWAN and the ability to repeatedly run SWAN calculations, Matlab is used. All the data are inserted into a database with a separate entry for each burst. For each set of consecutive sensors a separate simulation will be carried out. This means that for a single burst up to 5 separate simulations can be done, depending on the number of available sensors.

The calculation grid for the model is based on the locations of the sensors. In order to limit calculation times the length of the calculation grid is 10 points, which are evenly spread over the distance between every pair of consecutive sensors. On average this will result in a 2 metre distance between two grid points along the Palian transect and a 5 metre distance between the grid points along the Kantang transect. The bottom elevation is calculated for the corresponding grid points by interpolation of the available bottom level data.

The input spectrum for the SWAN calculation is determined by the wave data obtained by the most seaward wave sensor. It is assumed that the waves are propagating perpendicular to the coast. Wave spreading is ignored in the calculations.

Two energy dissipation methods can be used in this model. These are bottom friction and vegetation losses. However when trying to combine these losses in a single run, some simplifications in the SWAN model bring in some trouble. For the calculation of the energy dissipation by bottom friction the near bottom orbital velocity is used, which is determined based on a standard logarithmic distribution of orbital velocity over depth. The vegetation in the SWAN model is only accounting for a total energy loss, but does not affect the logarithmic distribution of this orbital velocity. In reality though, due to the high vegetation densities near bottom, the orbital velocity pattern is not following this logarithmic distribution. Near bottom the orbital velocity can be considerably lower. This makes the SWAN model can highly overestimate the bottom friction taking place within the mangroves. For this reason it is chosen not to implement bottom friction within the SWAN model, when vegetation is present.

The vegetation data implemented in SWAN is obtained from the data as well. The vegetation data is implemented in the 5 available layers (0-5 cm, 5-30 cm, 30-75 cm, 75-150 cm and 150+ cm).

The drag coefficient is the calibration parameter in these runs. Since it can be assigned a different value for the different layers, in theory there are 5 variables to be calibrated. Looking at literature, it was noted before that Mendez and Losada (2004) showed the influence of the KC number on the drag coefficient. Considering that the KC number contains the vegetation diameter, it is clear that the KC number, and accordingly the drag coefficient, will change over the different vegetation layers.

However, with only one known value of the energy dissipation, determining 5 different variables for the drag coefficients can in theory take an endless number of combination of values. In order to prevent this, the drag coefficient is assumed constant over all the layers.

The SWAN model was run for each data burst and for all sensor pairs, simulating the wave height at the location of the second sensor of each input pair. The output data can therefore be compared to the measured data at this sensor, which can be used to actually calibrate the drag coefficient.

3.2 CALIBRATION CRITERIA

The final aim of the model is to calibrate the drag coefficient. Based on values found in literature, which go up to a drag coefficient value of 15, under standard conditions, the calibration range for the drag coefficient has been set to 0- 100. The upper limit has been set this high, since in some extreme cases, drag coefficients can turn out higher than found in literature. Negative drag coefficients are ignored since they are not physically possible. They can either occur with problems in the data, or when other processes such as wind are influencing the data.

For the calibration, the total wave energy (Etot) is calculated, both from the model output, and from the measured data. This total wave energy is the sum of the bandwidth multiplied with the energy for each wave band (with E_f the energy for frequency band f , and Δf the width of the frequency band):

$$Etot = \sum E_f * \Delta f \qquad (3.1)$$

The model is iteratively run until the differences between observed and computed total energy is less than a certain threshold. When the difference between the computed and measured wave energy is lower than this threshold, the input drag coefficient will be considered the drag coefficient experienced in the field data. When the difference is larger than the threshold the midsection method is used to determine the new bandwidth for the drag coefficient (thus practically halving the bandwidth with each calculation step). The calibration threshold for the wave energy error between observed and calculated energy for a sensor, is set at a value of 10^{-7} J/m^2. This low limit is based on the measured energy values which go as low as $6*10^{-3}$ J/m^2. For these energy values the expected energy loss is low, and the proportion of this which can be assigned to mangroves even lower. This is estimated to be around 10^{-4} J/m^2 (or 1/60 of the total energy) in some extreme cases. Combining this with a required accuracy for the drag coefficient of about 0.1%, the given limit is obtained. In the end this limit can be considered very low though, and it can be questioned whether there is any reason for using such a low limit on field data which can never be this accurate. On the other hand, using such a low limit ensures that no extra inaccuracies are introduced in the dataset due to this transformation. Any inaccuracy in the data can be contributed to the measurements and unknown effects rather than the calculations.

A maximum number of iterations has been set, in order to prevent the model from running in an endless loop. This number of iterations has been set to 20. After these 20 iterations the remaining bandwidth for the drag coefficient is only 10^{-4}. Looking at expected drag coefficients at a value of about 0.5, combined with the observed variation in the data, a higher accuracy in the drag coefficient will not be of any use.

A schematization of the input, iteration process and output is shown in figure 18.

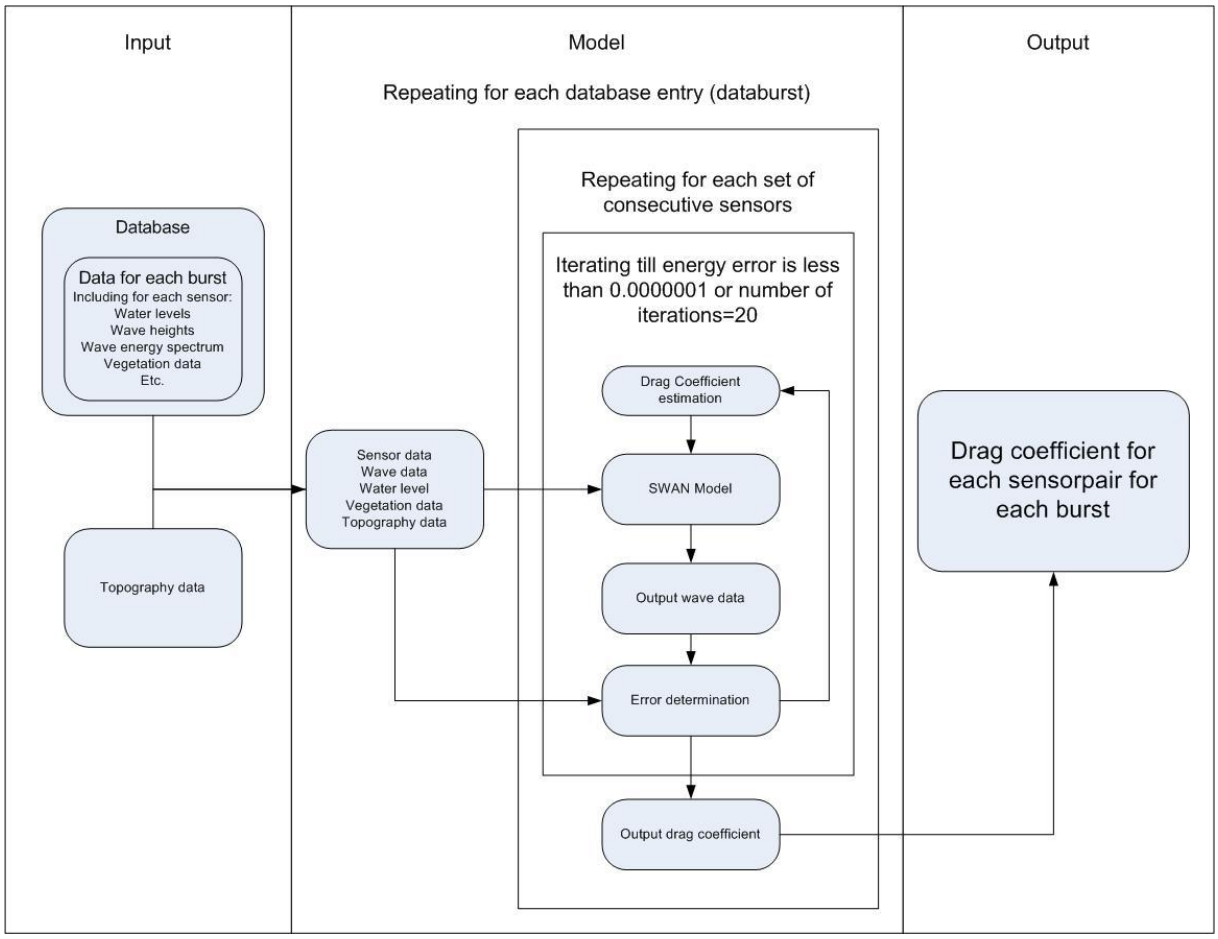

FIGURE 18 SCHEMATIZATION OF THE CALIBRATION PROCESS

3.3 RESULTS

In order to get a usable set of drag coefficients the extremes have to be filtered out. Any drag coefficient value which is at the set limits should be removed from the dataset. Considering the calibration procedure, C_D values below $0.5^{20} * 100$ (or about 10^{-4}), or C_D values above $100 - (0.5^{20} * 100) \approx 100$ are not possible. Any C_D values outputted at this values are therefore considered to end up outside the set limits. For the Kantang transects there are 270 drag coefficient values which are in the low limit of the simulation and 0 in the high limit of the simulation. For the Palian transect this were 602 in the low limit and 2 in the high limit. These values are removed from the data leaving a total of 11363 entries.

The average drag coefficients between sensors at the different transects, are in line with the values found in literature, with average C_D values between 2 and 4 (see table 6 and 7). The standard deviations though, are considerably high. When comparing the Kantang and Palian transects, the average C_D values follow the same trend, while the standard deviations at the Kantang transect are considerably higher.

TABLE 6 AVERAGE DRAG COEFFICIENTS AND STANDARD DEVIATIONS FOR THE FIELD DATA AT THE PALIAN TRANSECT

Palian	Average C_D	Standard deviation
Sensor 2-3	4.0	4.1
Sensor 3-4	4.0	4.1
Sensor 4-5	0.84	0.52
Sensor 5-6	0.59	0.34

TABLE 7 AVERAGE DRAG COEFFICIENTS AND STANDARD DEVIATIONS FOR THE FIELD DATA AT THE KANTANG TRANSECT

Kantang	Average C_D	Standard deviation
Sensor 2-3	2.4	2.4
Sensor 3-4	4.2	2.6
Sensor 4-5	3.2	1.6
Sensor 5-6	1.6	1.3

For both transects a decrease in C_D is observed with increasing densities, indicating some effects of sheltering. The only exception in this being sensor 2-3 at the Kantang transect which shows lower drag coefficients than sensor 3-4. This might for example be explained due to the differences in wave conditions.

4 DRAG COEFFICIENT

The first stage of investigating the parameterization of the drag coefficient is to derive relations between single variables and this drag coefficient. This can be used to identify which variables possibly affect the drag coefficient. In this chapter, these relations will be investigated for a number of variables, determined from literature and theories. The following variables were found to have a possible relation with the drag coefficient:

- Reynolds number
- KC-number
- Vegetation density
- Water depth
- Wave period
- Maximum flow velocity
- Mazda characteristic length scale
- Exposed area

For each of these variables a short description of the variable, and the expected relation are given. For those variables which allow for multiple implementations, a separate chapter is included describing the implementations which are performed and why these implementations have been chosen.

4.1 REYNOLDS NUMBER

From general flow theory around cylinders, the most important variable influencing the drag coefficient is the Reynolds number :

$$Re = \frac{\rho u L_c}{\mu} \qquad (4.1)$$

In this equation, ρ is the fluid density (kg/m^3), u is the flow velocity (m/s), L_c is the characteristic length scale (m) and μ is the dynamic viscosity (kg/ms). Depending on the flow regime, there are several different relations between the Reynolds number and the drag coefficient. For example at low Reynolds numbers, Stokes' law (originally for flow around spheres) shows an inverse relation between the drag coefficient and the Reynolds number. Flemming and Banks (1986), give the following equation for the drag coefficient of flow around spheres at low Reynolds numbers :

$$C_D = \frac{24}{Re} \qquad (4.2)$$

Even though the relation will be slightly different around cylinders, this relation will remain similar.

However at higher Reynolds numbers, different regimes can be found. Roshko (1960), collected data about those different regimes and bundled them in a single plot (see figure 19).

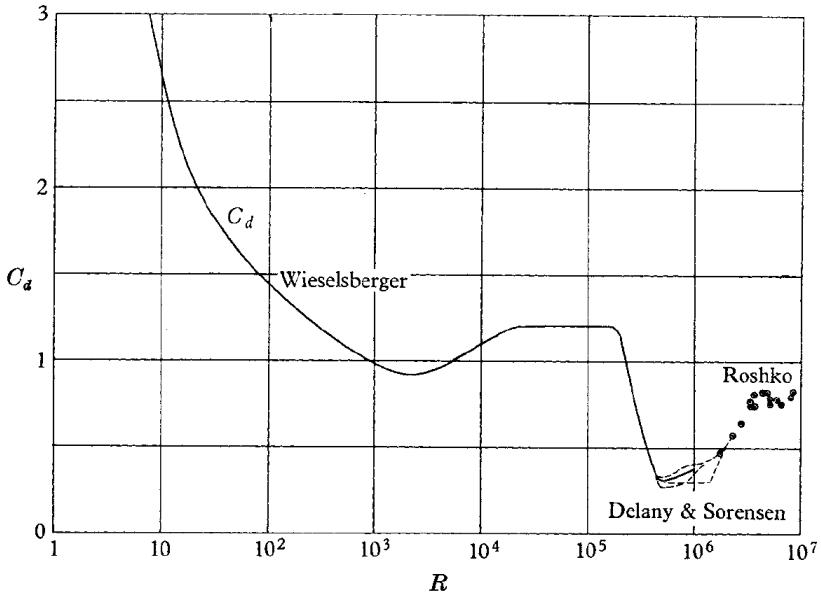

FIGURE 19 DRAG COEFFICIENT VS. REYNOLDS NUMBER, A COLLECTION OF DATA FROM DIFFERENT STUDIES (ADAPTED FROM ROSHKO, 1960)

Mazda et al. (1997b), investigated the relation between the drag coefficient and the Reynolds number for vegetation in general, again showing a clear relation between Reynolds number and drag coefficient. However, in the data from Mazda et al., the drag coefficient seems to be limited to a value of around 15, at low Reynolds numbers, rather than infinity (see figure 20). This might indicate an exponential function rather than a power function, but due to the limited range of this data set (with lowest Reynolds values being around 10^2) this cannot be verified.

These differences in the type of relations between the drag coefficient and the Reynolds number at low Reynolds numbers, show that there currently is no single definition for the drag coefficient as a function of the Reynolds number.

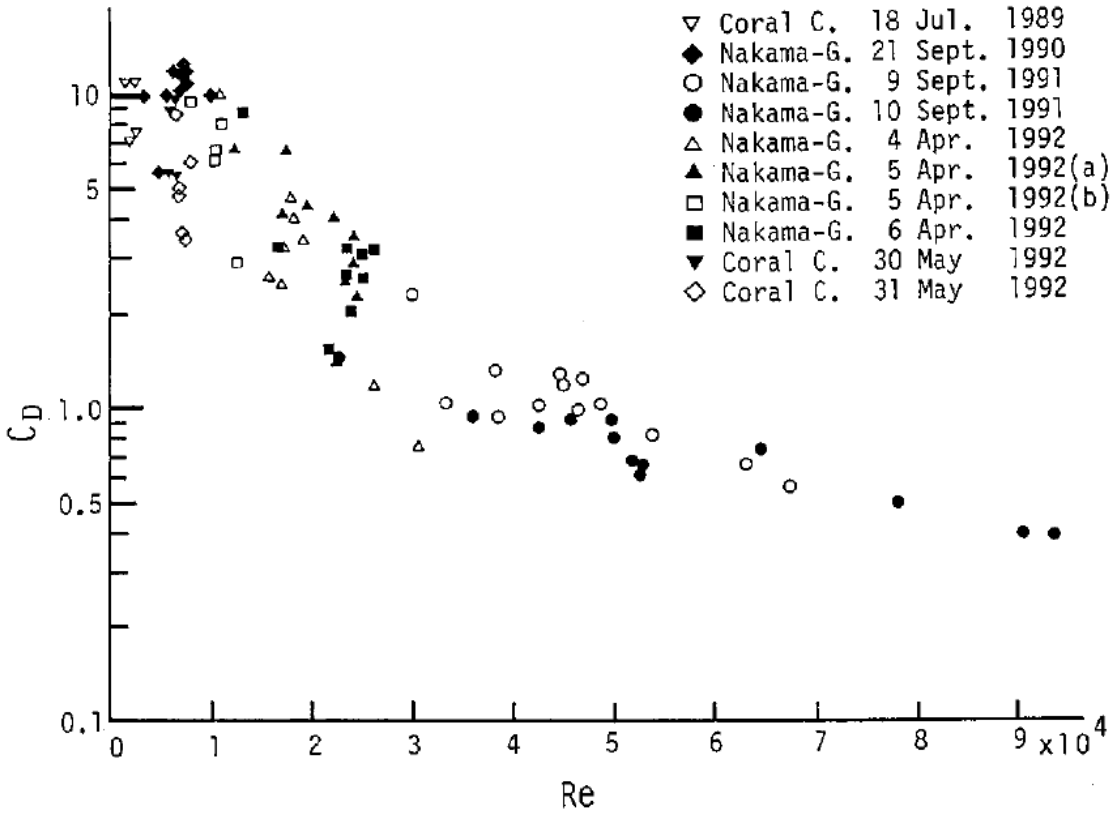

FIGURE 20 DRAG COEFFICIENT VS. REYNOLDS NUMBER (MAZDA ET AL., 1997B)

4.1.1 IMPLEMENTATION

The Reynolds number, as seen before, can be defined by the following equation:

$$Re = \frac{\rho u L_C}{\mu} \qquad (4.3)$$

In general, for oscillatory flow, the characteristic length scale (L_C) in this equation is generally defined as the maximum horizontal movement of a particle under the influence of the wave. This is defined as:

$$L_{max} = \frac{u * T}{\pi} \qquad (4.4)$$

This characteristic length scale includes no vegetation data. For this reason Mazda et al (1997b), came up with a different definition for this characteristic linear dimension:

$$L_E = \frac{(Vc - Vm)}{A_p} \qquad (4.5)$$

In this equation Vc is the control volume (m^3), Vm is the vegetation volume within this control volume (m^3), and A_p is the projected surface area of this vegetation (m^2), perpendicular to the direction of wave propagation. When using this definition, vegetation data is included in the

Reynolds number, thus this might give better results. However, since no other uses of this linear dimension have been found in literature, both definitions will be assessed in this thesis.

4.2 KC-NUMBER

Mendez and Losada (2004), demonstrated the importance of the Keulegan-Carpenter number, especially for the drag coefficient in case of vegetation. The Keulegan-Carpenter number has been introduced by Keulegan and Carpenter (1958), to account for the effects of changing values of drag coefficients with changing flow velocity or size of cylinders in oscillating fluids. The Keulegan-Carpenter number is defined as:

$$KC = \frac{uT}{L_c} \qquad (4.6)$$

In which u is the maximum flow velocity (m/s), T is the period of the oscillation (s) and L_c is the characteristic length scale (m). For cylinders this length scale is generally defined as the diameter.

Mendez and Losada (2004), calculated a bulk drag coefficient and KC values for a total of 115 data points, and obtained a clear relation. They specified the following relation:

$$C_D = 0.47\, e^{-0.052KC} \qquad (4.7)$$

This relation had a 76% correlation according to their calculation.
As can be seen in the plot they made (figure 21), some of their variation was caused by different values of α (the vegetation height relative to the water depth). In order to include this effect they suggested an adaptation to the Keulegan-Carpenter number (Q):

$$Q = \frac{KC}{\alpha^{0.76}} \qquad (4.8)$$

With this adaptation for the KC number the following relation with the drag coefficient was found:

$$C_D = \frac{e^{-0.0138*Q}}{Q^{0.3}} \qquad (4.9)$$

This relation had a correlation of 92% in their data.

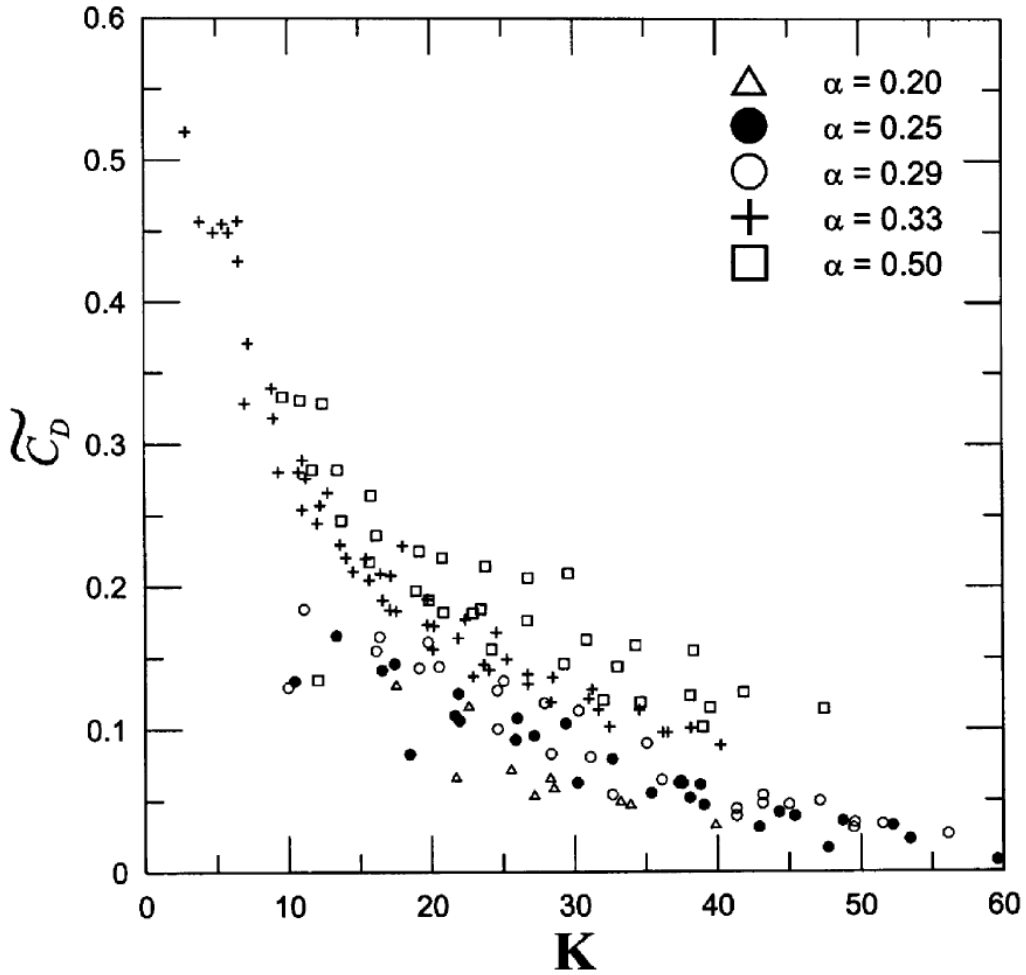

FIGURE 21 DRAG COEFFICIENT VS KEULEGAN CARPENTER NUMBER (MENDEZ AND LOSADA, 2004)

4.2.1 IMPLEMENTATION

As seen before, (Mendez and Losada, 2004) have shown the correlation between the KC number and the drag coefficient.

The period of the oscillation used for calculating the KC number, is the period corresponding to the maximum flow velocity. For this reason the peak period is implemented as the period of the oscillation.

In order to determine the influence of the KC number it is important to decide what vegetation characteristics will be used to compute the KC number. The KC number can differ between different vegetation layers. The main cause of this are the pneumatophores found at some locations. These strongly decrease the average diameter, and therefore give a high KC number.

It is therefore chosen to determine a depth-averaged KC number, which can be done in different ways. Two approaches are used for this thesis. Either the depth-averaged diameter is determined, after which the KC number is calculated as a function of this depth-averaged diameter, or the depth-averaged KC number is calculated as an average of the KC number of the different layers.

When averaging the diameter over the depth the following equations are used:

$$KC = \frac{uT}{Lavg} \qquad (4.11)$$

With:

$$Lavg = \sum_{h=0}^{hmax} L(h) * \frac{\Delta h}{h_{max}} \qquad (4.12)$$

In this equation h_{max} is the measured water depth, L(h) is the diameter of the vegetation layer (m) at height h (m), and Δh is the submerged depth of this vegetation layer (m).

When averaging the KC number over depth the following equation is used:

$$KC = \sum_{h=0}^{hmax} \frac{uT}{L(h)} * \frac{\Delta h}{hmax} \qquad (4.13)$$

Another, third possible implementation of the length scale in the KC number, is the length scale defined by Mazda. This was originally developed for use in the Reynolds number but since it is a representative length scale for vegetation, it might show good performance in the KC number as well. This gives:

$$KC = \frac{uT}{L_E} \qquad (4.14)$$

All three implementations are expected to have different results, and therefore all approaches will be tested to check which one correlates best with the drag coefficient.

4.3 VEGETATION DENSITY

In the Dalrymple et al. (1984) formulation, for wave dissipation by vegetation, vegetation density is used implicitly by the use of the diameter and number of stems per square metre. However, density might also be influencing the drag coefficient, which is part of this general formulation, for example due to sheltering (Tanino and Nepf, 2008).

The density used in this thesis is the depth-averaged density of the submerged vegetation only. This can be defined as follows:

$$\rho_v = \frac{Vm}{Vc} \qquad (4.15)$$

In which ρ_v is the density (-), Vm is the vegetation volume within the control volume (Vc).

What the relation between vegetation density and drag coefficient might look like is unknown, though from the sheltering effect a negative correlation is expected (e.g. lower drag coefficients at higher vegetation densities).

4.4 WATER DEPTH

Water depth has been shown to be correlate with the drag coefficient in different researches (e.g. Brinkman et al., 1997, Mazda et al., 2006). There are many different processes though which

can cause this correlation. In the dataset available for this research for example vegetation density is dependent on the water depth. Another example are the wave characteristics, which are as well related to water depth. Therefore it is unknown what the relation between the drag coefficient and the water depth will look like.

4.5 WAVE PERIOD

In the raw data, there were clear differences in the energy dissipation over different frequency bands (section 2.6). It should be investigated whether these relations are actually caused by the mangroves or not. This can be either investigated through the wave frequency or its inverse: wave period. Since the KC number also includes the wave period, it is chosen to use the wave period as the relating variable, since this will also enable analysing constituents of the KC-number.

For the wave period from the data both the peak period and the average period are defined. Again the peak period will be used, since this is the period corresponding to the waves with the greatest horizontal movement (and thus highest energy losses).

4.6 MAXIMUM FLOW VELOCITY

The maximum orbital flow velocity, as part of the KC number and the Reynolds number, is another variable that should be investigated. Just as the KC number and the Reynolds number, the maximum orbital flow velocity is expected to have a power or exponential relation with the drag coefficient.

4.7 MAZDA LENGTH SCALE

The Mazda characteristic length scale has been previously introduced for usage in the KC-number and the Reynolds number. Since analysing constituents of these numbers is also interesting, the Mazda length scale by itself is added to the list of variables potentially correlating with the drag coefficient. The definition of this Mazda length scale can be found in equation 4.5.

4.8 EXPOSED AREA

Quartel (2007) found a relation between the drag coefficient and the projected cross-sectional area of the underwater obstacles (A) according to the following function:

$$C_D = 0.6 * e^{0.15A} \qquad (4.17)$$

The exposed area of the vegetation is defined as the frontal surface of the vegetation, perpendicular to the dominant flow direction, within a plot of one square metre over the whole water depth. Therefore this variable has a correlation with the water depth itself, increasing the exposed area with an increasing water depth. Furthermore, the Mazda characteristic length scale depends on the exposed area of the vegetation as well.

5 PARAMETERIZATION OF THE DRAG COEFFICIENT

This chapter will focus on the derivation of a general parameterization of the drag coefficient from the field data. The first step in the process concerns single variable relations, between different variables and the drag coefficient. Based on these single variable relations, a multi variable analysis will be performed. Since it is hard to include all variables at once, this multi variable regression analysis will start with combinations of two variables. From there on, the inclusion of additional variables is studied, in order to find out whether the results can be significantly improved. The main focus will be to provide a simple and reliable parameterization for the drag coefficient. Based on this multi variable analysis a number of possible relations will be selected. These possible relations will next be scored on a number of criteria, after which a best parameterization will be selected.

5.1 SINGLE VARIABLE REGRESSION ANALYSIS

Prior to the regression analyses, filters have been applied to remove negative values and outliers: the used data may only contain decreasing energy values in landward direction and all C_D values should be within the set boundaries. This results in 1407 data bursts being used.

For all the relevant variables that were obtained from literature, correlations with the drag coefficient have been tested. This is displayed by the correlation coefficient, which has a value of 1 in case of a perfect positive correlation and a value of -1 for a perfect negative correlation. A value close to 0 means no correlation at all. The significance of the correlation is tested as well and displayed by the P-value. A P-value smaller than 0.05 indicates a significant correlation. Furthermore, for all variables curves have been fitted according to the different relations as found in literature, or as estimated. For each fit the R-squared value has been calculated. This R-squared value describes the amount of variation that can be explained by the fit, compared to simply taking the average value. An R-squared value of 1, represents a perfect fit, while an R-squared value close to 0, indicates the function has almost no added value, compared to simply taking the average. All these values are displayed in the following table, starting with the formulation that represents the variability of the drag coefficients best.

TABLE 8 SINGLE VARIABLE RELATIONS WITH THE DRAG COEFFICIENT

Variable	Relation type	R-squared	Correlation coefficient	P-value
KC-number (Mazda Length scale)	Power	0.39	-0.39	<<0.001
KC-number (Mazda Length scale)	*Exponential + Constant*	0.39	-0.39	<<0.001
Mazda length scale	Polynomial (1st degree)	0.32	0.56	<<0.001
Exposed area	Power	0.31	-0.45	<<0.001
KC-number (Depth-averaged)	Exponential + Constant	0.26	-0.29	<<0.001
KC-number (Depth-averaged)	*Power*	0.24	-0.29	<<0.001
KC-number (L averaged)	Exponential + Constant	0.21	-0.29	<<0.001
Water depth	Polynomial (1st degree)	0.21	0.46	<<0.001
KC-number (L averaged)	*Power*	0.18	-0.29	<<0.001
Vegetation density	Polynomial (1st degree)	0.15	-0.38	<<0.001
Reynolds Mazda	Power	0.051	0.18	<<0.001
Average period	Polynomial (1st degree)	0.044	-0.21	<<0.001
Reynolds number	Power	0.038	-0.10	<<0.001

Maximum flow velocity	Exponential + Constant	0.032	-0.032	0.26
Reynolds number	*Exponential + Constant*	0.014	-0.10	<<0.001
Peak period	Polynomial (1st degree)	0.0014	-0.037	0.19

As can be seen from table 8, the KC-number with Mazda length scale, gives the best representation of the variability of the observed drag coefficient best. However the Mazda length scale on itself as well performs relatively high, just as the exposed area.

5.2 DOUBLE VARIABLE REGRESSION ANALYSIS

For the double variable analysis six primary variables have been selected. These primary variables form the base of any possible regressions. The primary variables for this analysis are:

- KC-number (Mazda length scale)
- KC-number(Depth-averaged)
- Reynolds number
- Reynolds Mazda
- Maximum flow velocity
- Mazda length scale

The two variations of the KC number are, together with the Mazda length scale, the best performing variables. This makes it logical to include those as primary variables. The Reynolds number and Mazda Reynolds number, even though showing a poor fit, are expected to show good relations from literature. This makes it likely their performance can be improved by adding a secondary variable. Lastly the maximum flow velocity, being an important variable in both the KC and Reynolds number, is likely to increase performance as well when adding secondary variables. For the flow velocity this is expected especially because it is already showing an indication of an exponential relation (which is in line with literature).
All these base parameters show some clear common relations. For almost all, either a power or an exponential + constant relation type is found. The only exception is the Mazda length scale, showing a simple linear relation, but this is in essence just a power relation with power 1.

5.2.1 POWER AND EXPONENTIAL REGRESSION FUNCTIONS

Depending on the base function chosen (power or exponential), there are several options to implement a second variable. The standard power function is:

$$a * x^b \qquad (5.1)$$

In this formulation, four possible positions for implementation of a second parameter (y) can be defined: a second variable can be combined with the a, the b or the x in this equation, or it can simply be added to this equation independently. In order to prevent investigating an almost unlimited number of possible equations for including secondary variables, only simple dependent relations (thus influencing an already present variable or parameter) and linear independent relations will be considered in this analysis. These simple dependent relations are; adding, subtracting, multiplication or dividing. Based on this, the relations to be tested can be found in table 9.

TABLE 9 EQUATION IMPLEMENTATIONS USED FOR THE POWER FUNCTION

Equation number	Location	Type	Relation
1	a	+	(a+y)*x^b
2	a	-	(a-y)*x^b
3	a	*	a*y*x^b
4	a	/	a/y*x^b
5	b	+	a*x^(b+y)
6	b	-	a*x^(b-y)
7	b	*	a*x^(b*y)
8	b	/	a*x^(b/y)
9	x	+	a*(x+y)^b
10	x	-	a*(x-y)^b
11	x	*	a*(x*y)^b
12	x	/	a*(x/y)^b
13	linear independent		a*x^b +c*y+d

For the exponential function, a similar list of implementations can be obtained. The exponential function is:

$$a * \exp(b * x) + c \qquad (5.2)$$

Again, implementation of a second variable can take place at a, b and x (where multiplication and division at b and x are identical), and as a linear independent function (merging with c). Table 10 presents the resulting functions for this case.

TABLE 10 EQUATION IMPLEMENTATIONS USED FOR THE EXPONENTIAL FUNCTION

Equation number	Location	Type	Relation
14	a	+	(a+y)*exp(b*x)+c
15	a	-	(a-y)*exp(b*x)+c
16	a	*	(a*y)*exp(b*x)+c
17	a	/	(a/y)*exp(b*x)+c
18	b	+	a*exp((b+y)*x)+c
19	b	-	a*exp((b-y)*x)+c
20	b	*	a*exp(b*y*x)+c
21	b	/	a*exp((b/y)*x)+c
22	x	+	a*exp(b*(x+y))+c
23	x	-	a*exp(b*(x-y))+c
24	linear independant		a*exp(b*x)+c*y+d

It has to be noted that in the dependent equations, adding or subtracting (such as done in functions 1,2, 14 and 15) in most of the cases has no physical meaning and is expected not to show significant improvements in R-squared values. Nonetheless, these functions can have physical meaning, when considering dimensionless variables, and since these functions comply with the predefined requirements for the equations, they are included for completeness.

5.2.2 RESULTS

For each of the primary variables, combinations of all equations and secondary variables are tested and selected on accuracy of the representations. This results in table overviews. The results will be presented in the following sections, for each primary variable separately.

5.2.2.1 KC NUMBER MAZDA LENGTH SCALE

The regression results when using the KC number with Mazda length scale as primary variable are presented in table 11.

TABLE 11 R-SQUARED VALUES OF DOUBLE VARIABLE RESULTS WITH THE KC NUMBER WITH MAZDA LENGTH SCALE BEING THE PRIMARY VARIABLE

	Peak period	Average period	Water depth	Reynolds number	Maximum flow velocity	Reynolds number (Mazda)	Exposed area	Vegetation density	L_E
1	NaN	NaN	0.38	NaN	0.41	NaN	0.09	NaN	0.30
2	NaN	0.10	0.00	NaN	0.35	NaN	0.39	0.26	NaN
3	0.07	0.28	0.41	NaN	0.04	0.01	0.14	0.05	0.42
4	0.02	0.39	0.25	NaN	NaN	NaN	0.42	0.31	0.13
5	NaN	NaN	NaN	NaN	0.35	NaN	0.43	0.35	NaN
6	NaN	NaN	NaN	NaN	0.41	NaN	0.07	NaN	NaN
7	0.07	0.07	0.35	NaN	0.02	NaN	0.13	0.07	0.39
8	0.11	0.31	0.01	0.07	0.10	0.01	0.39	0.15	0.13
9	0.01	0.07	0.14	0.04	0.24	0.05	0.38	0.17	0.32
10	0.01	0.03	0.25	0.04	0.07	0.05	0.15	0.06	0.32
11	0.23	0.40	0.28	0.19	0.21	0.04	0.43	0.36	0.08
12	0.21	0.31	0.42	0.05	0.16	0.24	0.08	0.03	0.43
13	0.39	0.40	0.41	0.40	0.40	0.41	0.40	0.40	0.42
14	0.33	0.37	0.39	0.09	0.39	0.04	0.38	0.38	0.42
15	0.32	0.39	0.38	0.06	0.38	0.04	0.39	0.39	0.34
16	0.23	0.32	0.42	0.24	0.24	0.25	0.28	0.30	0.42
17	0.22	0.39	0.30	0.14	0.19	0.15	0.42	0.34	0.28
18	0.38	0.38	0.39	NaN	0.39	NaN	0.38	0.38	0.39
19	0.38	0.39	0.38	0.07	0.39	0.00	0.39	0.39	0.38
20	0.22	0.40	0.28	0.16	0.20	0.04	0.40	0.37	0.07
21	0.20	0.30	0.40	0.06	0.14	0.21	0.08	0.06	0.40
22	0.06	0.07	0.15	0.04	0.23	0.00	0.38	0.18	0.32
23	0.02	0.03	0.26	0.04	0.15	0.03	0.20	0.13	0.33
24	0.39	0.39	0.40	0.39	0.40	0.41	0.40	0.40	0.42
Max	0.39	0.40	0.42	0.40	0.41	0.41	0.43	0.40	0.43

No matter what secondary variable is added, there always is a small increase of the quality of the representation of the drag coefficient compared to the single variable relations (which had an R-squared of 0.39) for at least one equation. Especially for equations 13 and 24 (which are the linear independent relations), this becomes clear. Of course this is in line with what is expected from the behaviour of these functions, due to the added (independent) degree of freedom.

The best regression results are achieved by implementing the Mazda length scale (L_E), or the exposed area as second variable, even though these are already included in this variation of the

KC number. The parameterization scoring best for the Mazda length scale is the implementation according to equation 12, which would mean dividing the KC number by the Mazda length scale. For the exposed area, the best results are with an implementation according to equation 11, which means multiplying with the exposed area.

Even though small changes occur when implementing secondary variables, the improvements are only marginal considering the performance of the single variable parameterization based on the KC number with Mazda length scale . This is an indication that this version of the KC number by itself, already can give a good representation of the data.

5.2.2.2 KC-NUMBER DEPTH-AVERAGED

TABLE 12 R-SQUARED VALUES OF DOUBLE VARIABLE RESULTS WITH THE DEPTH-AVERAGED KC NUMBER BEING THE PRIMARY VARIABLE

	Peak period	Average period	Water depth	Reynolds number	Maximum flow velocity	Reynolds number (Mazda)	Exposed area	Vegetation density	L_E
1	NaN	0.19	0.26	NaN	0.24	NaN	0.22	0.18	0.36
2	NaN	0.26	0.21	NaN	0.24	NaN	0.26	0.28	NaN
3	NaN	0.12	0.31	NaN	NaN	NaN	NaN	NaN	0.36
4	NaN	0.25	0.04	NaN	NaN	NaN	0.36	0.39	NaN
5	NaN	NaN	0.24	NaN	0.24	NaN	0.03	NaN	NaN
6	NaN	0.17	0.13	NaN	0.23	NaN	0.31	0.34	NaN
7	0.17	0.25	0.16	NaN	0.06	0.00	0.31	0.36	0.01
8	0.07	0.17	0.25	0.09	0.14	0.22	0.01	0.00	0.31
9	0.08	0.22	0.16	0.04	0.23	0.05	0.26	0.27	0.00
10	0.00	0.00	0.07	0.04	0.24	0.05	0.20	0.14	0.00
11	0.15	0.26	0.12	0.12	0.13	0.00	0.34	0.38	0.00
12	0.11	0.17	0.30	0.01	0.09	0.19	0.00	0.00	0.34
13	0.25	0.27	0.32	0.25	0.26	0.29	0.34	0.33	0.39
14	0.25	0.26	0.27	0.08	0.26	0.04	0.26	0.26	0.33
15	0.23	0.27	0.26	0.06	0.26	0.03	0.26	0.27	0.24
16	0.19	0.24	0.31	0.19	0.18	0.19	0.21	0.21	0.32
17	0.16	0.27	0.20	0.12	0.16	0.10	0.32	0.33	0.21
18	0.03	0.00	0.32	NaN	0.27	NaN	0.22	0.01	0.00
19	0.10	0.26	0.18	0.00	0.26	0.00	0.28	0.35	0.05
20	0.15	0.28	0.14	0.12	0.14	0.00	0.32	0.37	0.00
21	0.15	0.20	0.32	0.01	0.11	0.17	0.00	0.00	0.32
22	0.09	0.25	0.18	0.04	0.26	0.00	0.28	0.28	0.00
23	0.04	0.11	0.31	0.04	0.27	0.03	0.23	0.13	0.30
24	0.26	0.28	0.33	0.26	0.27	0.30	0.35	0.34	0.39
Max	0.26	0.28	0.33	0.26	0.27	0.30	0.36	0.39	0.39

The results of the run with the depth-averaged KC number as primary variable are shown in table 12. The main difference between the depth-averaged KC number and the KC number with Mazda length scale can be found in the fact that the depth averaged KC number only takes account of the vegetation diameter. Vegetation density is not included. This can be observed in these results nicely, showing a good performance for the variables that do include more vegetation characteristics. The best performing parameterizations consequently include the

vegetation density and the Mazda characteristic length scale. Other interesting results are the exposed area (which is as well a vegetation characteristic) and the water depth (which highly correlates with vegetation density).

All in all, it is clear that the single variable parameterization with the depth-averaged KC number is outperformed by the KC number with Mazda length scale. However, when including vegetation data as a second variable, the performance of the depth-averaged KC number is improved, bringing it in the same range as the performance of the KC number with the Mazda length scale.

5.2.2.3 REYNOLDS NUMBER

TABLE 13 R-SQUARED VALUES OF DOUBLE VARIABLE RESULTS WITH THE REYNOLDS NUMBER BEING THE PRIMARY VARIABLE

	Peak period	Average period	Water depth	Maximum flow velocity	KC number (Mazda length scale)	Reynolds Mazda	Exposed area	Vegetation density	L_E
1	NaN	0.01	0.09	0.04	0.03	0.03	0.02	NaN	0.34
2	0.05	0.08	0.02	0.04	0.04	NaN	0.09	0.13	-0.06
3	NaN	NaN	0.23	0.08	NaN	0.41	NaN	NaN	0.38
4	NaN	0.12	NaN	NaN	0.41	NaN	0.38	0.13	NaN
5	NaN	NaN	NaN	0.06	NaN	NaN	NaN	NaN	NaN
6	NaN	NaN	NaN	NaN	0.26	NaN	0.36	0.01	NaN
7	0.01	0.12	0.10	0.00	0.34	NaN	0.36	0.17	0.18
8	0.01	0.01	0.25	0.02	0.33	0.09	0.18	0.06	0.36
9	0.04	0.04	0.04	0.04	0.04	0.05	0.04	0.04	0.04
10	0.04	0.04	0.04	0.04	0.04	0.06	0.04	0.04	0.04
11	0.08	0.06	0.00	0.03	0.19	0.00	0.21	0.19	0.01
12	0.01	0.02	0.10	0.08	0.05	0.39	0.01	0.01	0.21
13	0.07	0.10	0.25	0.09	0.17	0.22	0.27	0.22	0.37
14	0.03	0.04	0.09	0.04	0.04	0.01	0.04	0.03	0.36
15	0.03	0.07	0.04	0.04	0.04	0.01	0.10	0.15	0.03
16	0.03	0.06	0.23	0.00	0.19	0.23	0.21	0.15	0.35
17	0.04	0.08	0.16	0.04	0.40	NaN	0.35	0.14	0.21
18	NaN	NaN	0.00	NaN	NaN	NaN	NaN	NaN	NaN
19	NaN	NaN	0.00	0.03	0.10	NaN	NaN	NaN	NaN
20	0.07	0.05	0.01	0.03	0.16	NaN	0.19	0.17	0.00
21	0.00	0.03	0.10	0.07	0.03	0.39	0.00	0.00	0.20
22	0.04	0.04	0.04	0.04	0.04	NaN	0.04	0.04	0.04
23	0.04	0.04	0.04	0.04	0.04	0.04	0.04	0.04	0.04
24	0.06	0.09	0.25	0.07	0.15	0.20	0.26	0.21	0.36
Max	0.08	0.12	0.25	0.09	0.41	0.41	0.38	0.22	0.38

For the Reynolds number the same procedure has been done leading to the results as found in table 13. From these results it becomes clear that the Reynolds number does not represent vegetation characteristics. Adding the Mazda length scale, either by itself or through the KC number or Mazda Reynolds number, results in the greatest improvement of the parameterization, indicating a lack of vegetation data when using the Reynolds number by itself.

5.2.2.4 REYNOLDS MAZDA

TABLE 14 R-SQUARED VALUES OF DOUBLE VARIABLE RESULTS WITH THE REYNOLDS MAZDA NUMBER BEING THE PRIMARY VARIABLE

	Peak period	Average period	Water depth	Reynolds number	Maximum flow velocity	KC number Mazda length scale	Exposed area	Vegatation density	L_E
1	NaN	NaN	0.20	NaN	0.02	NaN	NaN	NaN	0.32
2	NaN	0.04	NaN	NaN	0.08	0.16	0.18	0.15	NaN
3	NaN	NaN	0.19	NaN	NaN	NaN	NaN	NaN	0.33
4	NaN	0.07	NaN	0.39	0.33	0.39	0.33	0.03	NaN
5	NaN	NaN	NaN	NaN	NaN	NaN	NaN	NaN	NaN
6	NaN	NaN	NaN	NaN	0.14	0.33	0.30	NaN	NaN
7	0.00	0.02	0.21	NaN	0.00	0.35	0.32	0.15	0.28
8	0.03	0.07	0.17	0.06	0.05	0.31	0.28	0.08	0.32
9	0.05	0.05	0.05	0.05	0.05	0.05	0.05	0.05	0.05
10	0.05	0.05	0.05	0.06	0.05	0.05	0.05	0.05	0.05
11	0.05	0.03	0.09	0.00	0.01	0.04	0.01	0.01	0.13
12	0.04	0.06	0.02	0.39	0.32	0.24	0.13	0.10	0.01
13	0.08	0.07	0.21	0.17	0.18	0.17	0.21	0.15	0.34
14	0.04	NaN	0.12	NaN	0.03	0.01	NaN	NaN	0.32
15	0.02	0.04	NaN	NaN	0.04	0.06	0.11	0.15	NaN
16	0.00	0.04	0.21	0.12	0.00	0.15	0.20	0.15	0.32
17	0.02	0.05	0.15	NaN	0.11	0.42	0.32	0.10	0.20
18	NaN	NaN	NaN	NaN	NaN	NaN	NaN	NaN	NaN
19	0.00	0.00	0.00	NaN	0.00	0.00	NaN	NaN	0.00
20	0.09	0.05	0.00	NaN	0.01	0.04	0.03	0.02	0.15
21	0.05	0.05	0.00	0.39	0.32	0.00	NaN	0.13	0.03
22	0.03	0.06	0.03	0.00	0.06	0.00	NaN	0.06	0.06
23	0.03	0.06	0.03	NaN	0.06	0.00	NaN	0.06	0.06
24	0.04	0.04	0.21	0.17	0.00	0.15	0.20	0.15	0.34
Max	0.09	0.07	0.21	0.39	0.33	0.42	0.33	0.15	0.34

From table 14, the results indicate that the Mazda Reynolds number is not a good representation of the drag coefficient. Even when adding a secondary variable the Mazda Reynolds number still performs poorly. The improved representations are mainly caused by the representation the secondary variables can give on their own.

5.2.2.5 MAXIMUM FLOW VELOCITY

When using the maximum flow velocity as primary variable, the Reynolds number and KC number are not regarded as possible second variables in the parameterization of the drag coefficient. These relations were not regarded since they are a combination of other available variables and thus they will always outperform these variables when adding them. When not including them as potential second variables, relations of the sub-variables can be tested better.

TABLE 15 R-SQUARED VALUES OF DOUBLE VARIABLE RESULTS WITH THE MAXIMUM FLOW VELOCITY BEING THE PRIMARY VARIABLE

	Peak period	Average Period	Water depth	Exposed area	Vegatation density	L_E
1	NaN	NaN	0.19	NaN	NaN	0.30
2	NaN	0.03	NaN	0.22	0.18	NaN
3	NaN	NaN	0.20	NaN	NaN	0.34
4	0.06	0.09	NaN	0.34	0.06	NaN
5	NaN	NaN	NaN	0.31	0.07	NaN
6	NaN	NaN	NaN	NaN	NaN	NaN
7	0.00	0.01	0.18	0.19	0.13	0.29
8	0.03	0.08	0.07	0.29	0.09	0.19
9	0.01	0.05	0.21	0.32	0.13	0.32
10	0.01	0.05	0.22	0.14	0.08	0.32
11	0.08	0.04	0.00	0.21	0.15	0.05
12	0.00	0.00	0.08	0.05	0.04	0.21
13	0.06	0.09	0.24	0.25	0.20	0.35
14	0.03	0.03	0.11	0.03	0.03	0.32
15	0.04	0.06	0.03	0.11	0.14	0.03
16	0.03	0.07	0.21	0.20	0.15	0.33
17	0.04	0.08	0.16	0.33	0.11	0.20
18	0.06	0.08	0.11	0.09	0.06	0.17
19	0.08	0.09	0.11	0.10	0.07	0.13
20	0.07	0.05	0.01	0.20	0.14	0.06
21	0.02	0.01	0.12	0.05	0.05	0.20
22	0.04	0.06	0.21	0.31	0.16	0.32
23	0.03	0.05	0.22	0.21	0.15	0.32
24	0.06	0.09	0.24	0.25	0.20	0.35
Max	0.08	0.09	0.24	0.34	0.20	0.35

From the results of this regression, it is clear that with the maximum flow velocity, just as for the Reynolds number, information about the vegetation is missing. Including the Mazda characteristic length scale as a secondary variable therefore gives the best results, closely followed by adding the exposed area. However, it can be concluded that these good relations are mainly due to the good relations these variables have with the drag coefficient by themselves, rather than due to their combination with the maximum flow velocity.

5.2.2.6 MAZDA LENGTH SCALE

TABLE 16 R-SQUARED VALUES OF DOUBLE VARIABLE RESULTS WITH THE MAZDA LENGTH SCALE BEING THE PRIMARY VARIABLE

	Peak period	Average period	Water depth	Maximum flow velocity	Exposed area	Vegetation density
1	NaN	NaN	0.30	0.30	0.30	0.17
2	NaN	0.15	0.10	0.33	0.31	0.24
3	NaN	0.13	0.29	NaN	0.32	0.15
4	0.02	0.34	0.30	0.06	0.32	0.21
5	NaN	NaN	0.07	0.30	0.32	0.27
6	NaN	-0.01	0.19	0.33	0.32	0.33
7	0.10	0.09	0.28	0.03	0.05	0.08
8	0.14	0.30	0.12	0.17	0.29	0.15
9	0.05	0.21	0.32	0.32	0.32	0.30
10	0.06	0.30	0.31	0.32	0.31	0.30
11	0.11	0.16	0.31	0.05	0.15	0.00
12	0.16	0.34	0.20	0.21	0.32	0.23
13	0.32	0.34	0.32	0.33	0.32	0.32
14	0.13	0.23	0.32	0.32	0.32	0.31
15	0.14	0.30	0.31	0.33	0.32	0.29
16	0.13	0.22	0.28	0.14	0.24	0.16
17	0.22	0.34	0.31	0.22	0.32	0.28
18	0.00	0.00	0.02	0.27	0.32	0.17
19	0.02	0.13	0.20	0.28	0.32	0.23
20	0.11	0.19	0.30	0.06	0.15	0.00
21	0.16	0.34	0.20	0.21	0.32	0.24
22	0.05	0.21	0.32	0.32	0.32	0.30
23	0.15	0.35	0.32	0.32	0.32	0.32
24	0.32	0.34	0.32	0.33	0.32	0.32
Max	0.32	0.35	0.32	0.33	0.32	0.33

The results of this regression (table 16) show only slight improvements to the single variable relation between the Mazda length scale and the drag coefficient. The best results are achieved by implementing the Average period as second variable, indicating the lack of wave characteristics in the Mazda length scale.

5.3 MULTI VARIABLE PARAMETERIZATION

The results of the double variable relations are used to define expectations of good performing parameterizations of the drag coefficient and test their performance. The double variable regressions showed that the Reynolds number as defined by Mazda and the maximum flow velocity perform poorly when implemented as primary variable. These primary variables only show reasonable results when adding secondary variables that were already regarded as primary variables by themselves. Therefore, there is no point in doing further analysis with these primary variables. Consequently, the following primary variables remain for the multi variable relations:

- KC-number (Mazda length scale)
- KC-number(Depth-averaged)
- Reynolds number
- Mazda length scale

For each primary variable, based on the type of relations and R-squared values obtained from the single and double variable regressions, secondary variables will be selected to be added.

5.3.1 KC NUMBER MAZDA LENGTH SCALE

As was shown in section 5.1, the best parameterizations of the drag coefficient are obtained with the KC number with Mazda length scale as primary variable. It can be motivated that this KC number on itself gives a sufficient representation of the drag coefficient, since adding extra variables has no significant impact on the R-squared values achieved. Even though this already gives a plausible equation, it is interesting to explore what can be achieved by adding additional variables.

As was shown in table 11 , the best results with adding a second variable are achieved when adding the Mazda length scale (L_E) according to equation 12, giving:

$$Cd = a * \left(\frac{KC_M}{L_E}\right)^b \qquad (5.3)$$

The R-squared value for this equation is 0.43 (for a=0.18 and b=-0.60).

However, within the exponential equations a good result can be found as well implementing L_E according to equation 16, giving:

$$Cd = a * L_E * \exp(b * KC_M) + c \qquad (5.4)$$

The R-squared value for this equation is 0.42 (when a=1.37, b=-29,5 and c=0.99).

Concerning the double variable relations, more variables showed to improve the R-squared value even though the effects were less than for the Mazda length scale. Nevertheless, it is required to verify whether adding another variable to the new equation might further improve the correlation. This will be done with both equations found here.

5.3.1.1 POWER EQUATION

The potential relations remaining with the power equation implementation are equations 1-13 (table 9). The implementation of the combined KC number and Mazda length scale can be performed simply by defining :

$$x = \frac{KC_M}{L_E} \qquad (5.5)$$

This is in line with the best performing equation from the double variable analysis, equation 12. The results for this implementation are presented in table 17.

TABLE 17 R-SQUARED VALUES OF MULTI VARIABLE RESULTS WITH THE IMPLEMENTATION OF THE KC NUMBER WITH MAZDA LENGTH SCALE, DIVIDED BY THE MAZDA LENGTH SCALE

	Peak period	Average period	Water depth	Reynolds number	Maximum flow velocity	Reynolds Mazda	Exposed area	Vegetation density	L_E
1	NaN	NaN	0.36	NaN	0.42	NaN	0.24	NaN	0.30
2	NaN	0.12	0.05	NaN	0.39	NaN	0.38	0.26	NaN
3	0.08	0.31	0.39	NaN	0.00	NaN	0.37	0.24	0.39
4	0.04	0.42	0.37	NaN	-0.01	NaN	0.39	0.32	0.37
5	NaN	NaN	NaN	NaN	0.38	NaN	0.40	0.25	NaN
6	NaN	NaN	NaN	NaN	0.42	NaN	0.36	NaN	NaN
7	0.08	0.09	0.33	NaN	0.02	NaN	0.10	0.05	0.36
8	0.12	0.33	0.06	0.09	0.12	0.00	0.36	0.16	0.10
9	0.01	0.07	0.15	0.04	0.21	0.05	0.33	0.14	0.32
10	0.01	0.03	0.24	0.04	0.04	0.05	0.30	0.10	0.32
11	0.32	0.44	0.40	0.29	0.31	0.21	0.42	0.41	0.39
12	0.29	0.37	0.42	0.13	0.24	0.28	0.39	0.31	0.42
13	0.43	0.44	0.43	0.43	0.44	0.44	0.43	0.44	0.43
Max	0.43	0.44	0.43	0.43	0.44	0.44	0.43	0.44	0.43

From the results, it is clear that small improvements in the accuracy of the representation are possible, but no significant increases can be found. However, since this equation is not dimensionless, it is interesting to see what can be done to do obtain a dimensionless equation again. Looking at the current dimensions of the equation (m^{-1}), two possibilities can be found to make the equation dimensionless again. Either the water depth (m), or the exposed area (m^{-1}) can be used to achieve this. For the water depth this means implementation according to equation 11, giving an R-squared value of 0.40, and for the exposed area, this means implementation through equation 12, giving an R-squared value of 0.39. When looking into the meaning of these implementations, implementing the exposed area, through equation 12, can be rewritten to dividing the KC number by 1 minus the vegetation density. Since the vegetation density is no more than 4%, this number will always be close to one, thus have little influence on the drag coefficient. This is visible in the results being similar to those of the KC number with Mazda length scale by itself. For this reason, combined with the slightly better representation, implementing the water depth as secondary variable is more interesting, giving:

$$Cd = a * \left(\frac{KC_M * h}{L_E}\right)^b \qquad (5.6)$$

This has an R-square value of 0.40, with the coefficients being a=0.13 and b=-0.67.

5.3.1.2 EXPONENTIAL EQUATION

The implementation in the exponential equation, results in the following adjustments:

$$a_n = a * \mathrm{L_E} \qquad (5.7)$$

In which a_n is the new replacement for a. The results of this implementation can be found in table 18.

TABLE 18 R-SQUARED VALUES OF MULTI VARIABLE RESULTS WITH THE IMPLEMENTATION OF THE KC NUMBER WITH MAZDA LENGTH SCALE AND THE MAZDA LENGTH SCALE BY ITSELF

	Peak period	Average period	Water depth	Reynolds number	Maximum flow velocity	Reynolds Mazda	Exposed area	Vegetation density	L_E
14	0.35	0.41	0.42	0.09	0.42	0.04	0.42	0.42	0.42
15	0.35	0.42	0.42	0.07	0.42	0.04	0.42	0.43	0.42
16	0.25	0.36	0.39	0.24	0.25	0.24	0.39	0.36	0.40
17	0.24	0.43	0.39	0.18	0.24	0.19	0.40	0.36	0.39
18	0.41	0.42	0.42	NaN	0.42	NaN	0.42	0.42	0.42
19	0.42	0.43	0.42	0.07	0.42	NaN	0.42	0.42	0.43
20	0.36	0.44	0.42	0.36	0.35	0.35	0.40	0.44	0.42
21	0.33	0.37	0.40	0.34	0.32	0.32	0.42	0.33	0.40
22	0.32	0.32	0.32	0.32	0.32	0.32	0.32	0.32	0.32
23	0.32	0.34	0.32	0.35	0.32	0.32	0.34	0.32	0.32
24	0.42	0.43	0.42	0.43	0.43	0.43	0.43	0.44	0.43
Max	0.42	0.44	0.42	0.43	0.43	0.43	0.43	0.44	0.43

Again, in order to achieve a dimensionless equation, either the water depth (with implementing equation 17), or the Exposed area (implementing equation 16) can be used. In both cases though, the R-squared value is reduced to 0.39, which is comparable to the value found when only using the KC number with Mazda length scale. For this reason it is decided to not try and make this equation dimensionless, but rather keep it as it is, thus:

$$Cd = a * L_E * \exp(b * KC_M) + c \qquad (5.8)$$

The R-squared value for this equation is 0.42 (when a=1.37, b=-29,5 and c=0.99).

5.3.2 KC NUMBER DEPTH-AVERAGED

For the depth-averaged KC number, as seen before, the vegetation density information is missing in the equation. The best improvement of the parameterization is thus obtained by adding either the vegetation density or the Mazda length scale. Of these two, adding the vegetation density is the most logical step, since this performs best at a dependent relation and is dimensionless, as opposed to the Mazda length scale that performs best at independent relations, while it has a dimension. All in all, two possible implementations are available to include the vegetation density. These consist of a division of the entire power equation (equation 4), or a multiplication of the exponent of the power or exponential equation (equations 11 and 20). When evaluating only the R-squared values of the two implementations, the differences are negligible (table 12). However, for the second implementation (equations 11 and 20), the equations become comparable to the KC number with Mazda length scale. For this reason this is not an interesting implementation to consider. This means the following implementation is remaining:

$$Cd = \frac{a}{\rho_v} * KC^b \qquad (5.9)$$

TABLE 19 R-SQUARED VALUES OF MULTI VARIABLE RESULTS WITH THE IMPLEMENTATION OF THE DEPTH-AVERAGED KC NUMBER AND THE VEGETATION DENSITY

	Peak period	Average period	Water depth	Reynolds number	Maximum flow velocity	Reynolds Mazda	Exposed area	Vegetation density	L_E
1	NaN	0.33	0.41	NaN	0.39	NaN	NaN	0.40	0.36
2	NaN	0.36	0.37	NaN	0.39	NaN	NaN	0.37	0.28
3	0.07	0.27	0.40	NaN	NaN	NaN	0.35	0.24	0.42
4	0.03	0.39	0.26	NaN	0.03	NaN	0.39	0.35	0.22
5	NaN	NaN	0.34	NaN	0.40	NaN	NaN	0.03	NaN
6	NaN	0.26	0.30	NaN	0.38	NaN	NaN	0.39	NaN
7	0.20	0.39	0.33	NaN	0.15	0.09	0.39	0.34	0.29
8	0.13	0.30	0.35	0.11	0.16	0.18	0.33	0.30	0.38
9	0.14	0.37	0.32	0.13	0.39	0.03	0.09	0.39	0.12
10	0.03	0.05	0.14	0.13	0.39	0.03	0.04	0.38	0.03
11	0.23	0.40	0.30	0.27	0.27	0.20	0.40	0.34	0.27
12	0.23	0.32	0.41	0.04	0.14	0.20	0.36	0.36	0.43
13	0.40	0.40	0.41	0.40	0.40	0.40	0.40	0.40	0.41
Max	0.40	0.40	0.41	0.40	0.40	0.40	0.40	0.40	0.43

From the results of this implementation (table 19) it is clear that the only real improvement of the representation of the data can be obtained by implementing the Mazda length scale according to equation 12. Doing so would mean the introduction of a dimension again to the equation, while on the other hand, transforming the KC number to resemble the KC number with Mazda length scale. Since this combination of parameters has already been addressed, there is no added value in adding this variable. Therefore, the final equation derived from the depth-averaged KC number is:

$$Cd = \frac{a}{\rho_v} * KC^b \qquad (5.10)$$

This has an R-squared value of 0.39 (with a=1.9 and b=-0.72).

5.3.3 REYNOLDS NUMBER

For the basic Reynolds number the best R-squared value was obtained by adding the KC number with Mazda length scale or the Reynolds number with Mazda length scale. However, another good relation can be achieved by adding the Mazda length scale. This single variable is less complex while still performing well. Therefore, this variable has been implemented according to equation 3, giving:

$$Cd = a * L_E * Re^b \qquad (5.11)$$

The results of running the model on this base equation can be found in table 20.

TABLE 20 R-SQUARED VALUES OF MULTI VARIABLE RESULTS WITH THE IMPLEMENTATION OF THE REYNOLDS NUMBER AND THE MAZDA LENGTH SCALE

	Peak period	Average period	Water depth	Maximum flow velocity	KC number (Mazda length scale)	Reynolds Mazda	Exposed area	Vegetation density	L_E
1	0.27	0.35	0.38	0.38	0.38	0.15	0.38	0.37	0.38
2	0.36	0.39	0.38	0.38	0.38	NaN	0.38	0.38	0.38
3	0.00	0.21	0.32	0.41	NaN	0.38	0.04	NaN	0.32
4	0.22	0.43	0.26	0.19	0.38	NaN	0.32	0.25	0.04
5	NaN	NaN	NaN	0.38	NaN	NaN	NaN	NaN	NaN
6	NaN	NaN	NaN	0.29	0.40	NaN	0.29	0.12	NaN
7	0.32	0.42	0.32	0.33	0.40	NaN	0.34	0.34	0.31
8	0.32	0.31	0.34	0.35	0.41	0.32	0.31	0.31	0.34
9	0.38	0.38	0.38	0.38	0.38	0.33	0.38	0.38	0.38
10	0.38	0.38	0.38	0.38	0.38	0.33	0.38	0.38	0.38
11	0.42	0.40	0.37	0.36	0.40	0.36	0.38	0.39	0.37
12	0.34	0.36	0.38	0.42	0.33	0.42	0.37	0.36	0.38
13	0.40	0.40	0.38	0.40	0.38	0.40	0.38	0.38	0.38
Max	0.42	0.43	0.38	0.42	0.41	0.42	0.38	0.39	0.38

In order to make the equation dimensionless again the implementation of either water depth (according to equation 4), or exposed area (according to equation 3) is required. However, from table 20 it is clear that these implementations strongly decrease the goodness of fit of the model. Improvements on the goodness of fit are possible though by implementing other variables, of which the best R-squared is achieved for implementing the average period according to equation 4. Thus giving:

$$Cd = a * \frac{L_E}{Tavg} * Re^b \qquad (5.12)$$

The results of trying to add another variable in this equation, can be found in table 21.

TABLE 21 R-SQUARED VALUES OF MULTI VARIABLE RESULTS WITH THE IMPLEMENTATION OF THE REYNOLDS NUMBER, THE MAZDA LENGTH SCALE AND THE AVERAGE PERIOD

	Peak period	Average period	Water depth	Maximum flow velocity	KC number (Mazda length scale)	Reynolds Mazda	Exposed area	Vegetation density	L_E
1	0.33	0.41	0.43	0.43	0.43	0.14	0.42	0.42	0.42
2	0.37	0.40	0.42	0.43	0.43	NaN	0.42	0.42	0.42
3	0.04	0.38	0.36	0.37	NaN	0.34	0.12	NaN	0.35
4	0.15	0.38	0.32	0.26	0.34	NaN	0.35	0.30	0.12
5	NaN	NaN	NaN	0.37	NaN	NaN	NaN	NaN	NaN
6	NaN	NaN	NaN	0.35	0.42	NaN	0.33	0.15	NaN
7	0.34	0.35	0.35	0.38	0.40	NaN	0.37	0.37	0.34
8	0.35	0.38	0.37	0.40	0.39	0.36	0.34	0.34	0.37
9	0.43	0.43	0.43	0.43	0.43	0.39	0.43	0.43	0.43
10	0.43	0.43	0.43	0.43	0.43	0.38	0.43	0.43	0.43
11	0.42	0.42	0.42	0.42	0.43	0.41	0.42	0.43	0.41
12	0.40	0.43	0.42	0.42	0.39	0.41	0.41	0.40	0.42
13	0.43	0.43	0.43	0.43	0.43	0.43	0.43	0.43	0.43
Max	0.43	0.43	0.43	0.43	0.43	0.43	0.43	0.43	0.43

It is clear from table 21, that no further improvements are possible by implementing extra variables. However, the current formulation does have dimensions (m/s). The only easy way to bring the formulation back to a dimensionless formulation is by adding the maximum flow velocity, according to equation 4, thus reducing the goodness of fit. Since other dimensionless parameters have already shown much better performances, it is chosen not to implement the maximum flow velocity here, giving the final equation:

$$Cd = a * \frac{L_E}{Tavg} * Re^b \qquad (5.13)$$

The R-squared value achieved for this function is 0.43 (with a=10 and b=-0.21).

5.3.4 MAZDA LENGTH SCALE

The results of the double variable regression with the Mazda length scale as primary variable (table 16) showed that the best results are achieved by adding the average period as second variable. Several implementations show good results, however subtracting (such as in equation 23) is not preferable due to the different units of the variables thus lack of physical meaning. Furthermore, independent relations are less preferable than dependant relations. This means the remaining equations are 4, 12, 17 and 21. These equations have in common that they all show a division. Considering the fact that the Mazda length currently has units (m), division within the power or exponential part of the equation (equation 12 or 21), is the most preferred combination. This implementation can be done simply by defining:

$$x = \frac{L_E}{Tavg} \qquad (5.14)$$

TABLE 22 R-SQUARED VALUES OF MULTI VARIABLE RESULTS WITH THE IMPLEMENTATION OF THE MAZDA LENGTH SCALE AND THE AVERAGE PERIOD

	Peak period	Average period	Water depth	Maximum flow velocity	Exposed area	Vegetation density
1	NaN	0.28	0.35	0.32	0.33	0.32
2	NaN	0.22	0.28	0.35	0.34	0.33
3	0.04	0.34	0.33	NaN	0.26	0.14
4	NaN	0.26	0.27	0.07	0.34	0.21
5	NaN	0.18	0.28	0.32	0.32	0.31
6	NaN	NaN	0.21	0.35	0.34	0.28
7	0.20	0.32	0.34	0.08	0.24	0.27
8	0.19	0.30	0.26	0.23	0.32	0.20
9	0.01	0.12	0.34	0.33	0.30	0.10
10	0.07	0.12	0.28	0.35	0.30	0.30
11	0.17	0.32	0.34	0.06	0.06	0.01
12	0.15	0.29	0.22	0.26	0.35	0.26
13	0.36	0.35	0.34	0.39	0.35	0.34
14	0.15	0.31	0.35	0.33	0.33	0.31
15	0.11	0.24	0.32	0.35	0.35	0.33
16	0.14	0.34	0.32	0.14	0.21	0.17
17	0.17	0.27	0.28	0.21	0.36	0.30
18	0.04	0.11	0.21	0.36	0.32	0.24
19	0.10	0.20	0.28	0.37	0.36	0.33
20	0.17	0.32	0.34	0.06	0.06	0.09
21	0.15	0.28	0.22	0.23	0.35	0.27
22	0.02	0.13	0.35	0.33	0.31	0.17
23	0.14	0.25	0.29	0.35	0.35	0.35
24	0.36	0.35	0.35	0.39	0.35	0.35
Max	0.36	0.35	0.35	0.39	0.36	0.35

The regression results of this implementation are summarized in table 22. Clearly, the best improvement is obtained by adding the maximum flow velocity with independent relations. This, however, will not lead to a dimensionless equation. The only way the equation can be made dimensionless is by dividing by the maximum flow velocity (equation 12 or 21), which effectively will reduce the effort to implementing the KC number with Mazda length scale, based on the average period rather than the peak period. As discussed before this is not an ideal implementation.

For other possible implementations (such as the inclusion of the water depth or exposed area as secondary variable), the resulting equation always maintains a dimension, while the results do not improve compared to the parameterization obtained with the KC number with Mazda length scale. All in all, it can be concluded that starting with any of the sub-variables, as presented above, has no added value compared to starting with the KC-number.

5.4 SELECTION

In the previous chapter four different definitions have been created trying to define the drag coefficient. Furthermore, the basic implementation of only the KC number with Mazda length scale according to exponential implementation is considered. This gives a total of five possible definitions for the drag coefficient. For implementation, however, only one will be selected. In order to assess which function has the best potential, they are compared according to several criteria. These criteria are:

- Accuracy
- Relations used
- Physical meaning
- Comparison to literature

For the accuracy of the parameterizations in this chapter, the differences between the equations are only marginal. However the best performance can be found in the equations which are not dimensionless (equation 3 and 5). The lowest accuracy is achieved by equation 1 and 4, while equation 2 lays somewhere in the middle.

When comparing the type of relations used, all equations only use dependent relations. Dependent relations use less calibration parameters, and are in general closer to a physical representation than independent relations do. Another important part in this criterion is the number of variables used to achieve the result. The first equation gets the best score for this criterion, because it only requires the KC number based on the Mazda length scale. The worst performing equation on this criterion is the third equation, because it needs a constant value to be added to the equation (thus requiring an extra calibration parameter).

Considering the physical meaning, not all equations are dimensionless. Since the drag coefficient should be a dimensionless parameter, the equations which are not dimensionless, have little physical meaning. Looking more in depth, all equations include both wave characteristics and vegetation characteristics, which indicates a good description of the physical processes. When looking at each equation separately, the first equation shows good physical meaning. The KC number contains wave parameters, describing the stroke of the wave, while the implemented Mazda length scale gives information about the distance between two consecutive stems. This distance is of physical importance, since when being close to each other, the wake of the first stems can influence the flow around the stems situated behind it. For the second equation the same underlying function is used, with good physical meaning, however the addition of the water depth divided by the Mazda length scale seems to have no physical meaning. This results in a neutral scoring for the second equations. Equation 3 and 5, both are not dimensionless, which makes them score very badly on this criterion. Equation 4 though, is dimensionless, and shows logical relations. Again the usage of the KC number (now with depth-averaged diameter), has been shown before to have physical meaning. Furthermore, the decrease of drag coefficients at higher densities is in line with expectations from the physical processes as well. Therefore this equation also scores good on this criterion.

When comparing with literature, first of all it is interesting whether the base variables have been used before. The use of the general KC number for mangroves can be found in literature in different occasions (i.e. Mendez and Losada, 2004). However, the use of the KC number with implementation of the Mazda length scale cannot be found in literature. This length scale has originally been developed by Mazda (1997b), for implementation in the Reynolds number. Since the Reynolds number and KC number are closely related, the implementation of the Mazda length scale in the KC number can still be seen in line with literature. The use of the Reynolds

number is even more widespread in literature. The Reynolds number is used in many different fields and many relations between Reynolds numbers and drag coefficients have been shown (i.e. Flemming and Banks, 1986).
When taking into account secondary variables as well, equation 1 still performs good. Since this equation does not need any secondary variables, it is closely related to the single parameter relations as shown in literature. The use of the water depth, as seen for equation 2, is also in line with literature some literature, describing a decrease in drag coefficient at increased water depths. However the use of the Mazda characteristic length scale, outside of the KC number, cannot be found in literature. Therefore this equation scores slightly lower here. The same goes for equation 3. The use of the KC number in an exponential equation is in line with literature, however the extra implementation of the Mazda characteristic length scale outside the exponential function is not found anywhere in literature. In equation 4, the normal KC number is used in a power equation, much in line with what is found in literature. Furthermore the use of the vegetation density, showing a decrease in drag coefficient with increasing vegetation densities, is also in line with literature, giving a perfect score for equation 4. The last equation, contains the use of the Reynolds number in line with literature. However this equation needs two more parameters, from which the relations as used here are not found in literature, thus giving this equation a neutral score on literature.

A total overview of all scores can be found in table 23.

TABLE 23 SCORE OVERVIEW OF THE MULTI CRITERIA ANALYSIS

Primary variable	Equation	Accuracy	Relation type	Physical meaning	Literature
KC number (Mazda)	$Cd = 0.24 * {KC_M}^{-0.78}$	R^2= 0.39	++	++	++
KC number (Mazda)	$Cd = 0.13 * \left(\frac{KC_M * h}{L_E}\right)^{-0.67}$	R^2= 0.40	+	0	+
KC number (Mazda)	$Cd = 1.37 * L_E * \exp(-29.5 * KC_M) + 0.99$	R^2= 0.42	-	--	+
KC number (depth-averaged)	$Cd = \frac{1.9}{\rho_v} * KC^{-0.72}$	R^2= 0.39	+	++	++
Reynolds number	$Cd = 10 * \frac{L_E}{Tavg} * Re^{-0.21}$	R^2= 0.41	+	--	0

The best overall scoring equations in this table are the first and the fourth. Even though the other equations perform slightly better on accuracy, they are outperformed at the rest of the criteria. The only difference between equation 1 and 4 can be found in the second column: Relation type, at which equation 1 scores slightly higher. This makes the first equation scoring the best out of the 5 equations.

5.5 CONCLUSION

Based on analysis of the available field data, five equations where derived to parameterize the drag coefficient. Out of the five multi variable parameterizations developed in this chapter, the equation with only the KC number with Mazda length scale as a variable has a slight preference over the other equations and therefore is considered the best equation to describe the drag coefficient. The equation is as follows:

$$Cd = 0.24 * {KC_M}^{-0.78} \qquad (5.15)$$

With:

$$KC_M = \frac{Vmax * Tpeak}{Le} \qquad (5.16)$$

Where C_D is the vegetation drag coefficient, L_E is the length scale defined by Mazda et al. (1997b), KC_M is the Keulegan-Carpenter number based on the Mazda length scale and Tpeak is the peak wave period.

6 VALIDATION

In this chapter the performance of the newly developed equation will be assessed, based on the performance on total energy dissipation in the field data, measured from the first to the last submerged sensor. Subsets, of consecutive sensors, are not considered in these calculations. This decreases the effects of possible measuring inaccuracies . To do so, a total of two runs will be considered. The first run will be the baseline, using the SWAN model in simple configuration with a single drag coefficient for each transect. The second run will be based on the previously defined drag coefficient which will be calculated as an average for the whole depth. The first of these runs will serve as a baseline for the results. The second run tests the goodness of the newly derived definition for the drag coefficient. Both implementations are based on the same model and parameters as used for the calibration of the drag coefficients. The dataset used is as well the same dataset as used before. No separate dataset was available to perform a validation on.

6.1 BASELINE

For the baseline run, a single vegetation drag coefficient has been determined for each transect. This drag coefficient, being the calibration parameter for these runs as well, is based on the energy losses observed in the data, determined in such a way that the average energy loss of the calculations is equal to the average energy loss in the data. Due to the balance in total energy loss in the data, a different weighing is used then seen when determining the average C_D values in chapter 3. Since high C_D values are often associated with low energy, the average C_D values derived here are lower. The drag coefficients determined for the transects can be found in table 24.

TABLE 24 DERIVED DRAG COEFFICIENTS FOR THE BASELINE RUN

Transect	Drag Coefficient
Palian	0.48
Kantang	1.63

With these drag coefficients for all available data bursts, the model has been run from the first to the last submerged sensor, calculating the total energy dissipation over this length.

The calculated total energy dissipation can be compared to the observed energy dissipation (figure 22). There is clearly a good relation between the two, showing to be close to equal to each other for most points. However a few outliers can be spotted as well. In order to determine the correlation between the measured and calculated data, the correlation coefficient is determined. The correlation coefficient found for this data is 0.90, which indicates a clear positive relation between the calculated and the observed data. This clearly indicates that, in general, the model with a single constant drag coefficient, has a good performance, but not all variation in the energy dissipation is represented. However since this only represents the correlation between the two sets of values, and does not include the scale of the errors, the R-squared is calculated as well. The R-squared for the simulated data is 0.74.

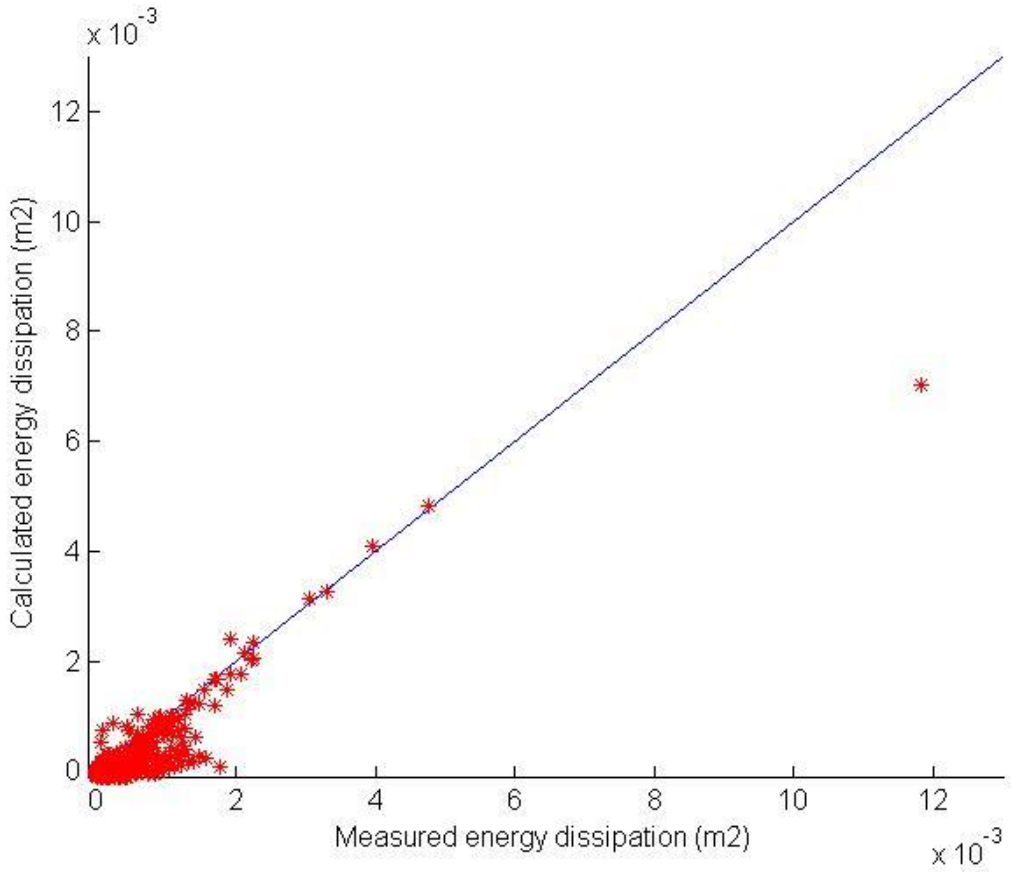

FIGURE 22 CALCULATED ENERGY DISSIPATION WITH A SINGLE CONSTANT DRAG COEFFICIENT, VS. MEASURED ENERGY DISSIPATION (INCLUDING A 1:1 TRENDLINE)

It is expected that some of this variation is due to inaccuracy of the sensors. To test this the same plots have been made, now only including bursts in which the whole transect was submerged. This reduces the relative effect of sensor inaccuracy since it will be spread over a longer calculation distance. The correlation coefficient in this case becomes 0.99 (see figure 23). The R-squared value for this subset of the modelled data is 0.98.

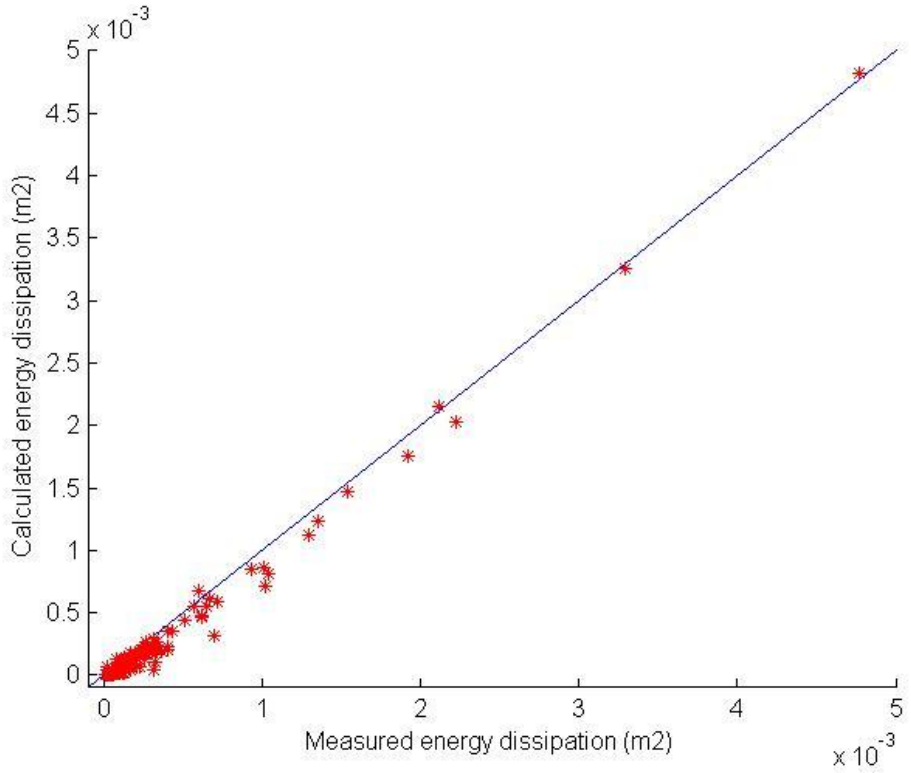

FIGURE 23 CALCULATED ENERGY DISSIPATION WITH A SINGLE CONSTANT DRAG COEFFICIENT, VS. MEASURED ENERGY DISSIPATION FOR COMPLETELY SUBMERGED BURSTS ONLY (INCLUDING A 1:1 TRENDLINE)

When applying this filter, much of the noise at low energy levels is removed, but combined with that, as well the point with the highest energy dissipation is removed from the data. Removing this point, which shows to be an outlier in the total dataset, of course will increase the correlation coefficient.

6.2 PARAMETERIZED DRAG COEFFICIENT

Total energy losses for the parameterized depth-averaged drag coefficient have been calculated using the same model again, with the only difference being the drag coefficient being calculated in each iteration based on the parameterization defined in chapter 5. The results are similar to the results for the single C_D value, although some differences can be found as well.

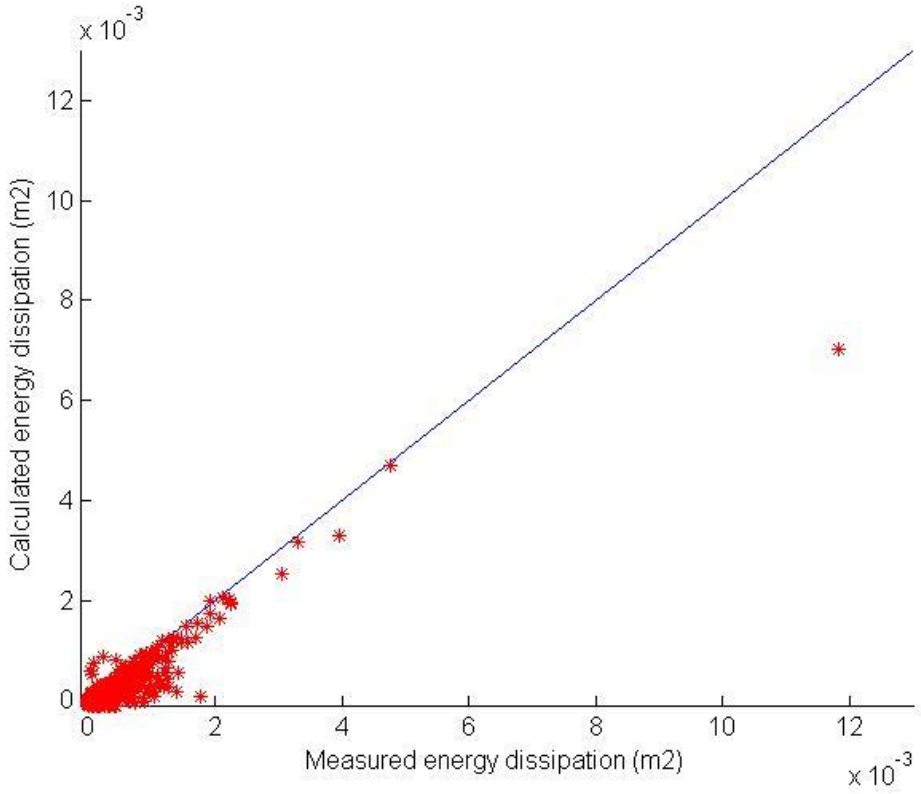

FIGURE 24 CALCULATED ENERGY DISSIPATION WITH FORMULATED DRAG COEFFICIENT, VS. MEASURED ENERGY DISSIPATION (INCLUDING A 1:1 TRENDLINE)

The calculated energy dissipation in general underestimates the measured energy dissipation (figure 24). Only at low observed energy dissipation the modelled dissipation shows to be higher in cases. The reason for this underestimation is probably that the data set used for the parameterization of the drag coefficient, is dominated be low energy bursts, and therefore high energy dissipation conditions are less well represented.

Even though this underestimation, the data do show a more linear pattern than observed for the single C_D value. This can as well be seen in the correlation coefficient which is 0.93 for this data, and the R-squared value of 0.80. It is important to notice that these values do not represent the goodness of fit for the C_D values, but for the formulation of energy loss as a whole (thus the Darlymple et al., (1984) formulation). Only the improvements in the correlation coefficient and R-squared value, compared to the base line calculations, can be contributed to the formulation of the drag coefficient.

Again, using only the bursts with completely submerged transects (see figure 25), a lot of the noise disappears and an even better correlation is achieved, which is 1.00. Again the R-squared value also increases to 0.99. Also large part of the underestimations of the wave dissipation disappear when applying this filter.

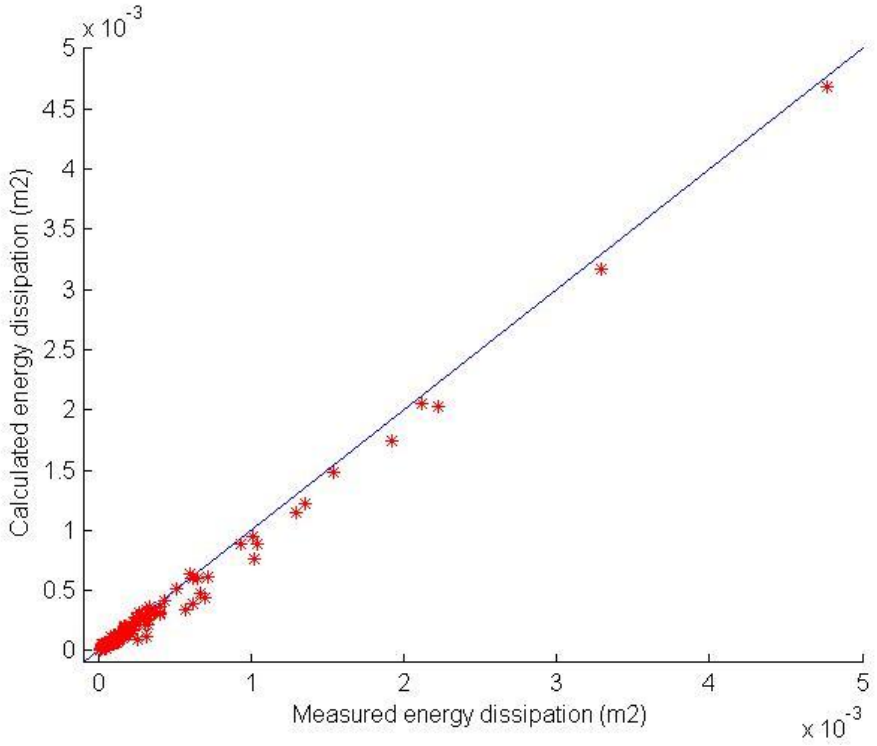

FIGURE 25 CALCULATED ENERGY DISSIPATION WITH FORMULATED DRAG COEFFICIENT, VS. MEASURED ENERGY DISSIPATION FOR COMPLETELY SUBMERGED BURSTS ONLY (INCLUDING A 1:1 TRENDLINE)

6.3 COMPARISON

All correlation coefficients and R-squared values determined before have been merged into a single table in order to make an easy comparison (table 25). It is clear that the depth-averaged drag coefficient performs better than the single drag coefficient. Even though on first sight this may sound logical since the formulation for the drag coefficient was determined based on this data, there is another point which comes into play here. For the single C_D run, both transect (Palian and Kantang) got their own C_D value. These values differs by a factor 3. However in the definition of the drag coefficient, a single definition was provided to deal with both transects. This means the difference between the two transects was therefore well captured within a single equation.

All in all, the run with the parameterized C_D values, outperforms the run with the single C_D value on each aspect for this data. It provides a better representation, shows more correlation with reality, and does not need separation of the two transects. However, since the model has also been fitted to this dataset a comparison is hard to make, and a validation on another dataset is needed.

TABLE 25 COMPARISON OF THE DIFFERENT MODEL RUNS

	Total data		Completely submerged transects only	
Model run	Corr.	R-squared	Corr.	R-squared
Single C_D	0,90	0,74	0,99	0,98
Parameterized C_D	0,93	0,80	1.00	0.99

7 DISCUSSION

Given the results of the validation, some good results were obtained by computing the wave dissipation due to mangroves, based on a variable, parameterized drag coefficient rather than a constant, calibrated drag coefficient. This study can provide a first step towards a complete parameterization of the drag coefficient in mangroves.

7.1 ADDED VALUE OF THIS RESEARCH

This research made a first step towards a general parameterization of the drag coefficient. Beside the improvement in representation of the wave dissipation data, this step towards a general parameterization has an added value for future calculations on coastal safety. By using the parameterized drag coefficient, the need for extensive field measurements in order to calibrate the drag coefficient can be eliminated. The only field data needed for running simulations on the wave dissipation concerns the mangroves. The number of stems, roots and branches at multiple elevations above the forest floor and the average diameter of these elements is the only data needed for making predictions. Even though getting this data might still be a major undertaking in many locations, it does mean a reduction of the field data needed for predicting the wave attenuation.

7.2 COMPARISON TO LITERATURE

When comparing the results of this study with literature some clear differences can be found. Mazda et al. (1997b) showed a clear relation between the drag coefficient and their adaptation of the Reynolds number. This relation is not as clear in the data used for this study (see table 8). However, it has to be taken into account that the data used by Mazda et al. (1997b) only considers two different vegetation densities. Therefore it might be possible that the relation they found is not valid for a wider range of vegetation characteristics. Due to the lack of vegetation data it was not possible to test the newly derived parameterization of this study on the Mazda et al. (1997b) data set. Still it can be concluded that the drag coefficients do show a comparable range. A second dataset in literature is the dataset from Mendez and Losada (2004). They showed an exponential relation between the drag coefficient and the Keulegan-Carpenter number. Their drag coefficient are considerably lower though, almost all being below 0.5. This is considerably lower than the lowest drag coefficients found in this study. This might be caused by the data being in a completely different wave regime, or having completely different vegetation characteristics, but information for exploring these differences was not available.

7.3 VERTICAL VARIATION OF VEGETATION

In this study the drag coefficient has always been assumed constant over depth, even though the vegetation is variable over depth. This assumption was needed in order to derive the drag coefficients from the data. However, in reality the drag coefficient will be different for each layer of the data. The exact effects of this assumption on the parameterization of the drag coefficient are not investigated, however, due to the large range of water depths used for calibration within this study, these effects should be taken into account to some extent.

7.4 DATA LIMITATIONS

It might be argued that by using only two transects for the collection of data, the derived parameterization might not be valid for other locations. However, the used data does represent a large range of conditions. Over the two transects, six different vegetation fields have been used, each of them changing vegetation over depth as well. This results in a factor 25 between the lowest and highest vegetation density used in this study. The range of wave conditions shows a large variance over the data set used as well, with significant wave heights ranging from 8 mm to 44 cm, and peak periods ranging from 1.5 up to 21 seconds. With this large range of data, the transects and conditions used in this study, should be able to represent many mangroves around the world.

7.5 SENSOR ACCURACY AND PRECISION

As seen before, the accuracy of the collected data cannot always be guaranteed. The sensors used in the measurements have shown some problems over time, with sensors failing or showing consistently deviating results. Furthermore, especially at low wave energy, the precision of the sensors might also be causing problems. Since for the determination of the drag coefficients the difference in wave energy between two wave sensors is used, at low energy levels, small errors in both wave sensors can have large effects on the derived drag coefficients. This is represented by the large range of C_D values at, for example, low KC numbers, and as well in the relatively high number of measurements that cannot be used, since they result in a negative drag coefficient. However, when assuming this to be caused by the sensor precision and accuracy, this can affect the final results. Since only drag coefficients with a certain negative deviation from the normal value for their conditions are removed, while other C_D values with the same conditions but a positive deviation from the normal value are kept, an unbalance in the data might exist. This will influence the fit through the data. Since the SWAN model cannot deal with negative drag coefficients though, it is not possible to add these data. It would be recommended for new field measurements to somehow be able to verify the accuracy of the sensors. This for example can be done by deploying multiple sensors at a single location (i.e. two or more sensors being placed next to each other). This way it would both be able to uncover structural errors and to determine confidence bounds for the measured data.

7.6 UNACCOUNTED PARAMETERS

Under some conditions, parameters such as wind can influence the results of the measurements. At low wave energies, wave build up between sensors can have significant influence, creating negative drag coefficients. However, no data is available on the local wind speeds observed during the measurements. This makes it impossible to say whether for example negative drag coefficients have been caused for example by wind, or simply are the result of the limits in the accuracy or precision of the sensors. In order to be able to check the influence of especially the wind, it is recommended for further field measurements, to collect in-situ weather data as well.

7.7 UNACCOUNTED PHYSICAL PROCESSES

Due to limitations of the model, and the available data, not all physical processes can be taken into account. As discussed before (section 3), bottom friction has not been included in the derivation of the drag coefficients, since the vegetation disturbs the orbital velocities. Another physical process which is not included in the SWAN model is wave reflection. When propagating through a vegetation field, a part of the wave energy will be reflected at the vegetation. This

might change local energy readings at certain sensors. However, there is no way in which this can be incorporated in the current SWAN model. Another physical process which has not been taken into account is the effect of mud. Mud differs from normal soils in its interaction with waves since it can be seen as a dense fluid. This creates extra wave damping (Winterwerp et al. 2012). By not taking these physical processes into account some deviations from reality are introduced. To what extend these are problematic is debatable. Both bottom friction and mud damping can be considered relatively low, due to the low orbital velocities just above the bed. Even though the effects of reflection might be relatively large for local conditions, overall this won't have much effect on the total energy dissipation. The effects of these processes are currently represented in the values of the drag coefficients, thus are represented as well by the parameterization of the drag coefficient. Considering, all these physical processes are present in any mangrove forest, the representation of these processes in the drag coefficient will not create large errors when using the parameterization of the drag coefficient for future predictions.

7.8 REPRESENTING FORMULATION

The drag coefficient as calculated from the field data showed a lot of variation. This can be caused by many aspects, which have not been taken into account by this study. This results in, the best representation of the drag coefficient having an R-squared value of slightly above 0.4. Furthermore, there were several different formulations of the drag coefficient, which showed similar results. Even though the selected formulation is based on a combination of both expressions presented in literature, and new field data, improvements or errors in the formulation are likely to be present. In order to extract the influence of all parameters though, physical model experiments in a lab environment would be needed, in which single parameters can be manipulated. However, the formulation derived in this study, contrary to physical model experiments in which it is hard to represent for example the surface roughness of the vegetation, does give a reliable estimation of the range of vegetation drag coefficients in mangroves. A combination of data acquired from physical modeling and data acquired from a field study, like this one, therefore is expected to result in an improved representation.

8 CONCLUSIONS

The aim of this research was to derive and validate a predictive relationship between the drag coefficient and vegetation and wave characteristics. This has been done by using field data and the SWAN model.

After deriving the drag coefficients from the field data, it has become clear that using a single drag coefficient for a certain transect is not a valid assumption. The drag coefficient is not only depending on the 'constant' vegetation characteristics, but on the changing wave characteristics as well.

From a list of parameters affecting the drag coefficient, the best correlation with the drag coefficient was found with an adaptation of the KC number, using the Mazda length scale as characteristic length scale, giving the dimensionless parameter:

$$KC_M = \frac{uTA}{(V - V_M)}$$

In which u is the maximum orbital flow velocity (m/s), T is the peak period (s), V is the control volume of water (m^3), A is the projected surface of the vegetation within this control volume (m^2), and V_M, is the volume of the mangroves within the control volume (m^3).

Using a multi variable regression analysis, five possible parameterizations for the drag coefficient have been defined, based on different primary and secondary variables. Even though these formulations do differ, they also have a lot in common. All possible parameterizations include both wave characteristics (either through a variation of the KC number, or the Reynolds number) and some vegetation characteristics (trough density, exposed area or a combination of those two).

Although the performance of the different parameterizations was comparable, a multi criteria analysis has been performed, comparing the different parameterizations, on their accuracy, the type of relations needed, their physical meaning, and their coherence with literature, resulting in a single 'best' parameterization of the data:

$$Cd = 0.24 * {KC_M}^{-0.78}$$

A validation of this parameterization has been performed by computing the total energy dissipation over the transects for each data burst and comparing this to the measured energy dissipation. Small improvements were found when implementing the parameterized drag coefficient compared to implementing a single, constant drag coefficient, for each transect. However, the greatest advantage of this parameterization is that this single parameterization is able to determine the drag coefficients for two transects with different vegetation and wave characteristics, while for the single drag coefficient per transect two fairly different drag coefficients were needed for the two transects.

By implementing this new general parameterization of the drag coefficient, there is no need for calibration of the SWAN vegetation model, when simulating the wave attenuation in a different mangrove forest. This results in a reduction of the data needed in order to be able to run predictions on wave dissipation by mangroves.

9 RECOMMENDATIONS

This study has provided a first step towards a general parameterization of the drag coefficient for mangrove vegetation. However, there is still room for improvements. Five possible parameterizations have been developed for the drag coefficient. The differences between these parameterizations in the used variables for the parameterization and the results though are only marginal. By using more field data, it might be possible to get clearer distinctions between the different parameterizations. Acquiring further sets of field data can as well provide a better validation of the final parameterization, which has been performed on the same dataset as the calibration. It is therefore highly recommended to acquire further sets of field data.

Due to the large variation in field data, it is hard to isolate the effects of a certain variable. Moreover, external variables and sensor inaccuracies might as well have affected the results. More accurate, controlled data will be needed in order to be able to isolate the effects of certain parameters. It is therefore recommended to set up physical model experiments in which conditions can be controlled and manipulated. Even though in these physical model experiments it is hard to simulate the roughness of mangroves, by combining results from physical model experiments and field measurements, a better parameterization can be achieved for the drag coefficient.

In this study the drag coefficient has been determined as a single drag coefficient for the complete water depth, however due to the variation of vegetation characteristics over water depth this is not physically accurate. The current wave data do not allow for a further derivation of drag coefficient for each vegetation layer. It can be interesting to do tests on the influences of different layers, by doing controlled tests in which vegetation characteristics of a single layer can be changed. This can lead to a parameterization which is valid for each layer of vegetation on itself, rather than all layers combined.

LITERATURE

Bao T.Q., (2011), Effect of mangrove forest structures on wave attenuation in coastal Vietnam, Oceanologia, vol. 53, pp 807-818.

Booij N., Ris R.C., Holthuijsen L.H., (1999) A third-generation wave model for coastal regions 1: Model description and validation, Journal of geophysical research, April 15, 1999, Vol. 104, pp 7649-7666.

Burger B. (2005), Wave Attenuation in Mangrove Forests: Numerical modeling of wave attenuation by implementation of a physical description of vegetation in SWAN, M.Sc. Thesis, TUDelft, Faculty of Civil Engineering and Geosciences, Section of Hydraulic Engineering.

Brinkman R.M., Massel S.R., Ridd P.V., Furukawa K., (1997), Surface wave attenuation in mangrove forests, Proceeding of the Combined Australasion Coastal Engineering and Ports Conference, Christchurch, 1997, pp 941-946.

Dalrymple R.A., Kirby J.T., Hwang P.A., (1984), Wave diffraction due to areas of energy dissipation, Journal of Waterway Port Coastal and Ocean Engineering, vol 110(1), pp 67-79.

Danielsen F., Sorensen M.K., Olwig M.F., Selvam V., Parish F., Burgess N.D., Hiraishi T., Karunagaran V.M., Rasmussen M.S., Hansen L.B., Quarto A., Suryadiputra N., (2005), The Asian Tsunami: A Protective Role for Coastal Vegetation, Science magazine, Vol 310, 28th October 2005, pp 643.

Dennis S.C.R., Chang G., (1970), Numerical solutions for steady flow past a circular cylinder at Reynolds numbers up to 100, Journal of Fluid Mechanics, vol. 42, part 3, pp. 471-489.

Flemmer R.L.C., Banks C.L. (1986), On the drag coefficient of a sphere, Powder Technology, Vol. 48, pp. 217-221.

Giri C., Ochieng E., Tieszen L.L., Zhu Z., Singh A., Loveland T., Masek J., Duke N., (2011), Status and distribution of mangrove forests of the world using earth observation satellite data, Global Ecology and Biogeography, vol 20, pp 154-159.

Hasselmann K., Barnett T.P., Bouws E., Carlson H., Cartwright D.E., Enke K., Ewing J.A., Gienapp H., Hasselmann D.E., Kruseman P., Meerburg A., Müller P., Olbers D.J., Richter K., Sell W., Walden H., (1973), Measurements of wind-wave growth and swell decay during the joint north sea wave project (JONSWAP), Deutschen Hydrographischen Zeitschrift, Reihe A 8, Nr. 12.

Horstman E., Dohmen-Janssen M., Narra P., van den Berg N., Siemerink M., Balke T., Bouma T., Hulscher S., (2012), Wave Attenuation in mangrove forests; Field data obtained in Trang Thailand, Coastal Engineering Proceedings, 1(33), waves.40.

Horstman, E.M. (2014). Data report: Field campaign Trang, Thailand; November 2010 - May 2011. University of Twente, Enschede, The Netherlands.

Horstman, E.M., C.M. Dohmen-Janssen & S.J.M.H. Hulscher (subm.). Wave attenuation in mangroves; a quantitative approach to field observations.

Keulegan G.H., Carpenter L.H., (1958), Forces on Cylinders and Plates in an Oscillating Fluid, Journal of Research of the National Bureau of Standards, vol. 60, May 1958, pp 423-440.

Kobayashi N., Raichle A.W., Asano T., (1993), Wave attenuation by vegetation, Journal of Waterway Port Coastal and Ocean Engineering, vol. 119(1), pp 30-48.

Kranenburg W.M., Winterwerp J.C., de Boer G.J., Cornelisse J.M., Zijlema M., (2011), SWAN-Mud: Engineering model for mud-induced wave damping, Journal of Hydraulic engineering, September 2011, pp 959-975.

Madsen O.S., Poon Y., Graber H.C., (1988), Spectral Wave Attenuation by Bottom Friction: Theory, Proceedings of 21st Conference on Coastal Engineering, Torremolinos, Spain, pp 492-504.

Massel S.R., Furukawa K., Brinkman R.M., (1999), Surface wave propagation in mangrove forests, Fluid Dynamics Research, vol. 24(4), pp 219-249.

Mazda Y., Magi M., Ikeda Y., Kurokawa T., Asano T., (2006), Wave reduction in a mangrove forest dominated by *Sonneratia* sp, Wetlands Ecology and Management, vol. 14(4), pp 365-378.

Mazda Y., Magi M., Motohiko K., Hong P.N., (1997a), Mangroves as a coastal protection from waves in the Tong King delta Vietnam, Mangroves and Salt Marshes, vol. 1, pp 127-135.

Mazda Y., Wolanski E., King B., Sase A., Ohtsuka D., Magi M., (1997b), Drag force due to vegetation in mangrove swamps, Mangroves and Salt Marshes, vol. 1, pp 193-199.

McIvor A.L., Möller I., Spencer T., Spalding M., (2012), Reduction of Wind and Swell Waves by Mangroves, Natural Coastal Protection Series: Report 1, Cambridge Coastal Research Working Paper 40, Published by The Nature Conservancy and Wetlands International.

Mendez F.J., Losada I.J.,(2004), An empirical model to estimate the propagation of random breaking and nonbreaking waves over vegetation fields. Coastal Engineering, vol. 51(2), pp 103-118.

Miche, A., (1944), Mouvement ondulatoires de mers en profondeur constante ou decroissante, Ann. Ponts Chaussees, Vol.114, pp 25–78.

Narra P., (2012), Attenuation of wave energy in mangrove forests, Master thesis, Universidade de Aveiro, Departamento de Engenharia Civil.

Park D., 1999, Waves tides and shallow water processes, second Edition, Published by Butterworth-Heinemann, Oxford, UK.

Quartel S., Kroon A., Augustinus P., Van Santen P., Tri N.H., (2007), Wave attenuation in coastal mangroves in the Red River Delta Vietnam, Journal of Asian Earth Sciences, vol. 29(4), pp 576-584.

Reeve D., Chadwick A., Fleming C., (2004), Coastal Engineering, Published by Spon Press, New York.

Roshko A., (1960), Experiments on the flow past a circular cylinder at very high Reynolds number, Journal of Fluid Mechanics, Vol. 10, Issue 3, May 1961, pp 345-356.

Son J.S., Hanratty T.J., (1968), Numerical solution for the flow around a cylinder at Reynlds numbers of 40, 200 and 500, Journal of Fluid Mechanics, vol.35, part 2, pp. 369-386.

Sumer B.M., Fredsoe J., (2006), Hydrodynamics around cylindrical structures (revised edition), Published by World Scientific Publishers.

Suzuki, T.(2011a). Wave Dissipation Over Vegetation Fields. Ph.D. thesis, Delft University of Technology

Suzuki T., Zijlema M., Burger B., Meijer M.C., Narayan S., (2011b), Wave dissipation by vegetation with layer schematization in SWAN, Coastal Engineering, vol. 59(1), pp 64-71.

Tanino Y., Nepf H.M., (2008), Laboratory investigation of mean drag in a random array of rigid, emergent cylinders, Journal of Hydraulic engineering, vol. 134, pp. 34-41.

Tomlinson P., (1986), The botany of mangroves, Cambridge University Press, New York.

TU Delft (2013), The official SWAN homepage: http://www.swan.tudelft.nl, Downloaded 3 May 2013.

Vo-Luong P., Massel S.R., (2006), Experiments on wave motion and suspended sediment concentration at Nang Hai, Can Gio mangrove forest Southern Vietnam, Oceanologia, vol. 48(1), pp 23-40.

Vo-Luong P., Massel S.R., (2008), Energy dissipation in non-uniform mangrove forests of arbitrary depth, Journal of Marine Systems, vol. 74(1-2), pp 603-622.

Vos W. de, (2004), Wave attenuation in mangrove wetlands, M.Sc. Thesis, TUDelft, Faculty of Civil Engineering and Geosciences, section of Hydraulic Engineering.

Winterwerp J.C., Boer G.J. de, Greeuw G., Maren, D.S. van, (2012), Mud-induced wave damping and wave-induced liquefaction, Coastal Engineering, Vol. 64, June 2012, pp. 102-112.

Yanagisawa H., Koshimura S., Goto K., Miyagi T., Imamura F., Ruangrassamee A., Tanavud C., (2009), The reduction effects of mangrove forest on a tsunami based on field surveys at Pakarang Cape Thailand and numerical analysis, Estuarine Coastal and Shelf Science, Vol 81, pp. 27-37.

APPENDIX I: OVERVIEW OF FIELD STUDIES

Several field studies have been performed looking at wave dissipation in mangroves. This appendix gives a short overview of the performed studies and their main results. These results are as well summarized in table 26.

The study of Brinkman et al. (1997) and Massel et al. (1999) was executed at Cocoa Creek, Australia and Iriomote Island in Japan. The main mangrove type encountered was the *Rhizophora stylosa* at Cocoa Creek and the *Bruguiera* at Iriomote Island. Brinkman et al. (1997) and Massel et al. (1999) introduced a wave energy transmission factor, which varied between 0.45 and 0.8 (at which 1 means no energy loss). They found that the wave energy transmission depended on tidal water level and the structure of the mangrove trees. At relative high mangrove densities, they observed increased drag. Furthermore, they found the wave energy transmission to increase with water depth, thus a decreasing energy loss at deeper water. This is possibly caused by the fact that there are fewer aerial roots higher up above the forest floor.

The study of Mazda et al. (1997a) has taken place at several locations in the Tong King delta in Vietnam, where *Kandelia candel* and *Sonneratia caseolaris* had been planted. They found wave height reductions of up to 20% over a 100m stretch of 6 year old *Kandelia candel* trees. Young mangroves were observed not to reduce the wave height. When water depths increased (but not overtopping the vegetation), they observed that the wave height reductions were still high due to the high vegetation density throughout the whole water depth.

The second study of Mazda et al. (2006) was performed during a typhoon on the Vinh Quang coast in northern Vietnam, where the mangroves mainly consisted of *Sonneratia*. The rate of wave reduction over 100m of mangrove forest was found to be 45% for a water depth of 0.2 m and 26% for a water depth of 0.6m. They found wave reductions to be dependant on water depth. Wave reduction decreased with increasing water depths, due to reducing extent of the root system higher above the bed, until the branch height was reached from which point it increased again.

Quartel et al. (2007) did measurements in the Red River Delta in Vietnam, where *Kandelia candel* was the dominant mangrove type. They found wave height reductions to be between 5-7.5 times larger as would be the case with bottom friction only. Wave height reductions again depended on water depth. Furthermore, they derived an approximation for the drag coefficient, which for their location came down to the following formula: $C_D = 0.6\, e^{0.15A}$ (in which A is the cross-sectional area of the underwater obstacles up to a certain depth).

The studies of Vo-Luong and Massel (2006,2008) have been executed at Nang Hai, Can Gio in southern Vietnam where the mangroves consisted of a mixture of *Avicennia* and *Rhizophora* in the first 100 metre. Beyond this point *Rhizophora* dominated. There was also a steep cliff at the edge of the mangrove forests (elevation change of approximately 1.4 metre). They found 50-70% of the wave energy to be dissipated over the first 20 metre of mangrove forests at water levels between 1.9 and 2.1 metre deep. After these first 20 metre, wave heights decreased at much lower rates. The greatest reduction in wave height occurred as the waves passed over the steep cliff between mudflat and mangrove.

Bao (2011) measured wave attenuation in 32 plots in 2 regions in Vietnam. There were six different mangrove species present at these locations. The mean wave height reduction was found to be 0.0054/m over an 80m stretch of mangrove forest. It was found that 71% of the variation in the gradient of the wave height reduction (which is related to the wave attenuation), could be attributed to the mangrove forest structure.

Horstman et al. (2012) measured wave attenuation at 2 locations in Thailand. In the front zone of the forest *Avicennia* and *Sonneratia* where the dominant species found while in the back forest *Rhizophora* was dominant. A wave energy dissipation of 72% was found for the first location over a 98 metre long transect, and a wave energy dissipation of 78% was found for the second location over a 142 metre transect. In both these locations no wave breaking occurred so all dissipation can be contributed to either vegetation or bottom friction.

	Location	Type of mangroves	Dissipation type	Dissipation	Influencing variables
Brinkman et al. (1997)	Cocoa Creek, Australia and Iriomote Island, Japan	Rhizophora and Bruguiera	Wave energy transmission factor	0,45-0,8	Tidal water level, structure of mangrove
Mazda et al. (1997a)	Tong King delta, Vietnam	Kandelia and Sonneratia	Wave height reduction over 100 metre stretch	20%	Age of the mangroves
Mazda et al. (2006)	Vinh Quang coast, Vietnam	Sonneratia	Wave height reduction over 100 metre stretch	26%-45%	Water depth (related to the root density)
Quartel et al. (2007)	Red River delta, Vietnam	Kandelia	Wave height reductions compared to wave height reductions caused by bottom friction	5-7.5 times larger	Drag coefficient depending on the cross-sectional area of the underwater obstacles up to a certain depth
Vo-Luong and Massel (2006,2008)	Nang Hai, Can Gio, Vietnam	Avicennia and Rhizophora	Wave energy dissipation	70% in the first 20 metre, after the first 20 metre much lower dissipation rates	Steepness of the bottom
Bao (2011)	32 plots in 2 regions in Vietnam	six different species	Wave height reduction per metre	0,54%	Mangrove forest structure
Horstman et al. (2012)	2 location in Thailand	Avicennia and Rhizophora	Wave energy dissipation	72% over 98 metre and 78% over 142 metre	Vegetation density

TABLE 26 SUMMARY OF RESULTS FROM PERFORMED FIELD STUDIES LOOKING AT WAVE DISSIPATION IN MANGROVES

APPENDIX II: OVERVIEW OF THE MAIN CHARACTERISTICS OF THE ACQUIRED DATA (NARRA, 2012)

Kantang Transect												
Etot (J/m2)							Change in Etot (%)					
Sensor	*TK1*	*TK2*	*TK3*	*TK4*	*TK5*	*TK6*	*1-2*	*2-3*	*3-4*	*4-5*	*5-6*	*Total*
Mean	3.41	3.30	2.29	1.99	1.28	1.32	-0.06	6.55	10.84	35.25	-21.34	62.89
Std	2.36	2.25	1.14	0.95	0.73	0.84	22.76	22.61	16.74	17.06	72.64	18.38
Maximum	14.22	13.86	8.03	7.31	5.61	4.55	55.51	46.10	47.36	71.96	70.65	92.46
Minimum	0.71	0.61	0.55	0.47	0.24	0.41	-87.58	-83.35	-38.97	-10.93	-309.89	6.09
Hs (m)							Change in Hs (%)					
Sensor	*TK1*	*TK2*	*TK3*	*TK4*	*TK5*	*TK6*	*1-2*	*2-3*	*3-4*	*4-5*	*5-6*	*Total*
Mean	0.071	0.070	0.059	0.055	0.044	0.045	0.60	3.98	5.99	20.25	-5.70	40.91
Std	0.022	0.022	0.014	0.013	0.012	0.013	11.27	11.29	8.84	10.75	31.15	14.89
Maximum	0.152	0.151	0.115	0.109	0.096	0.086	33.30	26.59	27.45	47.05	45.82	72.54
Minimum	0.034	0.032	0.030	0.028	0.020	0.026	-36.96	-35.41	-17.89	-5.32	-102.46	3.09
Hrms (m)							Change in Hrms (%)					
Sensor	*TK1*	*TK2*	*TK3*	*TK4*	*TK5*	*TK6*	*1-2*	*2-3*	*3-4*	*4-5*	*5-6*	*Total*
Mean	0.050	0.050	0.042	0.039	0.031	0.031	0.60	3.98	5.99	20.25	-5.70	40.91
Std	0.016	0.015	0.010	0.009	0.009	0.009	11.27	11.29	8.84	10.75	31.15	14.89
Maximum	0.108	0.106	0.081	0.077	0.068	0.061	33.30	26.59	27.45	47.05	45.82	72.54
Minimum	0.024	0.022	0.021	0.020	0.014	0.018	-36.96	-35.41	-17.89	-5.32	-102.46	3.09
T (s)							T shift (s)					
Sensor	*TK1*	*TK2*	*TK3*	*TK4*	*TK5*	*TK6*	*1-2*	*2-3*	*3-4*	*4-5*	*5-6*	*Total*
Mean	7.43	7.54	7.03	7.33	7.93	8.64	-0.11	-0.27	-0.31	-0.48	-0.56	-0.13
Std	2.26	2.25	2.22	2.22	1.79	1.50	0.86	0.79	0.54	0.76	0.92	1.57
Maximum	12.10	12.64	13.19	12.64	11.91	11.61	2.76	1.96	1.31	1.68	1.17	2.90
Minimum	2.96	2.80	2.88	3.07	2.93	5.07	-3.97	-2.81	-2.28	-2.75	-3.56	-4.19
Palian transect												
Etot (J/m2)							Change in Etot (%)					
Sensor	*TP1*	*TP2*	*TP3*	*TP4*	*TP5*	*TP6*	*1-2*	*2-3*	*3-4*	*4-5*	*5-6*	*Total*
Mean	3.51	2.47	2.35	2.89	1.99	1.01	15.16	58.63	-262.76	19.66	11.48	46.12
Std	4.66	4.94	3.60	3.54	2.06	1.06	18.69	34.86	1426.94	20.16	28.65	20.86
Maximum	48.96	44.00	34.10	27.33	12.16	5.72	86.09	99.74	30.57	74.60	69.56	90.63
Minimum	0.11	0.10	0.00	0.08	0.07	0.08	-61.66	-49.42	-	-79.70	-100.91	-30.94
Hs (m)							Change in Hs (%)					
Sensor	*TP1*	*TP2*	*TP3*	*TP4*	*TP5*	*TP6*	*1-2*	*2-3*	*3-4*	*4-5*	*5-6*	*Total*
Mean	0.066	0.051	0.049	0.059	0.051	0.037	8.50	41.32	-60.44	11.06	7.12	28.11
Std	0.037	0.037	0.038	0.035	0.026	0.017	10.63	26.39	102.75	11.16	15.05	14.84
Maximum	0.283	0.268	0.236	0.211	0.141	0.097	62.70	94.90	16.67	49.61	44.82	69.40
Minimum	0.013	0.013	0.001	0.012	0.011	0.012	-27.14	-22.24	-	-34.05	-41.74	-14.43
Hrms (m)							Change in Hrms (%)					
Sensor	*TP1*	*TP2*	*TP3*	*TP4*	*TP5*	*TP6*	*1-2*	*2-3*	*3-4*	*4-5*	*5-6*	*Total*
Mean	0.047	0.036	0.035	0.042	0.036	0.026	8.50	41.32	-60.44	11.06	7.12	28.11
Std	0.026	0.027	0.027	0.024	0.018	0.012	10.63	26.39	102.75	11.16	15.05	14.84
Maximum	0.200	0.190	0.167	0.149	0.100	0.068	62.70	94.90	16.67	49.61	44.82	69.40
Minimum	0.009	0.009	0.001	0.008	0.008	0.008	-27.14	-22.24	-	-34.05	-41.74	-14.43
T (s)							T shift (s)					
Sensor	*TP1*	*TP2*	*TP3*	*TP4*	*TP5*	*TP6*	*1-2*	*2-3*	*3-4*	*4-5*	*5-6*	*Total*
Mean	5.88	6.13	7.60	7.13	7.56	7.59	-0.74	-1.56	0.47	-0.43	-0.14	-2.19
Std	1.79	1.80	2.02	2.03	2.04	1.97	0.74	1.35	0.97	0.59	0.60	1.36
Maximum	12.42	12.32	14.08	13.39	14.15	12.60	1.43	1.42	5.25	1.29	2.03	0.62
Minimum	2.24	2.23	2.73	2.64	2.79	3.20	-3.69	-5.51	-2.43	-2.71	-2.24	-6.48

TABLE 27 OVERVIEW OF THE MAIN CHARACTERISTICS OF THE ACQUIRED DATA (NARRA, 2012)

APPENDIX III: ANALYSIS OF SENSOR ABNORMALITY

Two sensors have been defined as faulty or possibly faulty. This appendix will present and discuss all information available from these sensors.

PALIAN MEASUREMENT 1, SENSOR 3

Sensor 3 from measurement 1 at the Palian transect shows some very peculiar data. When looking at the average total energy for each sensor during this measurement some abnormal results are found.

Sensor	Average Total energy (J/m^2)
1	3.0173
2	2.6557
3	1.7916
4	2.1837
5	1.5195
6	1.0638

TABLE 28 AVERAGE TOTAL ENERGY PER SENSOR AT PALIAN MEASUREMENT 1

As can be seen in table 28, the average total energy at sensor 3 is much lower than observed at the surrounding sensors.

Even more clear becomes the problem when looking at bursts with relatively low energy (see table 29). For these burst sensor 3 often shows less than 1/3 of the energy of the surrounding sensors. These large deviations in not single burst, but in many consecutive bursts, make it unlikely for this error to be caused by some local physical process. Therefore it is concluded that sensor 3 in measurement 1 of the Palian transect is faulty.

Burst	Sensor 1	Sensor 2	Sensor 3	Sensor 4	Sensor 5	Sensor 6
63	1,881599	1,714363	0,419729	1,39192	1,211603	0,63357
64	1,653794	1,242021	0,309416	0,888301	0,862292	0,537684
65	1,515841	1,360181	0,275695	1,18942	0,886881	0,568319
66	1,274218	1,240619	0,329125	0,981486	0,672406	0,455675
67	0,973228	0,749603	0,192192	0,736171	0,740653	0,417295
68	1,07878	0,967984	0,306171	0,763513	0,644947	0,447225
69	0,88328	0,630048	0,241352	0,694956	0,490805	0,35109
70	0,750915	0,891383	0,070444	0,540178	0,548436	0,411335
71	1,237871	0,907702	0,046823	0,539724	0,57163	0,266569
72	0,632089	0,57634	0,08268	0,489893	0,765205	0,458892
73	0,954722	0,669485	0,071776	0,748473	0,549867	0,545927
74	0,805103	0,817779	0,097385	0,700048	0,5392	0,484984
75	0,954826	0,642353	0,093755	0,574434	0,483964	0,445477
76	0,669872	0,480559	0,094812	0,358588	0,470928	0,514615
77	0,504131	0,445733	0,06684	0,383836	0,402617	0,396579
78	0,64703	0,51937	0,06796	0,435602	0,422922	0,356374
79	0,287155	0,25568	0,036901	0,308649	0,323772	0,244306
80	0,309126	0,310401	0,035504	0,253852	0,215377	0,205296
81	0,449757	0,314683	0,049773	0,220753	0,244913	0,241518
82	0,606317	0,2569	0,056143	0,23772	0,208931	0,157616
83	0,404813	0,384517	0,071516	0,191871	0,182445	0,301499
84	1,301233	0,649171	0,029831	0,351857	0,374978	0,355725
85	0,579932	0,369336	0,115562	0,286106	0,354032	0,339029
86	0,552556	0,49348	0,106652	0,413415	0,406697	0,404504
87	1,159884	0,491636	0,125123	0,440223	0,367713	0,286548
88	0,567172	0,426567	0,085515	0,434588	0,269297	0,255336
89	0,454436	0,350777	0,094758	0,174943	0,313555	0,151002
90	0,310191	0,177984	0,037269	0,151614	0,124764	0,123771
91	0,118365	0,106172	0,02128	0,086569	0,104959	0,088325
92	2,00914	0,657902	0,032106	0,687059	0,472871	0,309927

TABLE 29 ENERGY PER SENSOR FOR SEVERAL LOW ENERGY BURSTS

PALIAN MEASUREMENT 2, SENSOR 3

Sensor 3 in measurement 2 at the Palian transect again shows some relatively low energy values (table 30).

Sensor	Average total energy (J/m^2)
1	4.9610
3	3.5183
4	4.3410
5	2.9346

TABLE 30 AVERAGE WAVE ENERGY PER SENSOR AT PALIAN MEASUREMENT 2

However, when comparing the data from this measurement to the data from the previous measurement no structural error can be found. At low energy values, sensor 3 is still outputting

lower energy values than sensor 1 and 4, but now the difference is scaled according to the values in sensor 1 and 4. This indicates two possible causes. Either the scaling of this sensor or calibration are wrong, resulting in a consistent underestimation of the wave energy, or there is some physical process which can explain these lower energy values.

When looking at possible physical processes that might cause the observed effects, reflection shows up as a possible candidate. Sensor 4, being situated just in front of the high density mangrove section, might be experiencing higher wave energies due to the reflection of the waves on the mangroves. If this indeed is the case there might be no error at all in the data.

However when looking further into the data reflection can be debated as well. When considering a one-dimensional wave transect with no wave spreading, reflected energy would not only be observed at sensor 4, but as well at sensor 1 and 3. Even though the reflected energy would also be dissipated partly by vegetation, considering a one-dimensional transect, this dissipation cannot be higher than the dissipation of the waves running towards the shore. Therefore the energy at sensor 3 will still be higher than at sensor 4.

This theory for one-dimensional transects though might not apply here. If sensor 4 is positioned close to a spot with high reflection, the local effects of the reflection observed at sensor 4 will be high. When this reflection is not equal everywhere along the shoreline, the reflected waves will experience spreading and might be hardly visible at sensor 3. In this case, due to the wave reflection and spreading, the energy at sensor 3 can indeed be lower than the energy at sensor 4.

However there is another point which indicates that wave reflection might not be the whole cause of the observed energy differences. When considering no friction at all at a one-dimensional wave transect, according to the conservation of energy, any energy reflected cannot be present any more further along the transect. In other words, the energy difference between sensor 3 and 5, in case of no energy losses, should be equal to the energy difference between sensor 4 and 3. When considering energy dissipation the energy difference between sensor 3 and 5, should even be larger than the energy difference between sensor 4 and 3.
When looking at these energy differences for the average energy at those sensors though, these requirements are not met. The difference between sensor 3 and 5 is 0.58 J/m^2, while the difference between sensor 4 and 3 is 0.82 J/m^2. In other words: More energy is reflected, than that is lost from the total energy, which according to the laws of physics is not possible.
Again this might be explained when looking at a two-dimensional wave transect, considering the reflection only to take place close to sensor 4. In this case wave spreading can result in smaller energy losses observed between sensor 3 and 5.

All in all it is hard to say whether these data indicate a defect sensor or do represent reflection on the vegetation. Reflection can only be the cause when the mangroves differ along the shore, and sensor 4 happened to be placed just before the highest density mangroves. It is impossible to draw definite conclusions from this without obtaining more information about the spatial variance in the mangroves in the alongshore direction.

APPENDIX IV

This appendix gives an overview of the fits through the data. For each relation the fits are shown, and shortly discussed. Furthermore for some relations sub-sets of the data will be considered as well, in order to further identify the type of relation.

STANDARD REYNOLDS NUMBER

Figure 29 shows the drag coefficient as calculated from the field data vs. the Reynolds number. This figure shows a clear trend which looks like either a power function or an exponential relation such as found by Mazda et al (1997b) (see figure 29). However when it is hard to actually fit the data, since especially at low Reynolds numbers the C_D values have a lot of variation. Looking at the shape of the graph this might be caused by the data being build up by many different power or exponential functions of which some are steeper than others.

When looking at all data both the exponential and the power equation seem to provide some description of the trend. However, there is a lot of variation which cannot be explained by the Reynolds number on itself. This is reflected in the R-square values for the fits, of 0.014 for the exponential fit and 0.038 for the power function fit (figure 26).

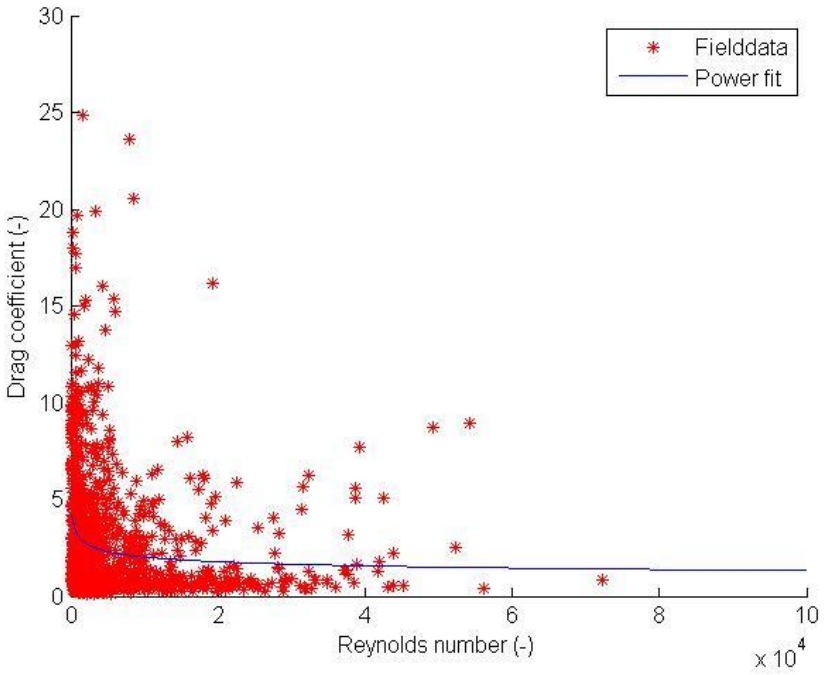

FIGURE 26 DRAG COEFFICIENT VS. REYNOLDS NUMBER FIELDDATA WITH EXPONENTIAL FUNCTION FIT

Even though here the power function shows to be better in describing the relation, this cannot be proved yet, since in the essence of the power function it can better deal with high Cd values at low Reynolds numbers. Furthermore the R-squared values are thus low that no preference between the functions can be decided.

MAZDA REYNOLDS NUMBER

When using the Reynolds number, as defined by Mazda et al (1997b), thus including vegetation characteristic, the results seem slightly improve compared to when using the normal Reynolds

number. This is represented by the R-squared values for the fit through this graph which are 0.030 for the exponential fit and 0.051 for the power fit (figure 27).

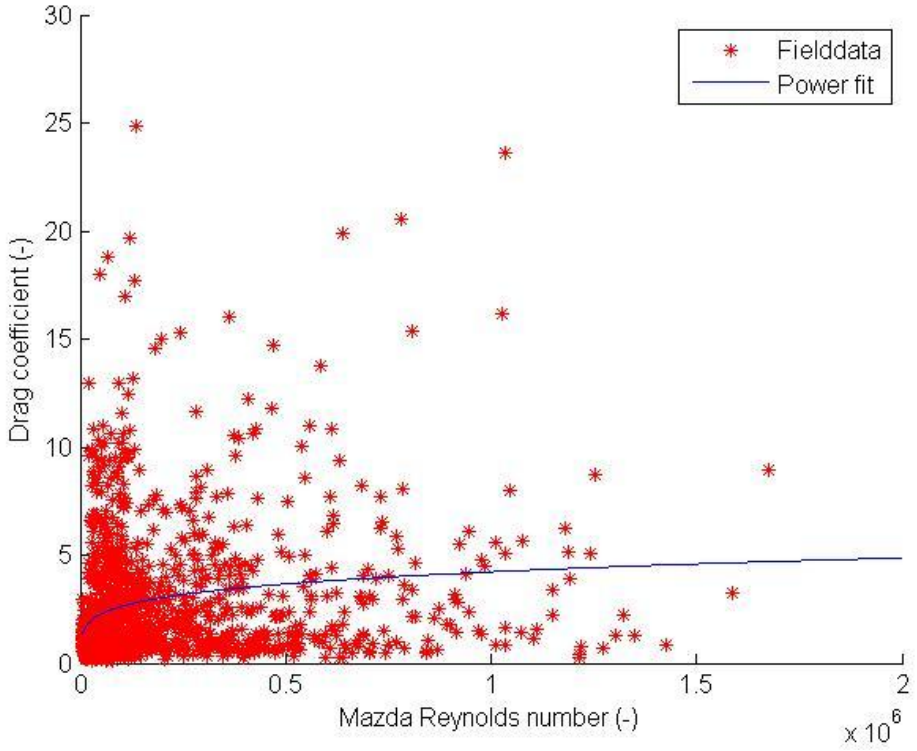

FIGURE 27 DRAG COEFFICIENT VS. REYNOLDS NUMBER ACCORDING TO ADAPTATION BY MAZDA

However as can be seen in figure 27, the shape of the fit is not in line with expectations, but is showing an inverse shape. Combined with the large spreading in the graph, this shows that the Mazda Reynolds number is not a very good variable for single variable relations.

KC NUMBER (DEPTH AVERAGED VEGETATION DIAMETER)

When plotting all data again a shape is seen which can either be represented by an exponential function or by a power function (figure 28). When fitting the complete data with these functions a R-squared value of 0.11 for the exponential fit, and 0.18 for the power fit.

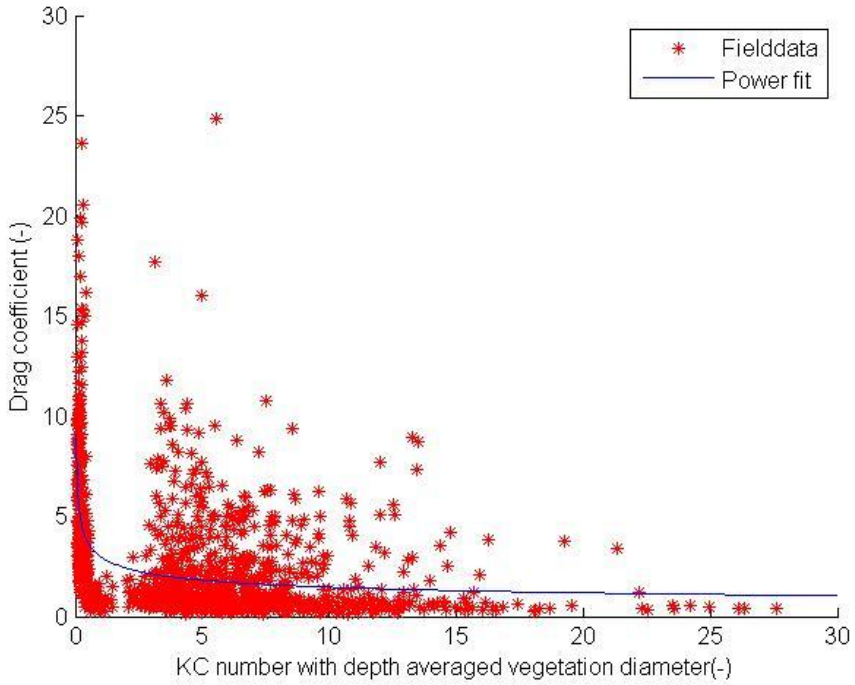

FIGURE 28 DRAG COEFFICIENT VS KC NUMBER BASED ON DEPTH AVERAGED VEGETATION DIAMETER

Looking at the fits, some clear power shape can be found for the low KC numbers, however at higher KC number the trend becomes less clear. This can indicate that this version of the KC number is not taking into account all effects, that are necessary for a good representation.

KC NUMBER (DEPTH AVERAGE)

When repeating the process as seen for the previous description of the KC number some differences can be found. When plotting all data and fitting them (figure 29), the R-squared values found are of 0.15 for the exponential fit, and 0.24 for the power fit. This slightly higher than the values seen for the KC number as a result of averaging the diameter over depth.

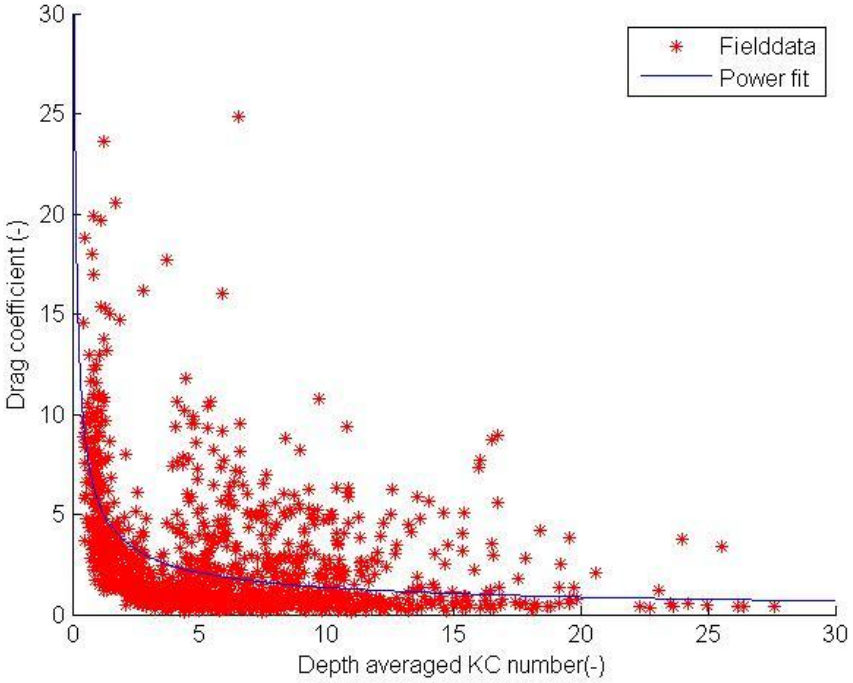

FIGURE 29 DRAG COEFFICIENT VS DEPTH-AVERAGED KC NUMBER

A very good trend is seen in part of the data, but some data seems to stand out here. The cause of this becomes clear when looking at the results for the Palian transect only (figure 30). The R-squared values achieved for fitting this data are 0.47 for the exponential equation and 0.45 for the power equation. This indicates that not all differences between the two transects can be captured within this depth-averaged KC number.

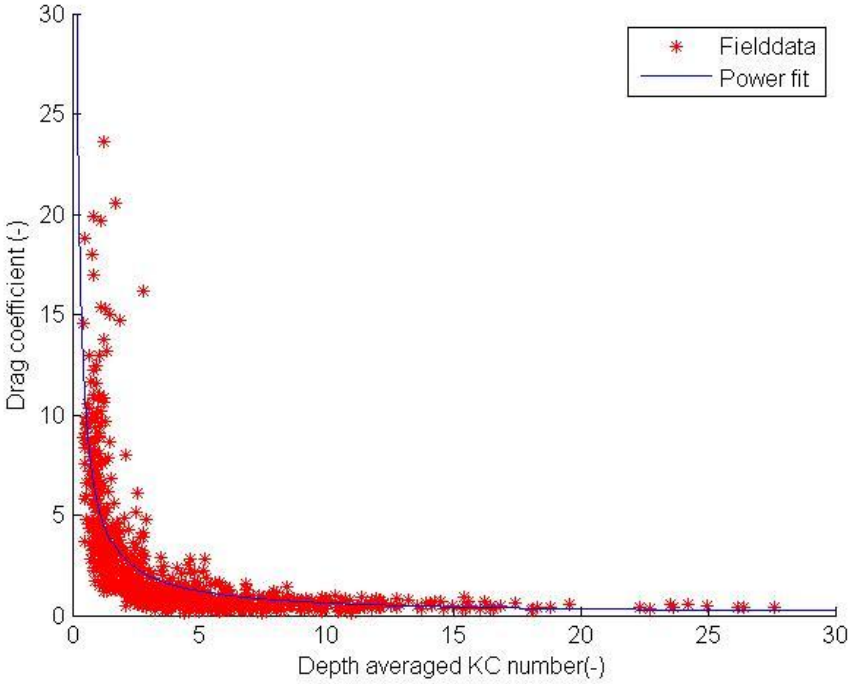

FIGURE 30 DRAG COEFFICIENT VS DEPTH AVERAGED KC NUMBER FOR THE PALIAN TRANSECT ONLY

KC NUMBER (MAZDA LENGTH SCALE)

When looking at the KC number with Mazda length scale, contrary to the versions of the KC number discussed before, the data is much more following a single trend (figure 31). This is represented in the R-squared values as well being 0.37 for the exponential fit an 0.39 for the power fit.

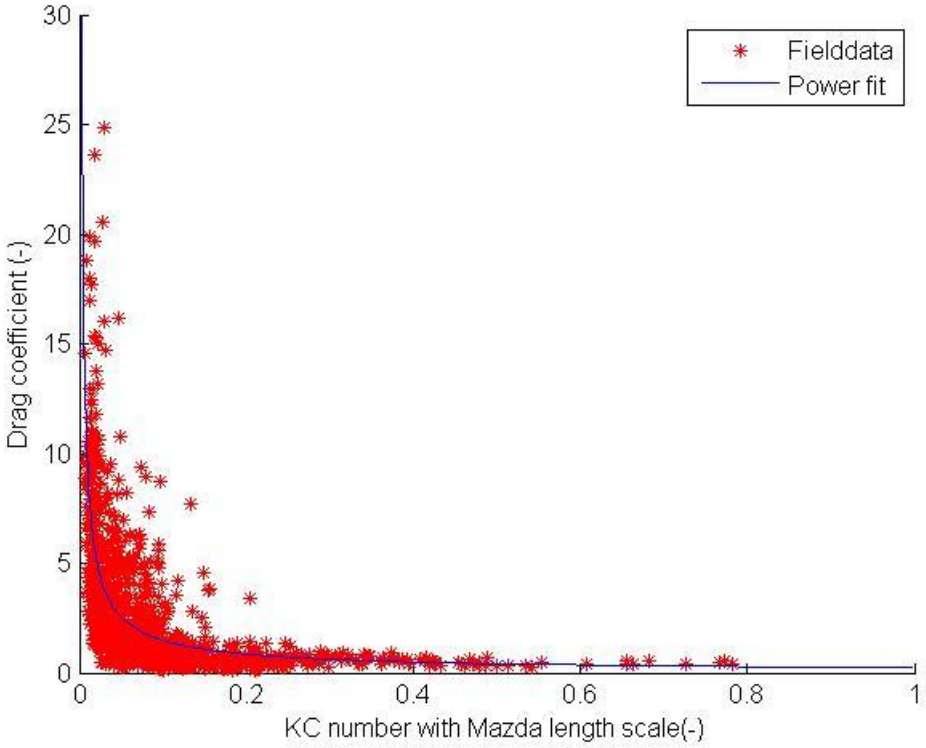

FIGURE 31 DRAG COEFFICIENT VS KC NUMBER WITH MAZDA LENGTH SCALE

It can be concluded that, due to the implementation of the Mazda length scale, suddenly the differences between the two transects, can be captured with a single trend. This makes the KC number with Mazda length scale outperform all other variables.

VEGETATION DENSITY

When looking at the vegetation density, as can be seen in figure 32, a negative trend can be found between vegetation density and drag coefficients. However, this trend is only able to explain part of the variation seen in the data. Several subsets in the data can be found, with their own behavioural pattern. These patterns cannot be captured by relating the drag coefficient to the vegetation density, which is represented in the R-squared value of 0.15.

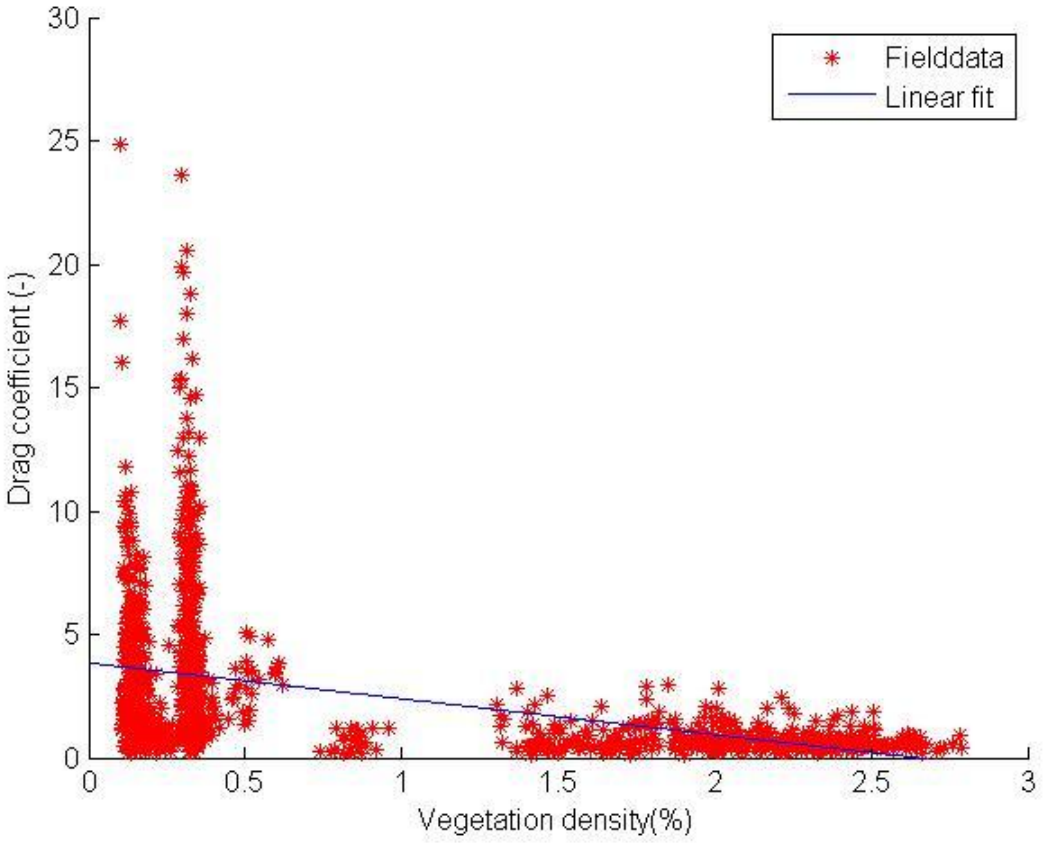

FIGURE 32 DRAG COEFFICIENT VS DEPTH AVERAGED VEGETATION DENSITY (%)

WATER DEPTH

When looking at figure 33 a relation between the water depth and the drag coefficient can clearly be found. A linear relation can best describe the trends seen here, showing an increased drag coefficient at increased water depths. This relation has an R-squared value of 0.21. However it can be debated whether this relation is caused by the water depth, or by some other variables. There is a clear negative trend between water depth and vegetation density, and combined with the earlier trend seen between the vegetation density and the drag coefficient, this can as well explain the positive trend seen here. Another point for debating the found relation is the negative values for the drag coefficient at low water depths. This of course is physically impossible.

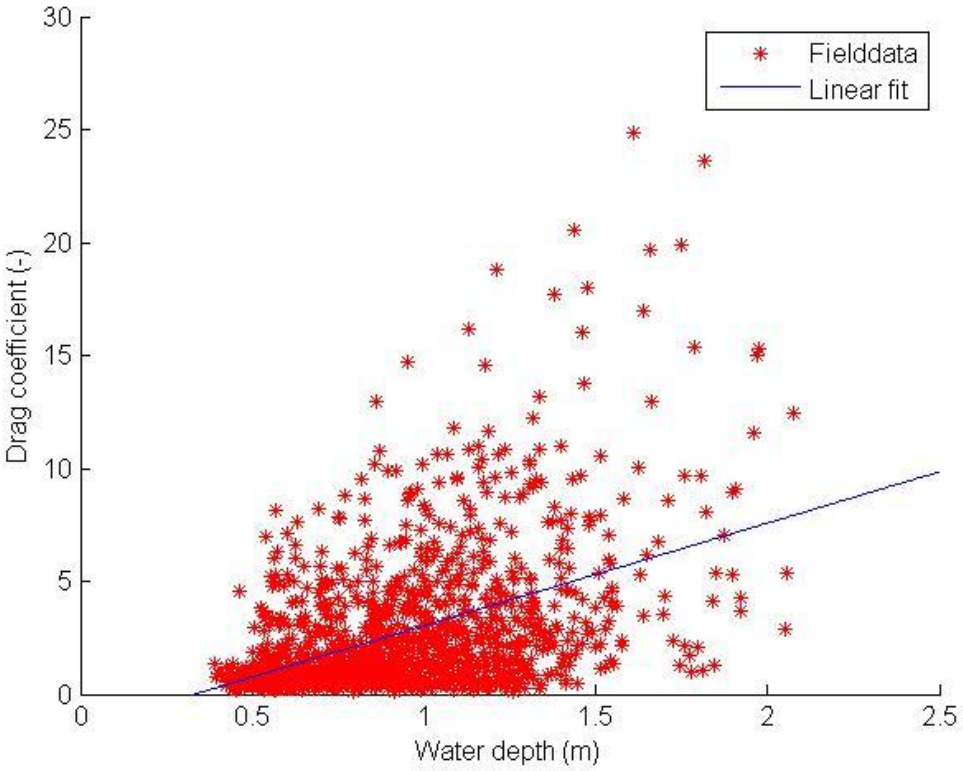

FIGURE 33 DRAG COEFFICIENT VS. WATER DEPTH (M)

PEAK PERIOD

When looking at the drag coefficient vs. the peak period (figure 34) no clear relation can be seen. The R-squared value for a linear fit through this data is 0.001. However due to the large variation in the data it is hard to actually draw conclusions. What is striking though is that for peak periods around 5 seconds the variation seems to be much lower than for lower or higher peak periods.

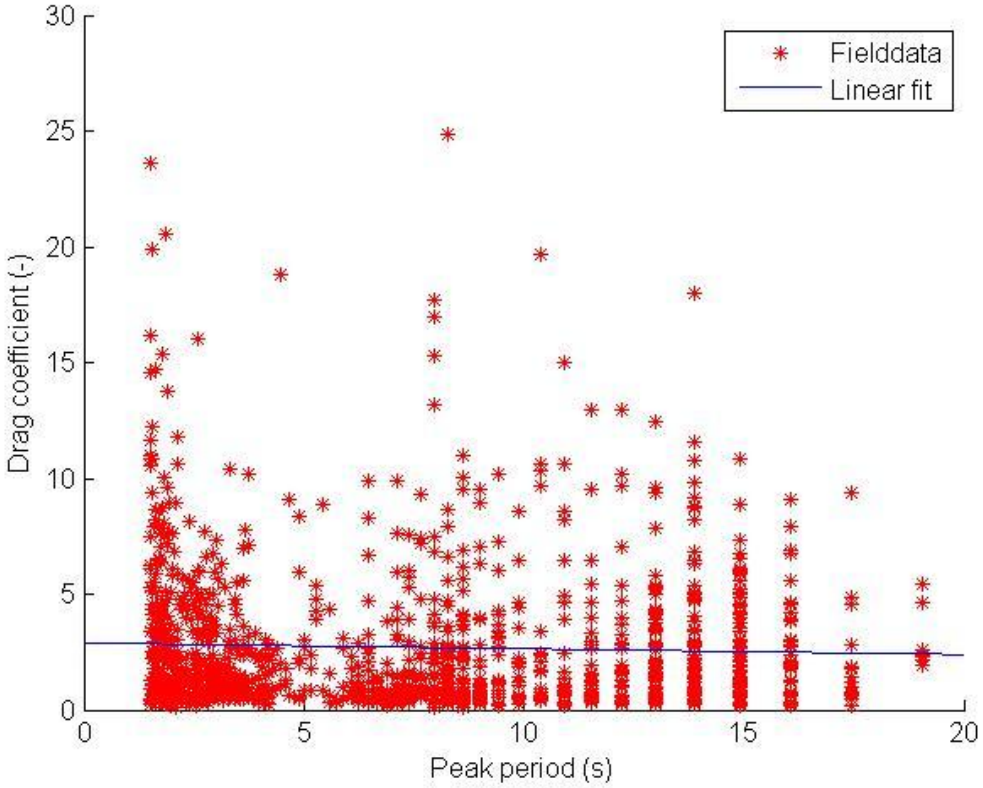

.

FIGURE 34 DRAG COEFFICIENT VS. PEAK WAVE PERIOD (S)

AVERAGE PERIOD

When looking at the drag coefficient vs. the average period (figure 35), a slight negative trend is visible. The R-squared value for this relation is 0.04. However it is unclear whether this relation is actually caused by the average period, or for example due to the change of the average wave period while propagating through mangroves.

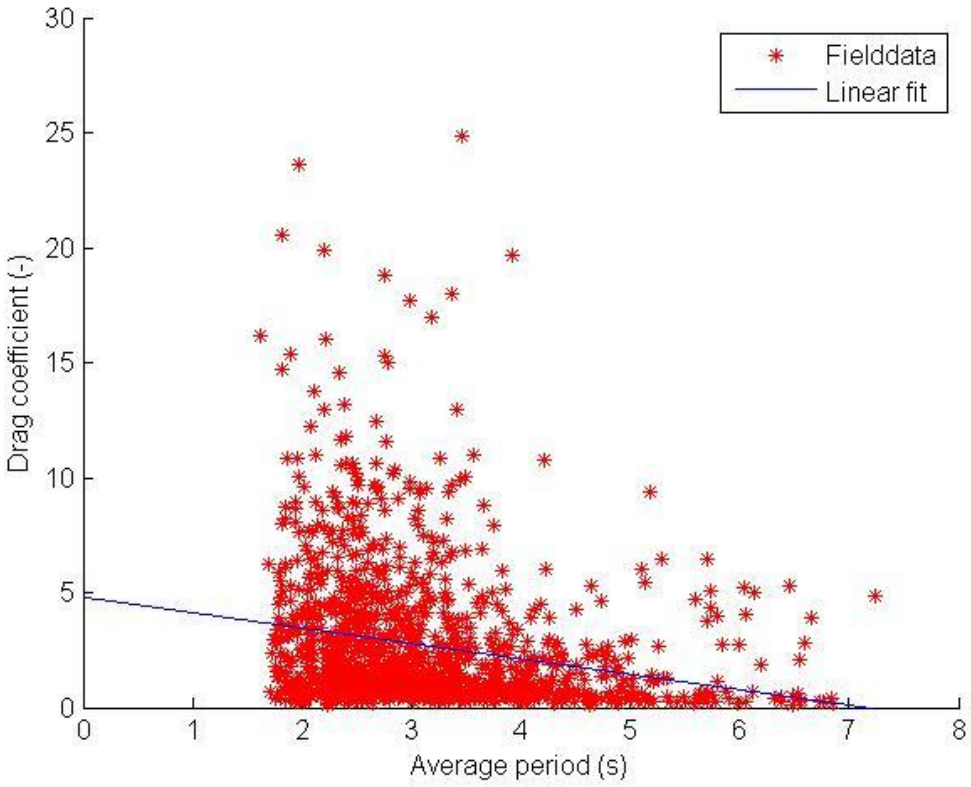

FIGURE 35 DRAG COEFFICIENT VS. AVERAGE WAVE PERIOD (S)

MAXIMUM FLOW VELOCITY

The relation which can be seen between the drag coefficient and the maximum flow velocity shows some indications of a power or exponential relation (figure 36). However, due to large variations in the data, with high drag coefficients still occurring at high flow velocities as well, it is clear that the maximum flow velocity cannot be used to describe the drag coefficient on its own. This is also clearly visible in the R-squared value found of 0.01 for the power relation.

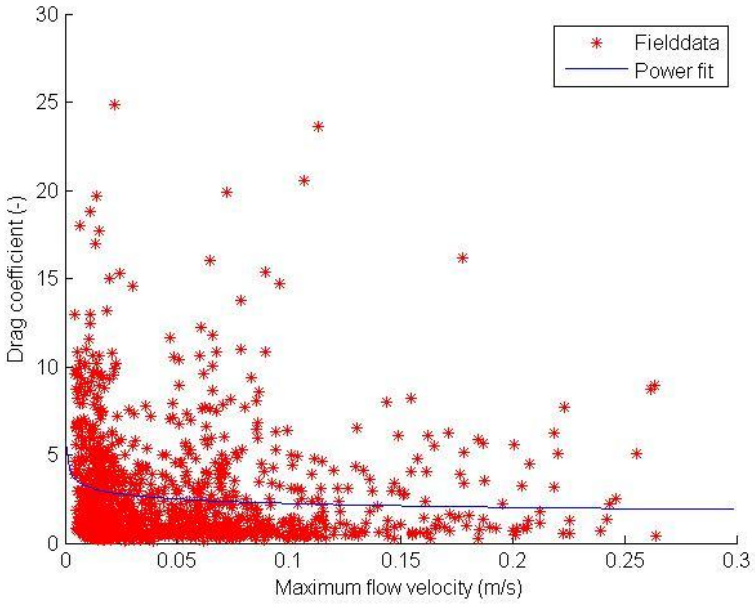

FIGURE 36 DRAG COEFFICIENT VS MAXIMUM FLOW VELOCITY

MAZDA LENGTH SCALE

When looking at the drag coefficient vs. the Mazda length scale a clear relation can be seen (figure 37). Higher drag coefficients are clearly found at high values for the Mazda length scale. However at higher values for the Mazda length scale, the variance in the data increases as well. A first degree polynomial (linear) fit shows to be a good estimation of the data here, with an R-squared value of 0.31.

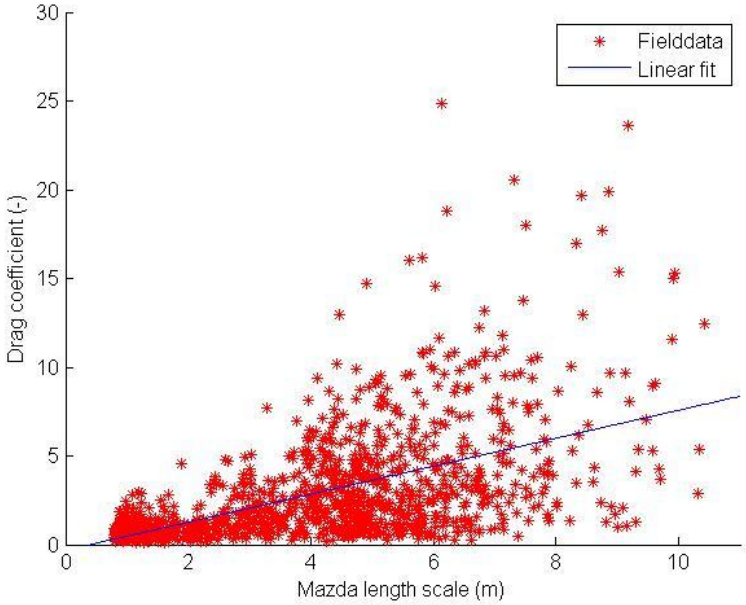

FIGURE 37 DRAG COEFFICIENT VS MAZDA LENGTH SCALE

The relation between the drag coefficient and the exposed area (figure 38), shows a trend. The best fit for this relation is a power fit, which has an R-squared value of 0.32.

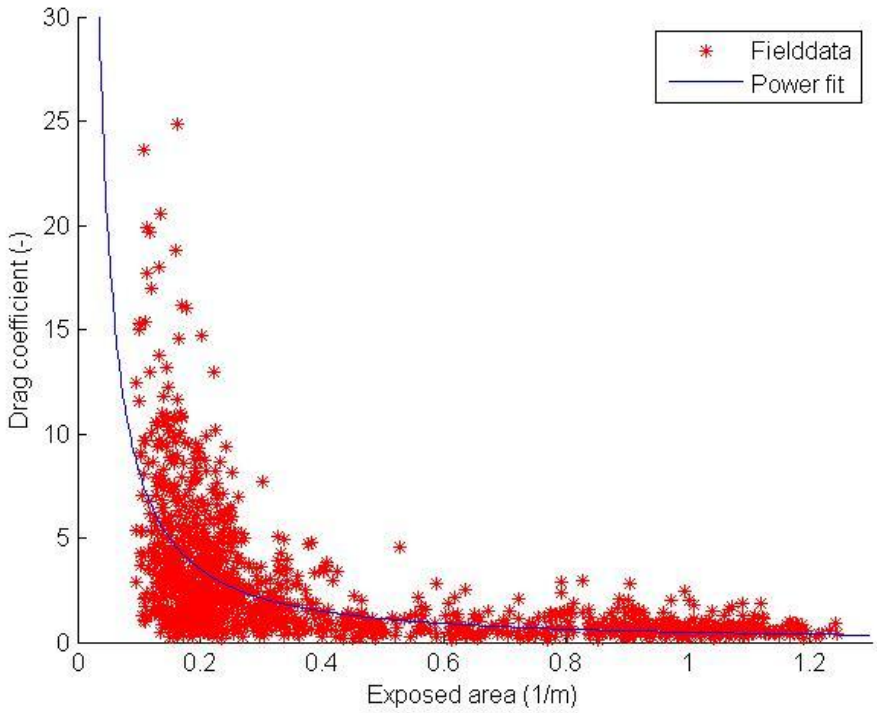

FIGURE 38 DRAG COEFFICIENT VS EXPOSED AREA

As seen before, Quartel (2007) found a relation between the drag coefficient and the projected cross-sectional area of the underwater obstacles (A) according to the following function:

$$C_D = 0.6 * e^{0.15A}$$

This however is clearly not in line with the relation found here. Where Quartel found a positive relation between exposed area and drag coefficient, in our data, there clearly is a negative relation. The cause for this difference is unknown.